



CCI Land Surface Temperature

End-To-End ECV Uncertainty Budget

WP2.5 – DEL-2.3

Ref.: LST-CCI-D2.3-E3UB

Date: 26-Nov-2021

Organisation: Consortium CCI LST



Signatures

	Name	Organisation	Signature
Written by	Claire Bulgin	University of Reading	
	Sofia Ermida	IPMA	
	Carlos Jimenez	Estellus	
Reviewed by	Karen Veal	University of Leicester	
Approved by	Darren Ghent	ULeic	
Authorized by	Simon Pinnock	ESA	

Change log

Version	Date	Changes
1.0	24-Jun-2019	First version
1.1	17-Sep-2019	Updated version taking into account RIDs raised by ESA
2.0	26-Nov-2021	Second version

List of Changes

Version	Section	Changes
2.0	5.1.3.1.2	<ul style="list-style-type: none"> • New section added to the ATSR/SLSTR detailing new TCWV uncertainty
2.0	5.2	<ul style="list-style-type: none"> • New section about MODIS, SEVIRI, GOES-16/ABI
2.0	5.3	<ul style="list-style-type: none"> • New section about SSM/I and SSMIS
2.0	6	<ul style="list-style-type: none"> • Harmonisation, Drift and Time corrections - this section is entirely new containing both IR and MW contributions

Table of Content

1. EXECUTIVE SUMMARY	1
2. INTRODUCTION	2
3. DEFINING NOMENCLATURE FOR UNCERTAINTY BUDGETS	3
3.1. Guidelines for defining terms relating to error and uncertainty	3
3.2. Definition of terms	4
3.2.1. Data Levels	4
3.2.2. Characterisation of error and uncertainty	4
3.2.3. Product assessment	5
3.2.4. Verification and Validation	6
3.3. Constructing an uncertainty budget	6
3.3.1. Uncorrelated uncertainties	6
3.3.2. Correlated uncertainties	7
4. EXPRESSION AND PROPAGATION OF UNCERTAINTY	8
4.1. Expression of uncertainty in a measurement equation	9
4.2. Defining sources of uncertainty in a measurement equation	10
4.3. Principles of propagating uncertainty	11
4.3.1. Introducing matrix notation for propagation of uncertainties: an example for propagating a Level 1 independent error effect for single pixel retrieval	12
4.3.2. Considering uncertainty propagation for structured error effects in single pixel retrievals	13
4.3.3. Relating the matrix notation to the definitions of terms and error effects	13
4.3.4. Propagation of uncertainties in averaged products	14
4.4. Reviewing the matrix notation for uncertainty propagation	15
4.5. Combining uncertainty components	17
4.6. Propagation of uncertainties to Level 4 products	17
5. CONSTRUCTING AN UNCERTAINTY BUDGET	18
5.1. ATSR-2, AATSR and SLSTR	18
5.1.1. Land Surface Temperature Retrieval	19
5.1.2. Level 1 data	22
5.1.2.1. Uncertainties due to random error effects	22
5.1.3. Level 2 data	23
5.1.3.1. Uncertainties due to locally systematic error effects	23
5.1.3.1.1 Uncertainty due to fractional vegetation cover	23
5.1.3.1.2 Uncertainty due to total column water vapour	24
5.1.3.1.3 Uncertainty due to geolocation	24
5.1.3.1.4 Uncertainty due to coefficient fitting (atmospheric effects)	25
5.1.3.2. Uncertainties due to large-scale systematic error effects	26
5.1.3.3. Correlation length scales of Level 2 uncertainty components	27
5.1.4. Level 3 data	27
5.1.4.1. Propagated Uncertainties	29
5.1.4.1.1 Uncorrelated (random) uncertainties	29
5.1.4.1.2 Fully correlated large-scale uncertainties	30
5.1.4.1.3 Locally systematic uncertainties	30
5.1.4.1.4 Propagation of locally-systematic surface uncertainty component	32
5.1.4.2. New uncertainties relevant to the processing level	35
5.1.5. L3C and L3S products	35
5.2. MODIS, SEVIRI and GOES-16/ABI	36
5.2.1. Land Surface Temperature Retrieval	37
5.2.2. Level 1 data	41
5.2.2.1. Uncertainties due to random error effects	42

5.2.2.1.1	Uncertainties due to instrument noise	42
5.2.3.	Level 2 data	42
5.2.3.1.	Uncertainties due to locally systematic error effects	43
5.2.3.1.1	Uncertainties due to total column water vapour	43
5.2.3.1.2	Uncertainties due to coefficient fitting (atmospheric effects)	44
5.2.3.1.3	Uncertainties due to emissivity estimation	45
5.2.3.2.	Uncertainties due to large-scale systematic error effects	45
5.2.3.3.	Correlations length scales of Level 2 uncertainty components	46
5.2.4.	Level 3 data	47
5.2.4.1.	Propagated uncertainties	49
5.2.4.1.1	Uncorrelated (random) uncertainties	49
5.2.4.1.2	Fully correlated large-scale uncertainties	49
5.2.4.1.3	Locally systematic uncertainties	49
5.2.4.2.	New uncertainties relevant to the processing level	51
5.2.5.	L3C and L3S products	51
5.3.	SSM/I and SSMIS	51
5.3.1.	Land Surface Temperature Retrieval	52
5.3.2.	L1 data	55
5.3.3.	L1 and L2 data together	56
5.3.4.	L3 data	59
6.	HARMONISATION, DRIFT AND TIME CORRECTIONS	61
6.1.	Harmonisation and calibration drift correction	61
6.1.1.	Harmonisation and calibration drift correction with reference to IASI	61
6.1.1.1.	How to quantify the uncertainties in the harmonisation to IASI	63
6.2.	Adjusting for differences in equator overpass time	64
6.2.1.	Adjustment for differences in equator overpass time for the single-sensor CDR	64
6.3.	Correcting data to a nominal satellite overpass time	65
6.3.1.	Time correction for microwave products	65
7.	SPECIFICATION OF UNCERTAINTY INFORMATION USED IN LST RETRIEVAL	69
7.1.	Look-up Table Structure	69
8.	PROVISION OF UNCERTAINTIES IN LST CCI PRODUCTS	73
8.1.1.	LST_cci product types	73
8.1.2.	L2P, L3U, L3C and L3S uncertainty information	74
9.	VALIDATION OF UNCERTAINTIES	76
9.1.	Techniques	76
10.	APPENDIX: HOW TO USE LST CCI UNCERTAINTY PRODUCTS	78
10.1.	Using uncertainty information from Level 2 products	78
10.1.1.	Example 1: Is the LST from a Level 2 product significantly different from a matched independent in-situ radiometer measurement?	78
10.1.2.	Example 2: What is the uncertainty in my calculation of outgoing LW infrared flux from the land surface arising from the measurement uncertainty in the Level 2 LST product I am using?	79
10.2.	Using uncertainty information from Level 3 products	79
10.2.1.	Example 1: What is the best estimate of the average LST over an area of 0.25 degrees latitude by 0.25 degrees longitude using L3U LST data?	79
10.2.2.	Example 2: What is the total uncertainty in the averaged LST calculated in example 1 (section 9.2.1)?	80

List of Figures

Figure 4-1: Illustration of uncertainty propagation through different satellite processing levels with the addition of new sources of uncertainty at each processing level.----- 8

Figure 4-2: Example of error effect indexing (k) with reference to terms (j) in the measurement equation. Figure is reproduced from RD-14. -----10

Figure 5-1: Example of pixel selection for calculating geolocation uncertainty. The retrieval is made for the central pixel (marked with an X), and the delta LST is calculated for the eight surrounding pixels. The retrieval for all pixels is consistent with the exception of the biome specification (indicated by the different colours). -----25

Figure 5-2: Example correlation matrix for a set of pixels (1-10) with associated biomes (A-D). The correlation matrix has off-diagonal non-zero elements where pixels share the same underlying biome. 31

Figure 5-3: Schematic showing the averaging steps for post-processing LST L2 retrievals to L3U and L3C.34

Figure 5-4: Illustration of a single-channel regression model and calibration dataset. A neural network is trained to retrieve LST from the SSM/I 37 GHz vertically polarized brightness temperatures (TB). Red dots are the samples in the calibration dataset, and the neural network output is represented in blue. The horizontal axis has been divided into 5 K TB bins, and for each bin the mean (black circles) and + one standard deviation (black line centred around the mean) are given. See the text for more details. -57

Figure 5-5: Illustration of (A) a traditional LST estimation with a Neural Network (NN), and (B) the proposed scheme where both the LST and an estimation of the LST error are provided by the NN. See the text for more details. Diagram adapted from Figure 2 in [RD-54].-----58

Figure 5-6: Example of retrieved LST (top) and associated uncertainty (bottom). Plotted the morning retrievals from the SSMI overpass at ~6.30 AM local time. -----59

Figure 9-1: An example of uncertainty budget validation. Data are retrieved sea surface temperatures validated using in-situ observations from buoys. Two different retrievals are shown for ATSR data – L2 per pixel datasets (top), and gridded L3 products (bottom). Retrievals are nadir two-channel (N2) and dual-view two-channel (D2) where the channels used are 10.8 and 12 microns. Dashed lines denote the idealised uncertainty model, whilst solid lines represent the standard deviation of the retrieval minus in-situ differences. The blue line shows the SST bias and the red lines are the uncertainties on the retrieved uncertainty. -----77

List of Tables

Table 1: Organisations jointly responsible for the content of the Guide to Uncertainty in Measurement [RD-1] and International Vocabulary of Metrology [RD-2]. ----- 3

Table 2: Definitions of processing levels for satellite data. These are extracted from Table 1 in RD-3. ---- 4

Table 3: An example table showing ‘j’ terms and ‘k’ associated effects. ‘i’ denotes independent (uncorrelated) error effects and ‘s’ structured (locally systematic) error effects.-----11

Table 4: Summary of terminology used in constructing an uncertainty budget. -----15

Table 5: Definition of matrix notation introduced in section 4.3 (in part specified from RD-14)). -----16

Table 6: Definition of variables and notation introduced in sections 4.1-4.3. -----16

Table 7: Instrument characteristics for ATSR-2, AATSR and SLSTR. -----	18
Table 8: Error effects for single pixel LST retrieval. Effects are categorised according to the measurement equation term. Where quantified, the values propagated for each effect are specified for AATSR. *denotes cases where the uncertainty is modelled rather than propagated using a sensitivity coefficient.-----	21
Table 9: T_{11} and T_{12} diagonal elements in the S_{ϵ} matrix for the ATSR-2, AATSR [RD-25] and SLSTR [RD-26, RD-27] instruments.-----	23
Table 10: Binning resolution of the factors used to define the coefficient fitting uncertainty. -----	26
Table 11: Correlation length scales for the error effects characterised in Level 2 data. -----	27
Table 12: Error effects for averaging LST products. Effects are categorised according to the measurement equation term. Where quantified, the values propagated for each effect are specified. *denotes cases where the uncertainty is modelled rather than propagated using a sensitivity coefficient.-----	28
Table 13: Instrument characteristics for MODIS Aqua and MODIS Terra. -----	36
Table 14: Instrument characteristics for SEVIRI aboard MSG1-4.-----	37
Table 15: Instrument characteristics for ABI aboard GOES-16. -----	37
Table 16: Error effects for single pixel LST retrieval. Effects are categorised according to the measurement equation term. Where quantified, the values propagated for each effect are specified for MODIS TERRA. *denotes cases where the uncertainty is modelled rather than propagated using a sensitivity coefficient. -----	40
Table 17: T_{11} and T_{12} diagonal elements in the S_{ϵ} matrix for the MOIS AQUA, MODIS TERRA, MSG1, MSG2, MSG3, MSG4 and GOES-16/ABI instruments.-----	42
Table 18: Residual uncertainties in the coefficient fitting process. Uncertainties are presented as standard deviations and would be squared when used as diagonal elements of the error correlation matrix, S_{ϵ} .-----	45
Table 19: Correlation length scales for the error effects characterised in Level 2 MODIS, SEVIRI and GOES-16/ABI data. -----	46
Table 20: Error effect for averaging MODIS, SEVIRI and GOES-16/ABI LST products. Effects are categorised according to the measurement equation term. Where quantified, the values propagated for each effect are specified. *denotes cases where the uncertainty is modelled rather than propagated using a sensitivity coefficient. -----	48
Table 21: Instrument characteristics for SSM/I [RD-46]and SSMIS [RD-47]. Vertically and horizontally polarized BTs are available at all frequencies, apart from the 22.235 GHz channel, which is only vertically polarized. SSMIS also observe at other frequencies, but only the ones used for the LST estimation are listed. The ground resolution corresponds to the 3db-Field of View (FOV) of the projected ground footprint.-----	52
Table 22: Main error effects for single pixel LST retrieval. Effects are categorised according to the measurement equation term. *denotes cases where the uncertainty cannot be propagated using a sensitivity coefficient. -----	55
Table 23: T_m diagonal elements in the S_{ϵ} matrix for the SSM/I [RD-1] and SSMI/S [RD-2] instruments.---	56
Table 24: Error effects for averaging LST products. Effects are categorised according to the measurement equation term. * denotes where the uncertainty cannot be propagated using a sensitivity coefficient.-----	60

Table 25: Error effects table for the harmonisation of infrared sensors with reference to IASI. -----	62
Table 26: Error effects table for adjustment of AATSR and SLSTR-A data to a nominal equator overpass time of 1030/2230.-----	64
Table 27: Error effects table for time differences corrections for microwave data -----	68
Table 28: Global attributes for look-up tables used in the uncertainty budget calculation for AATSR. ----	69
Table 29: Dimensions of the look-up tables used in the uncertainty budget calculation for AATSR. -----	70
Table 30: Variables contained within the look-up table used in the uncertainty budget calculation. Information provided includes the variable name, the variable type and the dimensions of the variable.	71
Table 31: Attributes associated with each variable contained within the look-up tables used in the uncertainty budget calculation. -----	72
Table 32: Description of data product types produced within the LST_cci project (taken from RD-21). --	73
Table 33: Mapping of uncertainty components to variable names within L2P, L3U, L3C and L3S products.	74
Table 34: Variable dimensions for uncertainty components in L2P data. -----	74
Table 35: Variable dimensions for uncertainty components in L3U, L3C and L3S data.-----	74
Table 36: ‘long_names’ for uncertainty components in L2P, L3U, L3C and L3S products.-----	75
Table 37: Common variable attributes for uncertainty components in L2P, L3U, L3C and L3S products. --	75

Reference Documents

Identity	Reference
RD-1	Joint Committee for Guides in Metrology, (2008), Evaluation of measurement data – Guide to the expression of uncertainty in measurement. JCGM 2008.
RD-2	Joint Committee for Guides in Metrology, (2012), International vocabulary of metrology – Basic and general concepts and associated terms (VIM). JCGM 2012.
RD-3	Mittaz, J., Merchant, C. J., and Wolliams, E. R. (2019), Applying Principles of Metrology to Historical Earth Observations from Satellites, <i>Metrologica</i> , 56(3), doi: https://doi.org/10.1088/1681-7575/ab1705 ..
RD-4	Merchant, C. J., Paul, F., Popp, T., Ablain, M., Bontemps, S., Defourny, P., Hollmann, R., Lavergne, T., Laeng, A., de Leeuw, G., Mittaz, J., Poulsen, C., Povey, A. C., Reuter, M., Sathyendranath, S., Sandven, S., Sofieva, V. F., and Wagner, W. (2017). Uncertainty information in climate data records from Earth observation. <i>Earth System Science Data</i> , 9(2), 511-527.
RD-5	Global Climate Observing System, (2016). The Global Observing System for Climate: Implementation Needs, GCOS-200.
RD-6	Bulgin, C. E., Embury, O., Corlett, G. and Merchant, C. J. (2016). Independent uncertainty estimates for coefficient based sea surface temperature retrieval from the Along-Track Scanning Radiometer instruments, <i>Remote Sensing of Environment</i> , 178, 213-222.
RD-7	Ghent, D., Corlett, G., Goettsche, F., and Remedios, J. (2017). Global land surface temperature from the Along-Track Scanning Radiometers. <i>Journal of Geophysical Research – Atmospheres</i> , 122, pp 12,167-12,193.
RD-8	Merchant, C. J., Ghent, D., Kennedy, J., Good, E., Hoyer, J. (2015). Common Approach to

	Providing Uncertainty Estimates Across All Surfaces. EUSTACE (640171) Deliverable 1.1.
RD-9	Bulgin, C. E., Embury, O., Merchant, C. J. (2016). Sampling uncertainty in gridded sea surface temperature products and Advanced Very High Resolution Radiometer (AVHRR) Global Area Coverage (GAC) data. <i>Remote Sensing of Environment</i> , 177, 287-294.
RD-10	Martin, M., Gottsche, F. M. (2016). Satellite LST Validation Report. WP4 – DEL-12, ESA DUE GlobTemperature Deliverable.
RD-11	Embury, O. and Merchant C. J. (2012) A reprocessing for climate of sea surface temperature from the Along-Track Scanning Radiometers: a new retrieval scheme. <i>Remote Sensing of Environment</i> , 116 pp 47-61.
RD-12	Ermida, S. L., DaCamara, C. C., Trigo, I. F., Pires, A. C., Ghent, D., Remedios, J. (2017). Modelling directional effects on remotely sensed land surface temperature. <i>Remote Sensing of Environment</i> , 190, pp 56-69.
RD-13	Merchant, C. J., Holl, G., Mittaz, J. P. D., Wooliams, E. R. (2019). Radiance Uncertainty Characterisation to Facilitate Climate Data Record Creation. <i>Remote Sensing</i> , 11(5), doi: https://doi.org/10.3390/rs11050474 .
RD-14	Merchant, C. and Wooliams E. (2019). Mathematical notation for FIDUCEO publications. Version 1.c.
RD-15	Embury, O., Merchant, C. J., and Corlett, G. K. (2012). A reprocessing for climate of sea surface temperature from the Along-Track Scanning Radiometers: Initial validation, accounting for skin and diurnal variability effects. <i>Remote Sensing of Environment</i> , 148, pp 16-27.
RD-16	Baret, F., Weiss, M., Lacaze, R., Camacho, F., Makhmara, H., Pacholczyk, P. and Smets, B. (2013). GEOV1: LAI and FAPAR essential climate variables and FCOVER global time series capitalizing over existing products. Part 1: Principles of development and production. <i>Remote Sensing of Environment</i> , 137, pp 299-309.
RD-17	Camacho, F., Cernicharo, J., Lacaze, R., Baret, F., Weiss, M. (2013). GEOV1: LAI, FAPAR essential climate variables and FCOVER global time series capitalizing over existing products. Part 2: Validation and intercomparison with reference products. <i>Remote Sensing of Environment</i> , 137, pp 310-329.
RD-18	Baret, F., Hagolle, O., Geiger, B., Bicheron, P., Miras, B., Huc, M., Berthelot, B., Nino, F., Weiss, M., Samain, O., Roujean, J. L. and Leroy, M. (2007). LAI, fAPAR and fCover CYCLOPES global products derived from VEGETATION Part 1: Principles of the Algorithm. <i>Remote Sensing of Environment</i> , 110, pp 275-286.
RD-19	Zeller, O., and Ghent, D. (2011). ATSR absolute geolocation accuracy: Observed shift between AATSR brightness temperature and Globcover biome structures (technical note for the ATSR Quality Working Group).
RD-20	Merchant, C. J., and Bulgin, C. E. (2018). SST CCI Phase-II Uncertainty Characterisation Report: Sea Surface Temperature v2. SST_CCI-UCR-UOR-201.
RD-21	Dodd, E. (2019). LST CCI Product Specification Document, LST-CCI-D1.2-PSD.
RD-22	Bulgin, C. E, Merchant, C. J., Ghent, D., Klueser, L., Popp, T., Poulsen, C., and Sogacheva, L. (2018). Quantifying uncertainty in satellite-retrieved land surface temperature from cloud detection errors, <i>Remote Sensing</i> , 10 (4), pp. 616.
RD-23	Prata, F. (2002). Land surface temperature measurement from space: AATSR algorithm theoretical basis document.
RD-24	Smith, (1999). AATSR infra-red radiometric calibration report.
RD-25	Smith, D. 2012, Envisat AATSR Instrument Performance – End of Mission Report
RD-26	Polehampton, E., Etxaluze, M., Smith, D., and Cox C. 2016. Sentinel-3 SLSTR RAL Phase E1 In-orbit Commissioning Report



RD-27	Polehampton, E., Etxaluze, M., Smith, D., and Cox C. 2018. Sentinel-3B SLSTR RAL Phase E1 In-orbit Commissioning Report
RD-28	Steinke, S., Eikenberg, S., Lohnert, U., Dick, G., Klocke, D., Di Girolamo, P., Crewell, S. (2015). Assessment of small-scale integrated water vapour variability during HOPE. Atmospheric Chemistry and Physics. 15, pp. 2675-2692.
RD-29	Vogelmann, H., Sussmann, R., Trickl, T., Reichert, A. (2015). Spatiotemporal variability of water vapour investigated using lidar and FTIR vertical soundings above the Zugspitze. Atmospheric Chemistry and Physics. 15, pp. 3135-3148.
RD-30	European Space Agency, Sea Surface Temperature Climate Change Initiative webpage, www.esa-sst-cci.org
RD-31	European Space Agency, Data User Element GlobTemperature webpage, www.globtemperature.info
RD-32	European Commission Fidelity and Uncertainty in Climate Data Records from Earth Observations webpage, www.fiduceo.eu
RD-33	Wan, Z., Dozier, J. A. (1996). A generalized split-window method for retrieving land-surface temperature from space. IEEE Trans. Geosci. Remote Sensing. 34, 892-905.
RD-34	Ghent, D., Veal, K., Trent, T., Dodd, E., Sembhi, H. and Remedios, J. (2019). A new approach to defining uncertainties for MODIS land surface temperature. Remote Sensing, 11, doi:10.3390/rs11091021.
RD-35	Dodd, E., Ghent, D., Jimenez, C., Ermida, S. (2019). CCI Land Surface Temperature Algorithm Theoretical Basis Document. WP2.1 – DEL-LST-CCI-D2.2-ATBD.
RD-36	Xiong, X., Chiang, K., Esposito, J., Guenther, B., Barnes, W. (2003). MODIS on-orbit calibration and characterization. Metrologia. 40, S89-S92.
RD-37	Liu, R. G., Liu, J. Y., Liang, S. (2006). Estimation of Systematic Errors of MODIS Thermal Infrared Bands. IEEE Geoscience Remote Sensing Letters. 3, 541-545.
RD-38	Xiong, X., Wu, A., Cao, C. (2008). On-orbit calibration and inter-comparison of Terra and Aqua MODIS surface temperature spectral bands. International Journal of Remote Sensing. 29, 5347-5359.
RD-39	Seemann, S. W., Borbas, E. E., Knuteson, R. O., Stephenson, G. R., Huang, H. L. (2008). Development of a global infrared land surface emissivity database for application to clear sky sounding retrievals from multispectral satellite radiance measurements. Journal of Applied Meteorological Climatology. 47, pp 108-123.
RD-40	Hulley, G. C., Hook, S. J., Abbott, E., Malakar, N., Islam, T., Abrams, M. (2015). The ASTER Global Emissivity Dataset (ASTER GED): Mapping Earth's emissivity at 100 meter spatial scale. Geophysical Research Letters. 42, pp 7966-7976.
RD-41	Friedl, M. A., McIver, D. K., Hodges, J. C., Zhang, X. Y., Muchoney, D., Strahler, A. H., Woodcock, C. E., Gopal, S., Schneider, A. Cooper, A. (2002). Global land cover mapping from MODIS: Algorithms and early results. Remote Sensing of Environment. 83, pp 287-302.
RD-42	Friedl, M. A., Sulla-Menashe, D., Tan, B. Schneider, A., Ramankutty, N. Sibley, A. Huang, X. (2010). MODIS Collection 5 global land cover: Algorithm refinements and characterization of new datasets. Remote Sensing of Environment. 114, pp 168-182.
RD-43	EOMF, IGBP land cover classification system, http://www.eomf.ou.edu/static/IGBP.pdf , Accessed 12 th Feb 2019.
RD-44	Peres, L. F., DaCamara, C. C. (2005). Emissivity maps to retrieve land-surface temperature from MSG/SEVIRI. IEEE Transactions in Geosciences Remote Sensing. 43, pp 1834-1844.
RD-45	WMO (2012). Guidelines on Ensemble Prediction Systems and Forecasting. WMO-No.1091
RD-46	Hollinger, J.P. 1989: DMSP Special Sensor Microwave/Imager Calibration/Validation. Final Report, Vol. I., Space Sensing Branch, Naval Research Laboratory, Washington D.C.

RD-47	Kunkee, David B.; Poe, Gene A.; Boucher, Donald J.; Swadley, Steven D.; Hong, Ye; Wessel, John E.; Uliana, Enzo A. (April 2008). "Design and Evaluation of the First Special Sensor Microwave Imager/Sounder". IEEE Transactions on Geoscience and Remote Sensing. 46 (4): 863–883. doi:10.1109/TGRS.2008.917980
RD-48	Fennig, K., Schröder, M., Andersson, A., and Hollmann, R.: A Fundamental Climate Data Record of SMMR, SSM/I, and SSMIS brightness temperatures, Earth Syst. Sci. Data, 12, 647–681, https://doi.org/10.5194/essd-12-647-2020 , 2020.
RD-49	Prigent, C., W.B. Rossow, E. Matthews, and B. Marticorena, 1999: Microwave radiometric signatures of different surface types in deserts. J. Geophys. Res., 104, 12147-12158, doi:10.1029/1999JD900153.
RD-50	Perry, M.; Ghent, D.J.; Jiménez, C.; Dodd, E.M.A.; Ermida, S.L.; Trigo, I.F.; Veal, K.L. Multisensor Thermal Infrared and Microwave Land Surface Temperature Algorithm Intercomparison. Remote Sens. 2020, 12, 4164. https://doi.org/10.3390/rs12244164
RD-51	Van der Baan, M. and Jutten, C. (2000) Neural networks in geophysical applications. Geophysics, 65 (4). pp. 1032-1047, doi.org/10.1190/1.1444797
RD-52	Aires, F., C. Prigent, W.B. Rossow, and M. Rothstein, 2001: A new neural network approach including first-guess for retrieval of atmospheric water vapor, cloud liquid water path, surface temperature and emissivities over land from satellite microwave observations. J. Geophys. Res., 106, 14887-14907, doi:10.1029/2001JD900085.
RD-53	Prigent, C., E. Jaumouille, F. Chevallier, and F. Aires, A parameterization of the microwave land surface emissivity between 19 and 100 GHz, anchored to satellite-derived estimates, IEEE TGRS, 46, 344-352, 2008
RD-54	F. Aires and V. Pellet, "Estimating Retrieval Errors From Neural Network Inversion Schemes--Application to the Retrieval of Temperature Profiles From IASI," in IEEE Transactions on Geoscience and Remote Sensing, doi: 10.1109/TGRS.2020.3026944.
RD-55	G. W. Milligan and M. C. Cooper, "An examination of procedures for determining the number of clusters in a data set," Psychometrika, vol. 50, no. 2, pp. 159–179, Jun. 1985.
RD-56	Veal, K., Ghent, D. Harmonization Documentation [LST CCI Technical Note], 2020.
RD-57	Badenas, C. and Onrubia, J. E. (2003). A mathematical study on effective wavenumber, an operative computation procedure, and its use with radiance temperature relationships. International Journal of Remote Sensing, 24(4). pp. 761-774. Doi:10.1080/01431160110115555.
RD-58	Bouillon, M., Safieddine, S., Hadji Lazaro, J., Whitburn, S., Clarisse, L, Doutriaux-Boucher, M., Coppens, D., August, T., Jacqueline, E. and Clerbaux, C. (2020). Ten Year Assessment of IASI Radiance and Temperature. Remote Sensing, 12, pp 2393, doi>10.3390/rs12152393.
RD-59	Fennig, K., Schröder, M., Andersson, A., and Hollmann, R.: A Fundamental Climate Data Record of SMMR, SSM/I, and SSMIS brightness temperatures, Earth Syst. Sci. Data, 12, 647–681, https://doi.org/10.5194/essd-12-647-2020 , 2020.
RD-60	Borbas, E., Hulley, G., Feltz, M., Knuteson, R., and Hook., S. (2018). The Combined ASTER MODIS Emissivity over Land (CAMEL) Part 1: Methodology and High Spectral Resolution Application. Remote Sensing, 10(4), pp. 643.
RD-61	Feltz, M., Borbas, E., Knuteson, R., Hulley, G., and Hook, S. (2018). The Combined ASTER MODIS Emissivity over Land (CAMEL) Part 2: Uncertainty and Validation. Remote Sensing, 10(5), pp 664.

1. Executive Summary

This document presents the end-to-end uncertainty budget as applied to the single-sensor Climate Data Record (CDR), single-sensor MODIS, SEVIRI and GOES-16 products and the microwave SSM/I and SSMIS land surface temperature (LST) data produced within the Climate Change Initiative (LST_cci) project. The CDR is generated using observations from the Along-Track Scanning Radiometer (ATSR) instruments, the Moderate Resolution Imaging Spectroradiometer (MODIS) and the Sea and Land Surface Temperature Radiometer (SLSTR). The provision of uncertainty information with LST data is motivated by the concept that this information is fundamental to the application of the data, particularly within the field of climate science. The aim is to provide uncertainty information with every datum within the LST_cci datasets, building on the work undertaken within the Sea Surface Temperature (SST) CCI project, and first applied to LST products within the ESA Data User Element GlobTemperature project.

The approach taken here is to construct an uncertainty budget for the LST data, recognising that uncertainties are introduced at each processing level (from satellite observations through to gridded products) and that uncertainties in lower-level products need to be correctly propagated into higher level products during the processing. In order to facilitate uncertainty propagation, we group error effects into three broad categories according to their correlation length scale:

- ❖ Uncertainties due to uncorrelated (random, independent) error effects
- ❖ Uncertainties due to locally-systematic (structured) error effects
- ❖ Uncertainties due to large-scale systematic (common) error effects

The methodology for propagating these uncertainties, based on the law of propagation of uncertainty is dependent on the correlation between terms used in the measurement equation; and for each of three cases identified above, the propagation is done independently. The uncertainty components once propagated can then be added in quadrature to give a total uncertainty for the LST retrieval. Where possible, the full uncertainty budget is provided to data users to enable correct propagation of uncertainties into user derived data products.

Within this document we build upon the metrological concepts for the quantification and propagation of uncertainty in Earth Observation developed within the Fidelity and Uncertainty in Climate Data Records from Earth Observations (FIDUCEO) project. These provide a basis for rigorous analysis of the sources of error in each data level and means to understand to what degree we can quantify these within our uncertainty budget. Using these principles, we have also been able to recommend areas for future development with regards to uncertainty budget calculation and propagation.

One advantage of providing uncertainty information calculated independently of in-situ datasets is that the uncertainties can be validated in addition to the LST retrievals. This enables data providers to understand the degree to which they can correctly characterise and propagate the uncertainties in their dataset and processing methodology. It also provides more detailed uncertainty information (datum specific) than is typically possible using comparisons against in-situ datasets. Uncertainties can also be used in the validation of the LST data to prescribe upper and lower bounds for measurement differences.

This document also contains information on the way in which uncertainty information is provided for users, and worked examples of how these data can be correctly applied across a few different applications.

2. Introduction

The maturity of Earth Observation (EO) products has increased significantly over the last decade with the longevity of the data record increasing their relevance for climate applications. With the development of these datasets, there has become an increasing awareness within the EO community of the importance of providing uncertainty estimates with data products, essentially informing the user of the degree to which these measurements are ‘in doubt’. This is intuitively important in the context of climate; to understand long-term changes in the geophysical world we need to ensure that the observed changes are not an artefact of the measurement process itself. These data now cover a period of time that is significant with respect to climate and have the potential to inform policy, adaptation and mitigation strategies.

This focus on quantifying uncertainties in EO products has been reflected in a number of recent research programs. Across the European Space Agency (ESA) Climate Change Initiative (CCI), funding has been provided to produce climate data records for twenty-three essential climate variables within the last decade, and within all of these projects, it is expected that uncertainties associated with the data be provided to the user. Horizon 2020 projects funded by the European Commission have also had a focus on understanding uncertainties in EO data, most notably in the FIDUCEO project [RD-32]. This particular project focuses on Level 1 satellite measurements (prior to any geophysical retrieval), providing a comprehensive overview of the uncertainties that arise as a function of the instrument and orbit characteristics. These can then feed into any higher-level application of these data in retrieving geophysical properties.

Focusing particularly on the retrieval of surface temperature, many of the concepts developed within the sea surface temperature (SST) CCI project [RD-30] are of relevance also to land surface temperature (LST) retrieval. Within this document we will take these principles, and apply them within the context of LST retrieval, building on work undertaken within the ESA GlobTemperature Data User Element (DUE) project [RD-31]. We will also exploit the methods and techniques developed within FIDUCEO to further understand the sources of uncertainty in our data products.

The remainder of this deliverable will be structured as follows: firstly we will define the nomenclature appropriate to characterising uncertainties. We will consider the sources of uncertainties specific to each instrument included in our infrared LST climate data record (ATSR2, AATSR, MODIS Terra and SLSTR), to the single-sensor products from MODIS, SEVIRI and GOES-16, and the microwave products from SSM/I and SSMIS. We will describe how uncertainties propagate from one level of product to another (i.e. from measurement uncertainty in Level 1 data right through to LST uncertainties in gridded Level 3 products). We will also consider uncertainties introduced through the process of harmonising instruments to make a continuous data record and correcting for differences in time both due to satellite in-orbit drift, and when providing continuous time series using data from multiple sensors. We will make some recommendations for future developments and finally we will describe how uncertainty data are provided within our products and how this information can be used within climate applications.

3. Defining nomenclature for uncertainty budgets

Only recently has the rigorous discipline of metrology begun to be applied within the domain of Earth Observation (EO). In the application of metrology to EO, the definition of terms is of paramount importance to prevent ambiguity and enable comparison of metrics between products. Unfortunately, terms such as ‘error’ are frequently misused within the English language, and very often the user’s meaning for the term has to be inferred from the context of its usage. Within the GlobTemperature project that preceded LST_cci, a survey was undertaken asking participants to match common terms used within the field of metrology, to their definitions. In the majority of cases, the user community were unable to match the correct definitions to each term, reflecting the common incorrect or ambiguous usage of many of these terms. Here we begin by defining the nomenclature that we will apply throughout the LST_cci project when referring to the uncertainty budgets provided with our data products.

3.1. Guidelines for defining terms relating to error and uncertainty

The basis for defining the metrology of uncertainty is the Guide to Uncertainty in Measurement (GUM) [RD-1], which should be read with reference to the International Vocabulary of Metrology (VIM) [RD-2]. These documents have been produced through the collaboration of seven international committees (Table 1) over the period of several decades, with regular updates to this documentation as understanding of the field has evolved. These documents aim to provide vocabulary and methods that are applicable across many fields of measurement, and the principles of applying metrology to EO build upon these.

Acronym	Organisation
BIPM	Bureau International des Poids et Mesures
IEC	International Electrotechnical Commission
IFCC	International Federation of Clinical Chemistry
ISO	International Organization for Standardization
IUPAC	International Union of Pure and Applied Chemistry
IUPAP	International Union of Pure and Applied Physics
OIML	International Organization of Legal Metrology

Table 1: Organisations jointly responsible for the content of the Guide to Uncertainty in Measurement [RD-1] and International Vocabulary of Metrology [RD-2].

RD-3 provides a comprehensive overview of how the concepts of metrology can be applied within the field of Earth observation. It considers the nature of satellite retrievals and various levels of processing required when generating geophysical data, defining the metrological concepts that need to be considered at each stage. Within the European Space Agency (ESA) Climate Change Initiative (CCI) program, the importance of providing uncertainties with climate data record (CDR) data from essential climate variables (ECVs) has been recognised. The domains covered by these ECV projects are diverse: including the biosphere, atmosphere and ocean. RD-4 is a review paper that includes a definition of terms relating to uncertainty estimation as applied consistently across the CCI ECV datasets. Uncertainty nomenclature is also specified within the GCOS Implementation Plan [RD-5], which defines the targets for dataset development within each of the ECVs.

3.2. Definition of terms

In this section we define the nomenclature relevant to characterising error and uncertainty within the LST_cci project. The terms defined here will be used consistently throughout this document and in other deliverables as appropriate. Unless explicitly stated otherwise, the definitions given here (and in Section 3.3) are consistent with those provided in the VIM [RD-2].

3.2.1. Data Levels

Retrieval of geophysical variables from satellite processing is a complex process involving a number of steps, commonly referred to as data processing levels within the EO community. These are referred to throughout this document so we begin by defining these in Table 2. The content of this table is extracted from RD-3.

Product Level	Description
Level 0 (L0)	Raw telemetry: timings, counts, instrument data etc.
Level 1 (L1)	Calibrated radiances (and/or counts and gain parameters) with location, time and viewing geometry.
Level 2 (L2)	Estimates of geophysical variables on the spatio-temporal sampling pattern of the L1 radiances ('swath data').
Level 3 (L3)	L2 data transformed to a fixed spatio-temporal sampling ('grid') often at reduced spatio-temporal resolution.
Level 4 (L4)	Spatio-temporally complete fields on a regular grid.

Table 2: Definitions of processing levels for satellite data. These are extracted from Table 1 in RD-3.

3.2.2. Characterisation of error and uncertainty

Considering now the terms related to the measurement process; firstly, the quantity we measure is the **measurand**:

- ❖ **measurand** : quantity intended to be measured

In measuring the **measurand** we then have a **measured quantity value**:

- ❖ **measured quantity value**: quantity value representing a measurement result

For Level 1 data this is typically the radiance (or derived reflectance or brightness temperature) but at Level 2 or above this is the value of the geophysical retrieval, in this case land surface temperature (LST). The value of the **measured quantity value** is typically different from the **true quantity value**, which is what we would ideally measure.

- ❖ **true quantity value**: quantity value consistent with the definition of a quantity

In some cases the **measurand** can be compared with a **reference quantity value** rather than a **true quantity value**.

- **reference quantity value**: quantity value used as a basis for comparison with values of quantities of the same kind

The difference between the **measured quantity value** and the **reference quantity value** is the **measurement error**.

- ❖ **measurement error:** measured quantity value minus a reference quantity value

In EO, we typically do not know the **measurement error**. If we did, we would correct for this in order to provide the **true quantity value**. Where we do not know the **measurement error** we can instead provide the **measurement uncertainty**.

- ❖ **measurement uncertainty:** non-negative parameter characterising the dispersion of the quantity values being attributed to a measurand, based on the information used.

Within LST_cci we provide the **standard measurement uncertainty, which assumes a normal distribution of errors**.

- ❖ **standard measurement uncertainty:** measurement uncertainty expressed as a standard deviation

Note here that the definitions of error and uncertainty are different. Uncertainties are an estimation of the spread of the distribution of errors, associated with a given measurement quantity value. These terms should not therefore be used inter-changeably.

3.2.3. Product assessment

Once we have generated a data product we can discuss the quality of this dataset and the degree to which it is appropriate to use it for a given application using a number of metrics. The first of these is the **measurement accuracy**.

- ❖ **measurement accuracy:** closeness of agreement between a measured quantity value and a true quantity value of a measurand.

It should be noted that the VIM explicitly states, “the concept ‘measurement accuracy’ is not a quantity and is not given a numerical quantity value. A measurement is said to be more accurate when it offers a smaller measurement error.” [RD-2].

A second metric is **measurement precision**.

- ❖ **measurement precision:** closeness of agreement between indications or measured quantity values obtained by replicate measurement on the same or similar objects under specified conditions.

Another common concept is **measurement bias**. Ideally any known measurement bias is removed from a dataset prior to calculating the uncertainty budget (section 3.3), so that this only represents the residual error sources that cannot be directly removed from the measurement quantity.

- ❖ **measurement bias:** estimate of a systematic measurement error (defined on page 7).

We can also consider the **stability of a measuring instrument** and **instrumental drift** over time.

- ❖ **stability of a measuring instrument:** property of a measuring instrument, whereby its metrological properties remain constant in time.
- ❖ **instrument drift:** continuous or incremental change over time in indication, due to changes in metrological properties of a measuring instrument (where indication is the quantity value provided by a measuring instrument or a measuring system).

We may also consider the **sensitivity of a measuring system**.

- ❖ **sensitivity of a measuring system:** quotient of the change in an indication of a measuring system and the corresponding change in a value of a quantity being measured.

3.2.4. Verification and Validation

Validation and data verification are typically undertaken together, independently of the dataset generation. Indeed validation is a specific form of verification. These terms are defined as follows:

- ❖ **verification:** provision of objective evidence that a given item fulfils specified requirements.
- ❖ **validation:** verification, where the specified requirements are adequate for an intended use.

In the case of a dataset where both the data and associated uncertainties are provided, the uncertainties can be validated in addition to the geophysical data.

3.3. Constructing an uncertainty budget

Our goal within the LST_cci project is to provide an uncertainty estimate for every datum in all of our products. In order to do this we need to construct an **uncertainty budget**.

- ❖ **uncertainty budget:** statement of a measurement uncertainty, of the components of that measurement uncertainty, and of their calculation and combination.

The uncertainty budget comprises all of the error sources for which we can characterise the error distribution either statistically or empirically or determine an uncertainty on the basis of expert analysis. These different methodologies fit into **Type A** and **Type B** uncertainties as defined below.

- ❖ **Type A evaluation of measurement uncertainty:** evaluation of a component of measurement uncertainty by a statistical analysis of measured quantity values obtained under defined measurement conditions.
- ❖ **Type B evaluation of measurement uncertainty:** evaluation of a component of measurement uncertainty determined by means other than a Type A evaluation of measurement uncertainty. Examples include:
 - Associated with authoritative published quantity values
 - Associated with the quantity value of a certified reference material
 - Obtained from a calibration certificate
 - Obtained from the accuracy class of a verified measuring instrument
 - Obtained from limits deduced through personal experience.

Within an uncertainty budget, the different error terms can have different correlation length scales. Categorising uncertainty components on the basis of the correlation length scales of the error source is important to ensure that these can be correctly propagated into higher-level products. We consider the different length scales over which errors sources can be correlated in the following sections (3.3.1 – 3.3.2).

3.3.1. Uncorrelated uncertainties

Uncorrelated uncertainties are those that arise from **random measurement error** effects.

- ❖ **random measurement error:** component of measurement error that in replicate measurements varies in an unpredictable manner.

These sources of uncertainty are treated independently of correlated uncertainties, because when gridded products are constructed (L3) these uncertainties cancel out to a certain degree where correlated uncertainties do not.

3.3.2. Correlated uncertainties

Correlated uncertainties arise from **systematic measurement error** sources.

- ❖ **systematic measurement error**: component of measurement error that in replicate measurements remains constant or varies in a predictable manner.

Within LST_cci as with other projects that have produced surface temperature data from satellite retrievals (e.g. SST CCI and Eustace) we intend to differentiate between locally systematic uncertainties (structured) and large-scale (common) uncertainties. The difference between the two is that locally systematic uncertainties are only correlated over a limited spatial or temporal range, beyond which they will behave like uncorrelated uncertainties, and will need to be treated as such in any uncertainty propagation. Large scale systematic uncertainties are correlated over much longer time or space scales, for example the lifetime of a given instrument, so are almost always treated as fully correlated in uncertainty propagation activities (with the exception of considering harmonisation between sensors).

4. Expression and Propagation of Uncertainty

As summarised in Table 2, there are a number of different processing levels for satellite data. At each new level of processing there are two sources of uncertainty:

1. The uncertainty already inherent in the data from the previous processing level will feed into the uncertainty budget for the new processing level.
2. Modification of the data introduces new sources of uncertainty (for example, making a retrieval of surface temperature through the atmosphere at Level 2).

The process described in (1) is known as ‘propagation of uncertainty’, which will be defined mathematically within this chapter. These concepts are illustrated in Figure 1, which shows a simplified version of the satellite data processing chain from levels 1 through to 4, with the propagation of uncertainties from one level to another and addition of new uncertainty sources at each level.

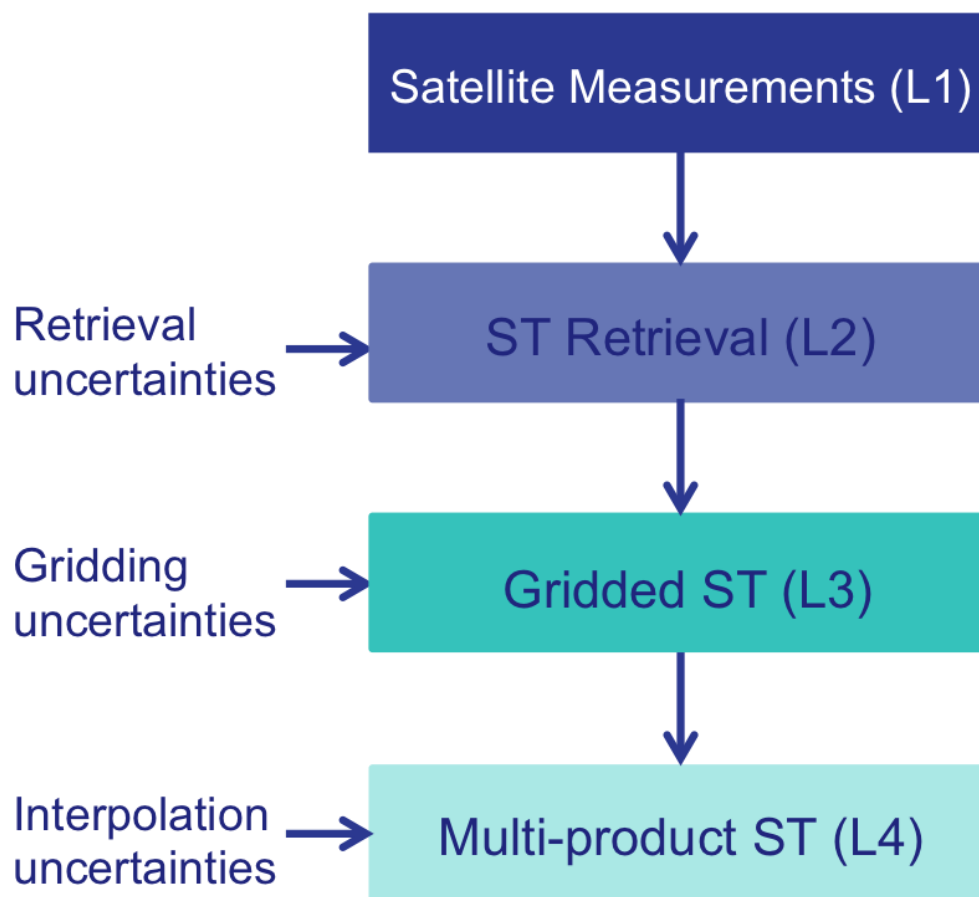


Figure 4-1: Illustration of uncertainty propagation through different satellite processing levels with the addition of new sources of uncertainty at each processing level.

4.1. Expression of uncertainty in a measurement equation

Here it is useful to introduce some generalised notation for defining measurement equations and uncertainties with a view to being able to express uncertainty calculations in matrix form [RD-14]. The advantage of this notation is the simplicity of the resulting equations, but it is understood that many people are more familiar with the traditional textbook expressions used in the GUM [RD-1]. Therefore the relationship between the two will be clearly explained here, so that the simplified matrix expressions can be used in later sections.

The focus of this project is on the retrieval of geophysical data from satellite observations. The measurement equation for a single pixel can therefore be expressed as a function (g) of the observations (\mathbf{y}) and retrieval parameters ($\boldsymbol{\beta}$), where z is the retrieved quantity [RD-13].

$$z = g(\mathbf{y}, \boldsymbol{\beta}) + 0 \quad (4.1)$$

There are three overall sources of uncertainty that contribute to the uncertainty in the retrieved quantity z [RD-13]:

1. Uncertainty in the observations (\mathbf{y}) propagated through g into the retrieved value z .
2. Uncertainty in the retrieval parameters ($\boldsymbol{\beta}$) propagated through g into the retrieved value z .
3. Uncertainty in the retrieved value z , that is not directly traceable via \mathbf{y} or $\boldsymbol{\beta}$ (resulting for example from approximations or assumptions made in the retrieval).

This equation includes a (+ 0) term to represent the uncertainties that we cannot trace through the retrieval process (point 3 in the above list).

Considering the case where the single pixel data are averaged to provide a gridded product, the measurement equation defines the weighted combination $\langle z \rangle$ of the n values of z that contribute to the averaged product [RD-13]. $\langle z \rangle$ is a function (h) of the input retrieved quantities, \mathbf{z} , and the parameters $\boldsymbol{\gamma}$.

$$\langle z \rangle = h(\mathbf{z}, \boldsymbol{\gamma}) + 0 \quad (4.2)$$

In this example, the parameters, $\boldsymbol{\gamma}$, could consist of weights, correlation length scales and correlation coefficients to give some examples [RD-13]. As with the measurement equation for single pixel retrieval, there are three sources of uncertainty associated with the calculation of an averaged product.

1. Uncertainty in the retrieved values (\mathbf{z}) propagated through h into the averaged value $\langle z \rangle$.
2. Uncertainty in the gridding parameters ($\boldsymbol{\gamma}$) propagated into the averaged value $\langle z \rangle$.
3. Uncertainty in the averaged value $\langle z \rangle$, which is introduced by incomplete sampling of the domain that the averaged value is said to represent (in either space or time).

4.2. Defining sources of uncertainty in a measurement equation

Each of the terms in a measurement equation has an associated uncertainty, which is comprised of contributions from one or more error effects. In the example of the measurement equation for the single pixel retrieval (4.1), the terms are the observations in vector \mathbf{y} and the parameters in vector $\boldsymbol{\beta}$. We can index these using the subscript 'j'. For each term (indexed using j), the error effects contributing the uncertainty in that term can be indexed using the subscript 'k'. An example of this indexing using an uncertainty analysis tree diagram is provided in Figure 4-2 [RD-14]. Here only the observation vector, \mathbf{y} , is expanded within the measurement equation but this is sufficient for illustrative purposes. Both the terms, j, and error effects, k, are numbered sequentially.

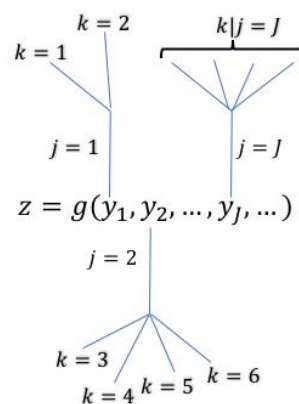


Figure 4-2: Example of error effect indexing (k) with reference to terms (j) in the measurement equation. Figure is reproduced from RD-14.

Having identified the effects, k, that relate to the terms, j, these can be further categorised according to their spatial correlation. This is important in the context of providing spatially or temporally averaged data (eg. equation 4.2) where the correct propagation of uncertainties is dependent on understanding their correlation length scale. Three further subscripts can be used to categorise the spatial correlations of error effects.

- ❖ 'i' denoting independent error effects. The uncertainties arising from these error effects are uncorrelated between pixels. These are often given the label 'random' in uncertainty products.
- ❖ 's' denoting structured error effects. The uncertainties arising from these error effects are correlated between pixels. For these effects, there will be an associated correlation coefficient and length scale. These are often labelled as 'locally systematic' in uncertainty products as they are correlated over a defined 'local' scale.
- ❖ 'c' denoting common effects. These uncertainties are correlated over large spatio-temporal scales, and are typically in common over the entire data record for a given sensor. These are often labelled as 'large-scale systematic' uncertainties in data products.

Table 3 provides an example of how error effects can be grouped according to terms and spatial correlation. This is an imaginary case and not representative of any particular measurement equation.

Subscript	Index											
j	1		2				3					
k	1	2	3	4	5	6	7	8	9	10	11	12
i	1		2	3					4			5
s		1			2	3	4	5		6	7	

Table 3: An example table showing ‘j’ terms and ‘k’ associated effects. ‘i’ denotes independent (uncorrelated) error effects and ‘s’ structured (locally systematic) error effects.

We can use this notation to define sets of error effects. For example, the valid values of k, given j = 3 would be as follows:

$$k|(j = 3) = \{7,8,9,10,11,12\} \quad (4.3)$$

Similarly we can group error effects given their spatial correlation.

$$k|i = \{1,3,4,9,12\} \quad (4.4)$$

$$k|s = \{2,5,6,7,8,10,11\} \quad (4.5)$$

From this table we can see that the sum over all error effects is equal to the sum over all independent effects plus the sum over all structured effects. This is true as each error effect, k, can be classified either as independent or structured but not both.

4.3. Principles of propagating uncertainty

Taking the two examples outlined in section 4.1, let us consider the propagation of uncertainty into:

- i. A single pixel retrieval, z.
- ii. An averaged product, ⟨z⟩.

The full equation for the propagation of uncertainty as given in the GUM [RD-1], can be defined firstly for the single pixel retrieval (equation 4.1), where u(z) is the uncertainty in z.

$$u(z)^2 = \sum_i^n \left(\frac{\partial g}{\partial y_i} \right)^2 u_i^2(y_i) + 2 \sum_{i=1}^{n-1} \sum_{j=i+1}^n \left(\frac{\partial g}{\partial y_i} \right) \left(\frac{\partial g}{\partial y_j} \right) u(y_i y_j) \quad (4.6)$$

The propagation of uncertainty assumes that the errors in z arising from errors in **y** are proportional to the derivative of the measurement equation (4.1) with respect to **y**. The first term in equation 4.6 relates to the propagation of uncertainties uncorrelated between the observations in the vector **y**. The second term represents the propagation of uncertainties that are correlated between observations, where pairs of observations are denoted by y_i and y_j . Note here that this is textbook notation from the GUM and ‘i’ and ‘j’ do not have the same definitions as those introduced in section 4.2.

Similarly we can apply the equation for the propagation of uncertainty to the case of an averaged product (equation 4.2).

$$u(\langle z \rangle)^2 = \sum_i^n \left(\frac{\partial h}{\partial z_i} \right)^2 u_i^2(z_i) + 2 \sum_{i=1}^{n-1} \sum_{j=i+1}^n \left(\frac{\partial h}{\partial z_i} \right) \left(\frac{\partial h}{\partial z_j} \right) u(z_i z_j) \quad (4.7)$$

In this case, the first term in equation 4.7 relates to the propagation of uncertainties uncorrelated between the retrievals, \mathbf{z} . The second term represents the propagation of uncertainties that are correlated between retrieved values, where pairs of retrieved values are denoted as z_i and z_j .

4.3.1. Introducing matrix notation for propagation of uncertainties: an example for propagating a Level 1 independent error effect for single pixel retrieval

We can use matrix notation to significantly simplify the uncertainty propagation equation. Taking equation 4.6 as the example here, let's consider the propagation of radiance uncertainty (an independent error effect) into a Level 2 per pixel product. The equation for the propagation of uncertainty can be written in matrix notation under the following assumptions [RD-13]:

- Errors in \mathbf{y} propagate linearly into errors in \mathbf{z} , in proportion to the derivative of the function g with respect to \mathbf{y} .
- Independent errors combine in quadrature.

Under these assumptions, equation 4.8 expresses the uncertainty in a single pixel retrieval $u(\mathbf{z})$ from independent errors in \mathbf{y} , as a function of the sensitivity coefficient matrix, \mathbf{C} , and the error covariance matrix, \mathbf{S}_ϵ .

$$u(\mathbf{z}) = \sqrt{\mathbf{C} \mathbf{S}_\epsilon \mathbf{C}^T} \quad (4.8)$$

\mathbf{C} represents the sensitivity of the measurand with respect to the observation vector, \mathbf{y} . This sensitivity coefficient matrix can be expressed in terms of the retrieval function (g) and observation vector (\mathbf{y}).

$$\mathbf{C} = \left[\frac{\partial g}{\partial y_1} \dots \frac{\partial g}{\partial y_n} \right]^T \quad (4.9)$$

In this case, errors are assumed to be independent and uncorrelated between observations in \mathbf{y} . \mathbf{S}_ϵ therefore becomes a diagonal matrix with off-diagonal terms of zero. A more traditional expression of the uncertainty under these conditions, relating back to equation 4.6, is:

$$u(\mathbf{z}) = \sqrt{\sum_i \left(\frac{\partial g}{\partial y_i} u(y_i) \right)^2} \quad (4.10)$$

We can further decompose the error covariance term, \mathbf{S}_ϵ , expressing this in terms of the uncertainty matrix (\mathbf{U}) and the correlation matrix (\mathbf{R}).

$$\mathbf{S}_\epsilon = \mathbf{U} \mathbf{R} \mathbf{U}^T \quad (4.11)$$

The uncertainty matrix, \mathbf{U} , is diagonal, with an uncertainty associated with each term in \mathbf{y} . The off-diagonal terms in the correlation matrix, \mathbf{R} , are equal to zero in this example (and therefore the off-diagonal terms in \mathbf{S}_ϵ are also equal to zero). In this case, \mathbf{R} is the identity matrix \mathbf{I} . We can use equation

4.11 to expand equation 4.8 which gives the uncertainty in the retrieved value for a single pixel, considering only the propagation of radiance uncertainty in the observations, \mathbf{y} .

$$u(z) = \sqrt{\mathbf{C}\mathbf{U}\mathbf{R}\mathbf{U}^T\mathbf{C}^T} \quad (4.12)$$

4.3.2. Considering uncertainty propagation for structured error effects in single pixel retrievals

Considering the ‘CURUC’ notation established in equation 4.12 for the propagation of radiance uncertainty, the same approach can be taken for any error effect. The terms are all fully transferable to structured error effects with the exception of the correlation matrix, \mathbf{R} . When error effects are fully correlated between input vectors (e.g. observations in \mathbf{y}) all terms in \mathbf{R} will be equal to 1. For convenience we define this as the \mathbf{J} matrix where all values are equal to 1. As a result, these error effects have to be treated separately in the propagation of uncertainty (as represented by the second term in equation 4.6).

4.3.3. Relating the matrix notation to the definitions of terms and error effects

It is useful now to link this derivation back to the notation discussed in section 4.2. Equation 4.12 is valid where we consider one single error effect, k , for a single term, j (remembering that term can be a vector, for example the satellite observations, \mathbf{y}). More strictly, this can be written with the appropriate subscripts to represent this.

$$u(z)_k = \sqrt{\mathbf{C}_j\mathbf{U}_k\mathbf{R}_k\mathbf{U}_k^T\mathbf{C}_j^T} \quad (4.13)$$

The sensitivity coefficient matrix, \mathbf{C} , is dependent on the term, j , whilst the uncertainty and correlation matrices (\mathbf{U} and \mathbf{R}) are defined for the effect, k . In the case where the total uncertainty in z is comprised of a number of error effects, k , relating to different terms, j , (as exemplified in Table 3), we can define the full error covariance matrix for all of the effects k .

$$u(z) = \sqrt{\sum_j \sum_{k|j} \mathbf{C}_j\mathbf{U}_k\mathbf{R}_k\mathbf{U}_k^T\mathbf{C}_j^T} \quad (4.14)$$

Here $u(z)$ is the total uncertainty from all of the contributing error effects (arising from terms in the \mathbf{y} vector in the measurement equation).

The calculation is a sum over all of the effects, k , within all of the terms, j (which include the observations, \mathbf{y}). Therefore, the uncertainty and correlation matrices do not average over effects and the sensitivity coefficient matrix does not average over terms. This means that each error effect, k , affecting each term, j , can have a unique correlation matrix \mathbf{R} . A similar process could also be undertaken with the terms in the $\boldsymbol{\beta}$ matrix, to derive the uncertainty in the retrieved variable, z , from the parameters used in the function, g .

Having calculated the uncertainties associated with each error effect, it is then helpful to group them according to spatial correlation scale (independent, locally systematic (structured) and large-scale systematic (common)). This ensures that the different error sources can be properly propagated into higher-level data. Note that as shown in Figure 4-1, some uncertainties at Level 2 may be propagated

	End-To-End ECV Uncertainty Budget <i>WP2.5– DEL-2.3</i>	Ref.: LST-CCI-D2.3-E3UB Version: 2.0 Date: 26-Nov-2021 Page: 14
---	---	--

from Level 1 data whilst others may be introduced at Level 2 (e.g. uncertainties associated with the retrieval process).

4.3.4. Propagation of uncertainties in averaged products

As the processing level increases, the data are typically provided at coarser resolutions (e.g. regularly gridded products as opposed to datasets on the satellite image grid), usually because these are the data formats that users can most easily exploit. Generation of data at higher levels typically involves averaging of higher resolution data (either spatially or temporally). Consider the case where we propagate uncertainties into an averaged product (eg. equation 4.7), the total uncertainty on the average value can be expressed as:

$$u(\langle z \rangle) = \sqrt{\mathbf{C} \mathbf{S}_\varepsilon \mathbf{C}^T} \quad (4.15)$$

In this case the sensitivity coefficients are now the derivative of h with respect to the retrieved values, \mathbf{z} , which contribute to the average.

$$\mathbf{C} = \left[\frac{\partial h}{\partial z_1} \dots \frac{\partial h}{\partial z_n} \right]^T \quad (4.16)$$

\mathbf{S}_ε is the error covariance matrix of the pixels, \mathbf{z} , being averaged. The propagation methodology in this averaging process is dependent on the correlation length scale of the uncertainty component. In the simplest case, where the errors in each retrieved pixel are independent, when calculating the average the total uncertainty is reduced by a factor of $1/\sqrt{n}$. This is under the assumption that the errors have a Gaussian distribution (zero mean), and will on average cancel out as the sample size increases. The opposing case is when the errors in each retrieved pixel are fully correlated. Under these conditions the uncertainty is essentially the ‘average uncertainty’ of all contributing points (i.e. these uncertainties do not reduce on averaging).

It is also possible for the correlation to vary as a function of the spatial or temporal separation of the retrieved pixels. The construction of the error covariance as the product $\mathbf{U} \mathbf{R} \mathbf{U}^T$ allows the appropriate correlation matrix to be used in these cases.

Let us consider the construction of the uncertainty budget for a Level 3 product. We separate the error effects into independent (i), structured (s) and common (c) groupings, considering j uncertainty inputs into the uncertainty calculation (from j L2 observations). On this basis we can define three uncertainty components, $u(\langle z \rangle)_i$, $u(\langle z \rangle)_s$ and $u(\langle z \rangle)_c$. We construct this equation, as it would be applied within LST_cci; the uncorrelated and common uncertainty components are propagated using a single value per pixel as provided with the Level 2 data. The structured uncertainties have an additional summation as two locally systematic uncertainties are provided with LST_cci Level 2 data.

$$u(\langle z \rangle)_i^2 = \sum_j \mathbf{C} \mathbf{S}_i \mathbf{C}^T \quad (4.17)$$

$$u(\langle z \rangle)_s^2 = \sum_j \mathbf{C} \left(\sum_{k|s} \mathbf{U}_s \mathbf{R}_s \mathbf{U}_s^T \right) \mathbf{C}^T \quad (4.18)$$

$$u(\langle z \rangle)_c^2 = \sum_j \mathbf{C} \mathbf{S}_c \mathbf{C}^T \quad (4.19)$$

As the uncertainty components are additive, these can be combined in a single equation to give a total uncertainty for an averaged product. Note that the part of the equation that is dependent on the correlation length scale of the uncertainty component is \mathbf{R} , the correlation matrix. The \mathbf{URU}^T products for each component (independent, locally-systematic (atmosphere and surface), and large-scale systematic) can be added inside the multiplication by the sensitivity matrix, \mathbf{C} .

$$u(\langle z \rangle)^2 = \sum_j \mathbf{C}_j \left(\mathbf{U}_i \mathbf{R}_i \mathbf{U}_i^T + \sum_{k|s} \mathbf{U}_s \mathbf{R}_s \mathbf{U}_s^T + \mathbf{U}_c \mathbf{R}_c \mathbf{U}_c^T \right) \mathbf{C}_j^T \quad (4.20)$$

4.4. Reviewing the matrix notation for uncertainty propagation

The previous sections have introduced both new language and notation for the expression and propagation of uncertainties. In this section we summarise these concepts in tables that can be easily referenced within the LST_cci project. Considering first the framework we outline for defining an uncertainty budget, we define the key terminology for this in Table 4.

Concept	Definition
Measurement Equation	The equation that defines how to calculate the desired quantity e.g. A single pixel retrieval or gridded average.
Terms	The quantities used within the measurement equation.
Observations	The input quantities in the measurement equation e.g. brightness temperatures for single pixel retrievals or retrieved values for the calculation of averaged products.
Parameters	Information used in the measurement equation in addition to the input values.
Error effects	A single source of error, affecting a single term in the measurement equation.
Correlation length scale:	Separation of uncertainty components on the basis of spatial correlation:
i. Independent ('random uncertainty')	i. no correlation between input values
ii. Structured ('locally systematic uncertainty')	ii. local correlation between input values
iii. Common ('large scale uncertainty')	iii. large-scale correlation between input values
Uncertainty budget	Statement of a measurement uncertainty, of the components of that measurement uncertainty, and of their calculation and combination [RD-2].

Table 4: Summary of terminology used in constructing an uncertainty budget.

Matrix notation is presented as a way of simplifying the equations for the propagation of uncertainty. The matrices used in these equations are defined in Table 5.

Matrix/Vector	Definition
C	Sensitivity matrix – matrix of sensitivity coefficients, non-square and filled in the contexts discussed in this document.
S_ε	Error covariance matrix – measurand covariance matrix
U	Uncertainty matrix – diagonal matrix of standard uncertainties relevant to a multi-variate measurand. If indexed with respect to k this refers to the uncertainty matrix for a particular effect.
R	Error correlation matrix – matrix of correlations of errors in a vector variable. If indexed with respect to k this refers to the error correlation matrix for a particular effect.
y	Vector of observations used as input to a single pixel retrieval.
z	Vector of single pixel retrievals used as input to an averaged product.
β	Vector of parameters used in the single pixel retrieval measurement equation.
γ	Vector of parameters used in the averaged product measurement equation.
I	Identity matrix
J	Matrix of ones

Table 5: Definition of matrix notation introduced in section 4.3 (in part specified from RD-14)).

In relation to the matrix notation described in this section and measurement equation construction, a number of variables have been defined, some used in equations and some as indices. These, along with their definition are summarised in Table 7. A few additional indices are included here for completeness (e.g. ‘p’ for pixel).

Index	Definition
k	A single error effect
j	A single term in the measurement equation
p	Denotes ‘pixel’, used to specify cross-pixel matrices
i	Independent error effect (spatially uncorrelated)
s	Structured error effect (locally spatially correlated)
c	Common error effect (spatially correlated over large scales)
z	Retrieved value (single pixel)
⟨z⟩	Averaged value (from sample of single pixel retrievals from one or more sensors)
g	Function for retrieving single pixel values
h	Function for retrieving averaged products

Table 6: Definition of variables and notation introduced in sections 4.1-4.3.

4.5. Combining uncertainty components

Components of the uncertainty budget grouped according to the correlation length scale of the contributing error sources (uncorrelated, locally systematic or large-scale systematic) can be combined in quadrature to give a total uncertainty for the measurement. Mathematically this can be expressed as follows, where u denotes uncertainty and subscripts 'i', 's', and 'c' refer to independent (random), locally systematic, and large-scale uncertainties respectively.

$$u = \sqrt{u_i^2 + u_s^2 + u_c^2} \quad (4.21)$$

4.6. Propagation of uncertainties to Level 4 products

Level 4 products are at the top of the satellite processing chain, usually consisting of blended, gap-filled datasets. LST_cci as a project will only provide products at levels 2 and 3. Therefore the propagation of these uncertainties to level 4 products is not considered here, but this note is included for completeness.

5. Constructing an Uncertainty Budget

Within the sea surface temperature (SST) climate change initiative project (CCI), a framework was established for calculating an uncertainty budget for SST retrievals [RD-6]. This approach has since been adopted within the land surface temperature and lake surface water temperature communities through the ESA DUE GlobTemperature and Horizon 2020 EU Surface Temperature for All Corners of Earth (EUSTACE) projects [RD-7, RD-8]. In LST_cci we build upon the approach taken in GlobTemperature, applying this to LST's from a wider range of instruments and improving consistency in how we calculate and present uncertainty information to users. In this section we focus on the instruments used to construct the climate data record (CDR) from polar orbiting sensors.

5.1. ATSR-2, AATSR and SLSTR

Within the single sensor climate data record, three of the instruments used share the same heritage; the (Advanced) Along Track Scanning Radiometers (ATSR-2 and AATSR) and the Sea and Land Surface Temperature Radiometer (SLSTR). These are dual-view instruments, all designed to measure surface temperature, and fly in sun-synchronous polar orbits with an equator overpass time of 10 or 10.30 am. The main characteristics of these instruments are presented in Table 8. These instruments have a relatively narrow swath, with nadir viewing angles between 0-23 degrees. Each instrument also has an oblique view at 52-55 degrees, in the forward direction for ATSR-2 and AATSR, and in the backward direction for SLSTR. The objective of the dual-view instrument was to facilitate surface temperature retrieval by better characterising atmospheric effects, using the two views, and this has proven very useful in sea surface temperature retrieval [eg. RD-11]. For LST retrieval, using two views becomes increasingly complex (although not impossible) due to the surface orography and directional effects of emitted and reflected radiance [RD-12], so nadir-view only retrievals are employed here.

Instrument	Channels (μm)	Availability	Equator Overpass Time
ATSR-2	0.55, 0.67, 0.87, 1.6, 3.7, 10.8, 12	Restricted telemetry results in reduced availability of visible channels and transmission swapping between the 1.6 and 3.7 μm channels. Ground segment problems lead to a data gap over part of Asia.	10:30, 22:30
AATSR	0.55, 0.67, 0.87, 1.6, 3.7, 10.8, 12	All channels available	10:00, 22:00
SLSTR	0.55, 0.66, 0.87, 1.38, 1.61, 2.25, 3.7, 10.85, 12 (plus two fire channels, 3.7 and 10.85).	All channels available	10:00, 22:00

Table 7: Instrument characteristics for ATSR-2, AATSR and SLSTR.

Given the commonality in design and orbit between this series of instruments, we apply a consistent LST retrieval methodology to these sensors and construct the uncertainty budget associated with this retrieval in the same way. In order to bridge the gap between the in-orbit communications failure of Envisat in April 2012 and the routine provision of data from SLSTR in 2016 (launched in February 2016) we use the Moderate Resolution Imaging Spectroradiometer (MODIS) Terra instrument. This

instrument is sufficiently different in its characteristics to the ATSRs that we apply a different retrieval scheme in this case for single sensor and merged products, and as our measurement equation is different we construct our uncertainty budget in a different way. Within the CDR, a consistent LST retrieval algorithm is applied to all algorithms. In this section we will describe the uncertainty budget for the ATSR-2, AATSR and SLSTR retrievals (used also for the full CDR including MODIS), and consider the MODIS single-sensor data record uncertainty budget separately (Section 5.2).

5.1.1. Land Surface Temperature Retrieval

The LST retrieval applied to the ATSR-2, AATSR and SLSTR sensors is a split window algorithm developed by F. Prata [RD-23] and modified for use in this context by the University of Leicester [RD-7]. It differs from the generalized split window approach due to non-explicit dependence on surface emissivity, as emissivity is included in the coefficient fitting process [RD-7]. The measurement equation (5.1) is dependent on brightness temperatures in two infrared channels; one at 10.8 μm (T_{11}) and one at 12 μm (T_{12}).

$$LST = a_{f,i,tcwv} + b_{f,i}(T_{11} - T_{12})^n + (b_{f,i} + c_{f,i})T_{12} \quad (5.1)$$

'a', 'b' and 'c' are the retrieval coefficients which have dependencies on fractional vegetation cover (f), biome (i) and total column water vapour (tcwv). Relating this back to equation 4.1, z is the retrieved LST, \mathbf{y} are the observations (T_{11} and T_{12}) and β the retrieval coefficients; a, b and c.

The variable n is related to the satellite zenith view angle (θ) via a parameter m. This introduces a weak non-linearity in the brightness temperature difference between T_{11} and T_{12} as this difference is dependent on the total column water vapour. T_{12} has greater attenuation as function of water vapour than T_{11} , which is important because the atmospheric path length of the retrieval increases with satellite zenith angle [RD-7].

$$n = \frac{1}{\cos(\theta/m)} \quad (5.2)$$

The coefficients are also dependent on the satellite zenith angle and time of day (partitioned into day/night). Each coefficient is constructed from two components with subscripts 'v' for 'fully-vegetated' and 's' for 'bare soil' corresponding to f=1 and f=0 respectively. Each coefficient component ('v' and 's') is determined as a function of biome and time of day (as in equations 4.3-4.5).

$$a_{f,i,pw} = d(\sec(\theta) - 1)tcwv + fa_{v,i} + (1 - f)a_{s,i} \quad (5.3)$$

$$b_{f,i} = fb_{v,i} + (1 - f)b_{s,i} \quad (5.4)$$

$$c_{f,i} = fc_{v,i} + (1 - f)c_{s,i} \quad (5.5)$$

The derivation of coefficient 'a' is also dependent on a fourth coefficient 'd', which accounts for changes in atmospheric attenuation of water vapour in both channels due to the increase in atmospheric path length at higher satellite zenith angles [RD-7]. Coefficient 'd' is also dependent on biome and time of day. 'd' is determined with regression from the radiative transfer modelling under different viewing zenith angles.

Given the definition of the measurement equation for single pixel retrieval (equation 5.1), the error effects associated with each of the terms in this equation can be determined. It won't necessarily be

possible to quantify all of these effects within the uncertainty budget at present, but it provides a good indication of how far we can currently go in characterising uncertainties in LST retrieval. A breakdown of the error effects for each of the terms in the measurement equation is provided in Table 9. The measurement terms in the first column relate back to the specification of the measurement equation for single pixel retrievals in 4.1 where $z = g(\mathbf{y}, \boldsymbol{\beta})$.

Measurement term	Normal notation	Effect	Effects expected	Correlation length scale	Attributed uncertainties	Sensitivity
$\boldsymbol{\beta}$	a	1	Fractional vegetation error	s	FCOVER uncertainty	$\frac{\partial g}{\partial f}$
		2	Fitting error (atmospheric and emissivity)	s	Fitting residual	*
		3	Total column water vapour error	s	Ensemble spread of total column water vapour	$\frac{\partial g}{\partial tcwv}$
	b	4	Fractional vegetation error	s	FCOVER uncertainty	$\frac{\partial g}{\partial f}$
		5	Fitting error (atmospheric and emissivity)	s	Fitting residual	*
	c	6	Fractional vegetation error	s	FCOVER uncertainty	$\frac{\partial g}{\partial f}$
		7	Fitting error (atmospheric and emissivity)	s	Fitting residual	*
\mathbf{y}	T_{11}	8	Noise	i	0.05 K	$\frac{\partial g}{\partial T_{11}}$
		9	Calibration error	c	Not attributed	$\frac{\partial g}{\partial T_{11}}$
	T_{12}	10	Noise	i	0.05 K	$\frac{\partial g}{\partial T_{12}}$
		11	Calibration error	c	Not attributed	$\frac{\partial g}{\partial T_{12}}$

+ 0	Geolocation	12	Correction of known geolocation mismatch	s	Delta LST weighted by biome classification in neighbouring pixels	*
		13	Re-projection of native instrument grid to image grid	s		
	Cloud Detection	14	Undetected cloud	s	Not attributed	*
	RTM	15	Error in RTM simulation (trace gas profiles, parameterisation).	c	0.03 K	$\frac{\partial g}{\partial T_{11}}$
	NWP	16	Error in RTM inputs (surface temperature and total column water vapour).	c		$\frac{\partial g}{\partial T_{12}}$

Table 8: Error effects for single pixel LST retrieval. Effects are categorised according to the measurement equation term. Where quantified, the values propagated for each effect are specified for AATSr. *denotes cases where the uncertainty is modelled rather than propagated using a sensitivity coefficient.

From Table 9 we can see that there are 7 error effects associated with the parameter vector, β . The parameter vector contains three coefficients, ‘a’, ‘b’ and ‘c’. Each coefficient has a dependence on the fractional vegetation cover and the radiative transfer model (RTM) simulations used to calculate the coefficients. Both of these errors are explicitly specified in the uncertainty budget, one by calculating the sensitivity of the retrieval to the fractional vegetation cover, and the other using the residuals from the retrieval fitting process. Coefficient ‘a’ has a further error effect associated with it, as it is directly reliant on the total column water vapour (TCWV) quantification. The TCWV uncertainty is estimated via the ensemble spread of the Numerical Weather Prediction model used to provide the atmospheric data.

The observation vector, \mathbf{y} , containing the brightness temperatures T_{11} and T_{12} , has four associated error effects. Two of these are related to instrument noise, which is specified individually for each channel. This is propagated through the retrieval equation according to the sensitivity of the retrieved quantity to the observations. The other two are related to instrument calibration of each channel and these are not quantified in the uncertainty budget as the information is not provided with the L1 data.

The ‘+0’ term contains any error effects not explicitly related to the observation or parameter vectors. Five additional error effects fall into this category. First there are geolocation errors. These are decomposed into two error effects; 1) error in the correction of a known geolocation mismatch, and 2) error in the re-projection from the native instrument grid to the image grid [RD-7]. Both are quantified within the uncertainty budget. Two other error effects arise from the RTM simulation; 1) errors in the model parameterisation and 2) errors in the boundary conditions (e.g. input numerical weather prediction fields including surface temperature and total column water vapour). These are error effects with a structure common across all retrievals and are characterised in the uncertainty budget together. The parameterisation used here is calculated with reference to sea surface temperature retrievals [RD-15], where the surface conditions are more uniform and stable than over land, so this is likely to be an underestimate of the true value when applied to land surface temperature retrievals. The last error

effect is the result of cloud detection errors. If a cloud is undetected in a retrieval, it has the potential to affect the retrieved surface temperature (often biasing this cold). At present this error effect is not quantified within the uncertainty budget.

In the next sections we describe in detail the error effects that we can propagate through the measurement equation to provide an uncertainty budget with our single pixel retrieval (sections 5.1.2 and 5.1.3). The measurement equation for averaged products is considered separately in section 5.1.4.

5.1.2. Level 1 data

Level 1 data that are used to retrieve Level 2 geophysical variables (e.g. LST) have an associated uncertainty comprised of error effects that arise from the instrument characteristics and measurement process. Constructing an uncertainty budget for Level 1 data requires detailed knowledge of the instrument and in-orbit characteristics, and to make the propagation of such information into a geophysical retrieval feasible, these uncertainties should be provided with the Level 1 data themselves [RD-13]. In the absence of a rigorous expression of the uncertainties in Level 1 data, we can propagate only the information that is routinely provided with the data into our geophysical retrieval.

5.1.2.1. Uncertainties due to random error effects

One source of uncertainty due to a random error effect in Level 1 data is instrument noise (effects 8 and 10 in Table 9). Each of the channels \mathbf{y} (T_{11} and T_{12}) used in the LST retrieval has an associated instrument noise, and this is propagated through the retrieval equation to calculate the uncertainty due to noise in the retrieved LST.

In this case, the sensitivity coefficient matrix, \mathbf{C} , (equation 4.9) becomes:

$$\mathbf{C} = \begin{bmatrix} \frac{\partial g}{\partial T_{11}} & \frac{\partial g}{\partial T_{12}} \end{bmatrix} \quad (5.6)$$

where:

$$\frac{\partial g}{\partial T_{11}} = \frac{\partial LST}{\partial T_{11}} = nb_{f,i}(T_{11} - T_{12})^{n-1} \quad (5.7)$$

$$\frac{\partial g}{\partial T_{12}} = \frac{\partial LST}{\partial T_{12}} = (-1)nb_{f,i}(T_{11} - T_{12})^{n-1} + (b_{f,i} + c_{f,i}) \quad (5.8)$$

The error correlation matrix, \mathbf{S}_ϵ , is diagonal with each non-zero element representing the variance due to instrument noise in each channel. At present this is specified as the square of the prescribed noise equivalent delta temperature (NEdT) at 300 K for each channel (T_{11} and T_{12}) given in the instrument specification. The values used for each instrument are detailed in Table 10.

Instrument	Variance T_{11} NEdT	Variance T_{12} NEdT
ATSR-2	$(0.036)^2$	$(0.034)^2$
AATSR	$(0.033)^2$	$(0.034)^2$
SLSTR A	$(0.011)^2$	$(0.017)^2$
SLSTR B	$(0.014)^2$	$(0.016)^2$

Table 9: T_{11} and T_{12} diagonal elements in the S_e matrix for the ATSR-2, AATSR [RD-25] and SLSTR [RD-26, RD-27] instruments.

5.1.3. Level 2 data

Level 2 data are the retrieved geophysical variable, z , in this case LST. As illustrated in Figure 4:1, each level of data processing introduces new sources of error that should be quantified within the uncertainty budget for the data product. In this section, the error sources introduced in the retrieval process and the corresponding uncertainty parameterisation are described.

5.1.3.1. Uncertainties due to locally systematic error effects

5.1.3.1.1 Uncertainty due to fractional vegetation cover

The LST retrieval (equation 5.1) is dependent on the specification of the surface fractional vegetation cover in the calculation of the retrieval coefficients (equations 5.3-5.5). Within the retrieval, fractional vegetation cover is specified using the Copernicus Global Land Services FCOVER dataset [RD-16, RD-17]. This product is available globally at a 1/112 degree resolution, close to the desired 1 km resolution of the ATSR and SLSTR sensor observations. The fractional vegetation cover used within the retrieval is matched to the satellite observations using a nearest neighbour approach [RD-7]. The fractional vegetation cover product provides an uncertainty on a per datum basis, using a theoretical model based on the residuals in a comparison against a validation dataset [RD-18].

For this uncertainty (effects 1, 4 and 6 in Table 9), the sensitivity coefficient matrix, \mathbf{C} , consists of the differential of the LST retrieval equation with respect to fractional vegetation cover (f).

$$\mathbf{C} = \left[\frac{\partial g}{\partial f} \right] \quad (5.9)$$

The differential can be calculated using equations 5.3, 5.4 and 5.5, where the retrieval coefficients, 'a', 'b' and 'c' are defined with respect to fractional vegetation cover (f), in the retrieval equation (5.1).

$$\frac{\partial g}{\partial f} = \frac{\partial LST}{\partial f} = (a_{v,i} - a_{s,i}) + (b_{v,i} - b_{s,i})(T_{11} - T_{12})^n + ((b_{v,i} - b_{s,i}) + (c_{v,i} - c_{s,i}))T_{12} \quad (5.10)$$

The uncertainty matrix, \mathbf{U} , is a single value, comprising of the uncertainty specified for the FCOVER dataset. This error effect is not channel dependent.

5.1.3.1.2 Uncertainty due to total column water vapour

The retrieval algorithm (equation 5.1) is also dependent on the specification of the total column water vapour in the calculation of one of the retrieval coefficients (equation 5.3). The TCWV estimate at a given instant and location is obtained from Numerical Weather Prediction (NWP) models. A commonly used measure of uncertainty in NWP models is the ensemble spread that is generally available together with the variable best estimate. The ensemble systems consist of a set of model runs with perturbed initial conditions; some systems also include perturbations to the model physics, more than one model within the ensemble or different physical parameterisation schemes [RD-45]. Processing of ensemble data can be quite demanding, and therefore we currently approximate the instantaneous TCWV spread to a climatology of this spread that depends on actual TCWV, latitude and month.

Here the sensitivity coefficient matrix, \mathbf{C} , consists of the differential of the retrieval equation with respect to total column water vapour (TCWV).

$$\mathbf{C} = \left[\frac{\partial g}{\partial tcwv} \right] \quad (5.11)$$

The differential can be calculated using equation 5.3, since only the retrieval coefficient ‘a’ is defined with respect to TCWV in the retrieval equation.

$$\frac{\partial g}{\partial tcwv} = \frac{\partial LST}{\partial tcwv} = d(\sec(\theta) - 1) \quad (5.12)$$

The uncertainty matrix, \mathbf{U} , is a single value, comprising the value obtained from the TCWV LUT based on TCWV, latitude and month. This error effect is not channel dependent.

5.1.3.1.3 Uncertainty due to geolocation

Uncertainties due to geolocation (error effects 12 and 13 in Table 9), fall into two categories [RD-7]:

- i. Errors in the correction of the known geolocation offset
- ii. Errors in the re-projection of the satellite data from the native grid to the image grid.

The uncertainty in the geolocation is estimated to be 0.5 km [RD-19], and this is propagated into the LST retrieval by calculating the probability that the biome assigned to a given 1km pixel (when matching the observations and GlobCover dataset) is correct [RD-7]. To do this requires analysis of the eight pixels surrounding the pixel for which the retrieval is being made (a 3x3 pixel block centred on the retrieved pixel). For each of these pixels the delta LST is calculated in response to the specified biome (whilst observations, atmospheric and radiative transfer components remain constant). Therefore if the biome in one of the surrounding pixels is the same as that assigned to the central pixel, the delta LST for this pixel will be zero.

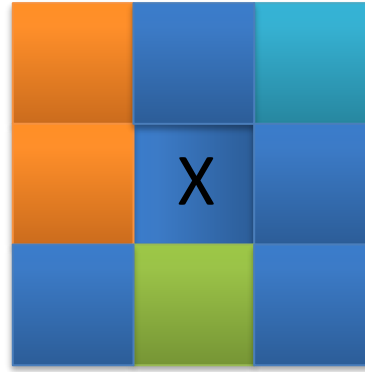


Figure 5-1: Example of pixel selection for calculating geolocation uncertainty. The retrieval is made for the central pixel (marked with an X), and the delta LST is calculated for the eight surrounding pixels. The retrieval for all pixels is consistent with the exception of the biome specification (indicated by the different colours).

The Haversine function is used to calculate the distance between each of the surrounding pixels (p_n) and the central pixel (c) (equations 5.13 – 5.15). Please note that this definition uses constants a , c and d which are not consistent with the ones defined above (this is a self-contained derivation).

$$d = earth_{radius} * c \quad (5.13)$$

$$c = 2 * \arctan(\sqrt{a}, \sqrt{1-a}) \quad (5.14)$$

$$a = \sin^2\left(\frac{\varphi_c - \varphi_{p_n}}{2}\right) + \cos(\varphi_c) * \cos(\varphi_{p_n}) * \sin^2\left(\frac{\lambda_c - \lambda_{p_n}}{2}\right) \quad (5.15)$$

The mean radius of the Earth is 6,371 km. φ_c is the latitude of the central pixel, and φ_{p_n} the latitude of the pixel to which the distance is being calculated. Here the subscript 'c' denotes 'centre' and the subscript 'p_n' the nth pixel. Similarly, λ_c and λ_{p_n} denote the longitude of the central pixel and the one to which the distance is calculated respectively. Each of the eight surrounding pixels (1 to n) are assigned a weight (w), which is used in the calculation of geolocation uncertainty.

$$w_n = \frac{1}{d_n^2} \quad (5.16)$$

The geolocation uncertainty (u_g) is specified as:

$$u_g = \sum \frac{w_n * \Delta LST_n}{\sum w} \quad (5.17)$$

Where ΔLST_n is the LST delta for each pixel (n) and $\sum w$ is the sum over all of the weights. The ΔLST calculated between each biome 'pair' is stored in a look-up table, which is read during the retrieval.

5.1.3.1.4 Uncertainty due to coefficient fitting (atmospheric effects)

The uncertainty due to coefficient fitting (error effects 2, 5 and 7 in Table 9) arises primarily from limitations in the model structure in fully representing the physical system (in this case, the radiative transfer between TOA and surface). Part of this uncertainty will also be associated with errors in the atmospheric state (dominated by the specification of the water vapour column) and errors in the surface emissivity, used within the radiative transfer model simulations to derive the retrieval

coefficients. The combined uncertainties from these components can be estimated empirically using the residuals from the fitting process. The uncertainties are derived as the standard deviation (σ) of the double differences between the retrieved and input surface temperatures [RD-7].

$$\sigma = \sqrt{\frac{\sum(x - \bar{x})^2}{n}} \quad (5.18)$$

Where
$$x = (LST_{sim} - LST_{ret}) - (LST_{sim} - LST_{NWP}) \quad (5.19)$$

The double difference is defined in equation 5.19 where the subscripts ‘sim,’ ‘ret,’ and ‘NWP’ denote simulated, retrieved and input (numerical weather prediction) surface temperatures respectively. The standard deviations are calculated as a function of biome, day/night, water vapour and satellite viewing angle. The binning resolution for each of these factors is provided in Table 10., with the resolution chosen to adequately capture the dependence on these factors. More information on the specification of the look-up tables used in the code is provided in Section 6.

Fitting uncertainty dependence	Binning resolution
Biome	Biome
Day/night	90 degrees solar zenith angle
Water vapour	Not banded by TCWV
Satellite viewing angle	5 degrees

Table 10: Binning resolution of the factors used to define the coefficient fitting uncertainty.

5.1.3.2. Uncertainties due to large-scale systematic error effects

Large-scale systematic uncertainties are correlated over long spatio-temporal scales, for example over the lifetime of an instrument. Two sources of large-scale uncertainty include [RD-7]:

1. Uncertainty in the calibration of the measuring instrument.
2. Uncertainty in the radiative transfer modelling used to simulate radiances in the retrieval coefficient derivation.

The uncertainty (1) is what remains following the correction of any known bias in the data. At present, these uncertainties are assumed to be negligible in the absence of more detailed information from the data producer. The uncertainty (2) can be estimated by assessing the sensitivity of the radiative transfer model to perturbations in the input data. Following RD-15, the radiative transfer modelling is found to be consistent to within 0.03 K for the 11 μm channel over ocean, and this value (although likely to be an underestimation over land) is used for both T_{11} and T_{12} .

The uncertainty is propagated using the sensitivity matrix with respect to the observation vector, \mathbf{y} , which is described by equations 5.6-5.8.

5.1.3.3. Correlation length scales of Level 2 uncertainty components

At Level 2, the contributing uncertainty components are grouped according to their spatial correlations to facilitate correct propagation to higher data levels. The correlation length scales of all the error effects discussed in this section and included in the uncertainty budget are summarised in Table 11.

Error effect	Correlation length scale
Instrument noise	Uncorrelated
Fractional vegetation cover	Biome dependent
Geolocation	Biome dependent
Atmospheric fitting	5 km / 5 minutes [RD-28, RD-29]
Radiative Transfer Modelling	Instrument record

Table 11: Correlation length scales for the error effects characterised in Level 2 data.

For the purposes of data distribution, at Level 2, four uncertainty components are provided (see Section 9). These are comprised of uncorrelated (random) uncertainty, large-scale systematic uncertainty and two locally systematic uncertainty components: surface and atmosphere. The surface component includes the fractional vegetation cover and geolocation uncertainties whilst the atmospheric component includes the atmospheric fitting uncertainty.

For the locally systematic atmospheric uncertainty component, the spatial and temporal correlation length scales are currently assumed to be 5 km and 5 minutes respectively [RD-28, RD-29]. These correlation length scales differ to those used over the ocean for sea surface temperature retrieval (100 km and 1 day). The values used over land are taken from the literature [RD-28, RD-29] and more localised metrological conditions can exist over the land than over the ocean. However, given the nature of weather systems, which develop on synoptic timescales, these correlation length scales may be too short, even at mid-latitudes. An in-depth study of the most appropriate correlation length scales for this application is recommended for Phase II of LST CCI. It is possible that correlation length scales need to vary latitudinally or longitudinally.

Updating the correlation length scales for the atmospheric uncertainty component would impact the generation of Level 3 products. Increasing the spatial length scale would require this component to be propagated as a systematic uncertainty over a larger area, which would need to be considered when generating coarser resolution products. Increasing the temporal correlation length scale would impact the L3C and L3S generation methodology, as LST retrievals close in time would have correlated atmospheric uncertainties.

5.1.4. Level 3 data

Level 3 products are those where data are placed onto a common grid at 0.01 or 0.05-degree resolution. Three types of Level 3 products can be produced in any given processing chain: 1) L3U – these are ‘uncollated’ products, where a single L2 orbit or full disk observation is placed on a regular latitude-longitude grid. 2) L3C – these are ‘collated’ products, where two or more orbits/disks are combined from the same instrument. 3) L3S – these are ‘synthesised’ products, which combine L3 data from two or more sensors.

The LST value within any given grid box is typically calculated as the arithmetic mean of all LST retrievals that fall within the geographical limits of the box (up to 25 for ~1km data gridded at 0.05-degree resolution). For the 0.01 resolution data, typically only 1-2 pixels fall into any given grid cell, sometimes with fractions of pixels overlapping the defined bounds of the cell. In this case the partially overlapping observations are also averaged, weighted by their fractions. Similarly, the uncertainties are propagated following the methodology described here, but weighted by their fraction.

$$LST_{grid} = \frac{1}{n} \sum_{i=1}^n LST_i \tag{5.20}$$

We can use the form of the measurement equation given in 4.2, $\langle z \rangle = g(\mathbf{z}, \boldsymbol{\gamma})$, along with equation 5.20 to define the error effects associated with the averaged LST product. These are shown in Table 13.

Measurement term	Normal notation	Effect	Effects expected	Correlation length scale	Attributed uncertainties	Sensitivity
\mathbf{z}	z_n	1	LST noise	i	Quantified at L2	$\frac{\partial h}{\partial z}$
		2	Retrieval error– surface effects (fractional vegetation, geolocation).	s	Quantified at L2	$\frac{\partial h}{\partial z}$
		3	Retrieval error – atmospheric effects (coefficient fitting).	s	Quantified at L2	$\frac{\partial h}{\partial z}$
		4	RTM and NWP simulation error	c	Quantified at L2	$\frac{\partial h}{\partial z}$
		5	Cloud Detection	s	Not attributed	*
$\boldsymbol{\gamma}$	Weighting	6	Weighting of retrieved pixels contributing to averaged product	s	0	*
+0	Sampling uncertainty	7	Clear-sky pixel representivity of LST across gridded domain	s	Modelled	*

Table 12: Error effects for averaging LST products. Effects are categorised according to the measurement equation term. Where quantified, the values propagated for each effect are specified. *denotes cases where the uncertainty is modelled rather than propagated using a sensitivity coefficient.

At Level 3, there are five error effects associated with the single pixel input vector, \mathbf{z} . These consist of four uncertainties that are quantified in the Level 2 data that can be propagated into the gridded product (instrument noise, retrieval uncertainty from surface effects, retrieval uncertainty from atmospheric effects and the RTM/NWP simulation uncertainty). One further effect (5 in Table 13) from cloud detection error is not quantified within the Level 2 data.

There is one error effect associated with the measurement equation parameters, \mathbf{v} , which is the weighting associated with the LST retrievals contributing to the gridded average. There are two options available for calculating the mean:

- i. A simple arithmetic mean with equal weight given to each contributing LST estimate (currently used).
- ii. A weighted mean reflecting the difference in the uncertainties associated with each contributing LST estimate.

An argument can be made for either approach as follows:

- i. If significant LST variability were expected across the 0.05-degree cell, the first approach would ensure that all contributing LST estimates are evenly represented in the average.
- ii. If minimum uncertainty in the LST estimate across the 0.05-degree domain is required, assuming that LST variability across the cell is negligible then the 25 LST estimates are essentially repeated measurements of the same LST.

For LST, it is likely that (i) may be the best approach in heterogeneous regions where the biome varies rapidly, but (ii) may be more appropriate in regions where the land cover is more homogeneous. Applying a weighting (as in option ii) would result in another source of error that should be quantified in the uncertainty budget. Using option 1 gives the same weight to all pixels and the attributed uncertainty from this approach is zero. This is the approach currently used.

At Level 3 the '+0' term includes the sampling uncertainty [RD-9] introduced when a gridded domain is not fully observed due to the limitation of having clear-sky observations only (for infrared LST retrievals).

5.1.4.1. Propagated Uncertainties

There are four uncertainty components in Level 2 data that are propagated into Level 3 data; uncorrelated (random) uncertainty, locally systematic surface parameter uncertainty, locally systematic atmospheric uncertainty and large-scale systematic uncertainty. When propagating the locally systematic uncertainty components from Level 2 to Level 3, the correlation length scales of the surface and atmosphere components differ and these have to be propagated independently. In this section we describe the propagation for each component.

5.1.4.1.1 Uncorrelated (random) uncertainties

The sensitivity coefficient for the propagation of uncertainty in \mathbf{z} into $\langle z \rangle$ is the derivative of the measurement function with respect to \mathbf{z} . This is consistent across all of the uncertainty components.

$$\mathbf{C} = \left[\frac{\partial h}{\partial z_1} \dots \frac{\partial h}{\partial z_n} \right] \quad (5.21)$$

The uncorrelated (random) uncertainty component is provided for each LST retrieval at Level 2 and the \mathbf{R} matrix is the identity matrix, \mathbf{I} , as these uncertainties are uncorrelated between pixels. The sensitivity coefficient is obtained by differentiating h with respect to \mathbf{z} , resulting in an uncertainty scaled by the familiar $1/\sqrt{n}$ (equation 5.20).

$$\frac{\partial h}{\partial z} = \frac{1}{n} \quad (5.22)$$

$$u(\langle z \rangle)_i = \frac{1}{\sqrt{n}} \sum_n u(z)_i \quad (5.23)$$

5.1.4.1.2 Fully correlated large-scale uncertainties

The large-scale uncertainty component is fully correlated over the gridded domain. The sensitivity coefficient matrix in this case is the same as that defined in equation 5.21. The correlation matrix, \mathbf{R} , will be equal to \mathbf{J} , i.e. all values are equal to 1 as the uncertainties are full correlated. The resultant propagated uncertainty is an average of the input large-scale uncertainties.

$$u(\langle z \rangle)_c = \frac{1}{n} \sum_n u(z)_c \quad (5.24)$$

5.1.4.1.3 Locally systematic uncertainties

For the locally systematic uncertainties, gridding data at a resolution of 0.05 degrees requires the atmospheric and surface components to be propagated separately. The correlation length scale of the atmospheric uncertainty component is 5 km, so this is assumed fully correlated across a grid cell at this resolution. For this component, the sensitivity coefficient matrix, \mathbf{C} , is defined in equation 5.21 and the correlation matrix, \mathbf{R} , is equal to \mathbf{J} . The atmospheric uncertainty component at Level 3 is therefore given by equation 5.25 (using the subscript ‘atm’ to represent ‘atmosphere’).

$$u(\langle z \rangle)_{atm} = \frac{1}{n} \sum_n u(z)_{atm} \quad (5.25)$$

The given spatial correlation length scale of the atmospheric uncertainty component is 5km. This may be an underestimate as atmospheric effects can be correlated over longer spatial scales corresponding to synoptic systems. However, given the value currently adopted, this means that this uncertainty component becomes uncorrelated (random) for the purpose of further propagation into derived products by users. As such, this component is then added to $u(\langle z \rangle)_i$ (see equation 5.28).

For the surface uncertainties, the assumption is made that these are correlated where the biome is consistent, but uncorrelated between biomes. In this case the correlation matrix in the uncertainty calculation would include off-diagonal terms dependent on the underlying biome of the pixels included in the average. This is illustrated for example data in Figure 5.2.

Pixel	Biome	Correlation Matrix									
1	A	1	1	0	0	0	0	1	0	1	0
2	A	1	1	0	0	0	0	1	0	1	0
3	D	0	0	1	0	0	0	0	1	0	0
4	C	0	0	0	1	1	0	0	0	0	1
5	C	0	0	0	1	1	0	0	0	0	1
6	B	0	0	0	0	0	1	0	0	0	0
7	A	1	1	0	0	0	0	1	0	1	0
8	D	0	0	1	0	0	0	0	1	0	0
9	A	1	1	0	0	0	0	1	0	1	0
10	C	0	0	0	1	1	0	0	0	0	1

Figure 5-2: Example correlation matrix for a set of pixels (1-10) with associated biomes (A-D). The correlation matrix has off-diagonal non-zero elements where pixels share the same underlying biome.

The current approach is to do the uncertainty propagation in two stages. This does not strictly follow the law of propagation of uncertainty and this would be relatively easy to update in the uncertainty budget calculation. In the current approach, all of the contributing LST retrievals in \mathbf{z} are first grouped by their biome. Within each biome grouping, the uncertainties are fully correlated. The sensitivity matrix is as equation 5.17 and the correlation matrix is equal to \mathbf{J} . For each biome ‘group’, an uncertainty estimate is calculated by averaging the contributing uncertainties.

$$u(\langle z \rangle)_{biome} = \sqrt{\frac{1}{n^2} \sum_n u(z|biome)^2} \quad (5.26)$$

Following this process we now have ‘ m ’ uncertainties (one for each biome) where $m \neq n$ unless each contributing LST retrieval in \mathbf{z} has a different biome. The subset of uncertainties in ‘ m ’ is now independent as the surface uncertainty component is correlated only as a function of biome. These then average as a function of $1/\sqrt{m}$ to give the surface component of uncertainty at Level 3, denoted by the subscript ‘surf’.

$$u(\langle z \rangle)_{surf} = \sqrt{\frac{1}{\sqrt{m}} \sum_m u(z)_{biome}^2} \quad (5.27)$$

The surface uncertainty component is the only contributor to the locally systematic uncertainty at Level 3.

$$u(\langle z \rangle)_s = u(\langle z \rangle)_{surf} \quad (5.28)$$

5.1.4.1.4 Propagation of locally-systematic surface uncertainty component

The assumption made about the correlation length scale of the locally systematic surface uncertainty component is that it is:

- ❖ Perfectly correlated for pixels with the same underlying biome
- ❖ Uncorrelated between pixels with differing biomes

As outlined throughout this document, uncertainties should be propagated using the law of the propagation of uncertainty. In this case, the **R** matrix contains a mix of terms depending on the biomes of the contributing pixels. The current implementation of uncertainty propagation in pre-cursor studies does not use this **R** matrix in a single calculation, but instead uses a two-step process to calculate the uncertainty. The two approaches are not consistent, and give different answers as shown in the worked example below. The metrological method would be to do a single calculation using the correct **R** matrix, for which all of the required information is available, and this is recommended for implementation, improving the state-of-the-art for LST uncertainty calculation.

5.1.4.1.4.1 Worked example

Let us consider a worked example for the case where there are five clear-sky LST observations contributing to an averaged LST (using the data mean). In this example, the surface component of the uncertainty associated with these five observations will be as follows:

$$U = [0.3, 0.35, 0.2, 0.4, 0.6]$$

As the LST calculated as an arithmetic mean, the measurement equation is as follows (used in the L3U LST calculations):

$$\langle z \rangle = \frac{1}{n} \sum_{i=1}^n LST_i \quad (5.29)$$

For which the derivative of the measurement equation with respect to the input LST is:

$$\frac{\partial \langle z \rangle}{z_i} = \frac{1}{n} \quad (5.30)$$

We can then substitute this into the law for the propagation of uncertainty to give the equation for the locally systematic uncertainty component as follows:

$$u(\langle z \rangle)^2 = \sum_i^n \left(\frac{1}{n}\right)^2 u_i^2(z_i) + 2 \sum_{i=1}^{n-1} \sum_{j=i+1}^n \left(\frac{1}{n}\right) \left(\frac{1}{n}\right) u(z_i) u(z_j) r \quad (5.31)$$

Now, let's assume that in this example, the 1st and 2nd observation in the sample share the same biome and the 3rd and 5th also share a biome (but one that differs from that of observations 1 and 2). Following the law of propagation of uncertainty (8.3), the propagated locally systematic uncertainty can be calculated.

$$u(\langle z \rangle)^2 = \frac{1}{5^2} \sum_i^n u_i^2(z_i) + 2 \left(\frac{1}{5^2} \right) (0.3)(0.35) + 2 \left(\frac{1}{5^2} \right) (0.2)(0.6) \quad (5.32)$$

$$u(\langle z \rangle)^2 = 0.0489 \quad (5.33)$$

The method currently applied within LST_cci is a two-step process:

1. The uncertainty for pixels with the same biome is calculated using a simple average.
2. The uncertainty for each biome group is then propagated assuming independence between biomes.

In taking this approach, the measurement equation is no longer the arithmetic mean but equivalent to:

$$\langle z \rangle = \frac{\frac{z_1 + z_2}{2} + \frac{z_3 + z_5}{2} + z_4}{3} \quad (5.34)$$

Calculating the uncertainty using this equation yields the following result.

$$U(1) = \frac{u(z_1) + u(z_2)}{2}, U(2) = \frac{u(z_3) + u(z_5)}{2}, U(3) = u(z_4) \quad (5.35)$$

$$u(\langle z \rangle)^2 = \frac{\sum U^2}{9} \quad (5.36)$$

$$u(\langle z \rangle)^2 = 0.0472917 \quad (5.37)$$

The current implementation underestimates the true uncertainty in the surface component. The magnitude of the difference between using the metrological propagation and the current implementation will depend on the magnitude of the surface uncertainty component in the LST data (with larger uncertainties resulting in greater discrepancies). Changing the approach to the metrological propagation is recommended for Year 2/3 of the project to progress the 'state of the art' LST uncertainty estimation.

5.1.4.1.4.2 Retention of biome information for uncertainty propagation to higher level products

At present, information about the underlying biome for each retrieved LST is used in the propagation of the surface component of the locally systematic uncertainty from L2P to L3U data. Following this propagation, this information is no longer retained, but is of relevance when generating higher-level products including both synthesised datasets (L3C or L3S) and for gridding at coarser resolutions than 0.05 degrees.

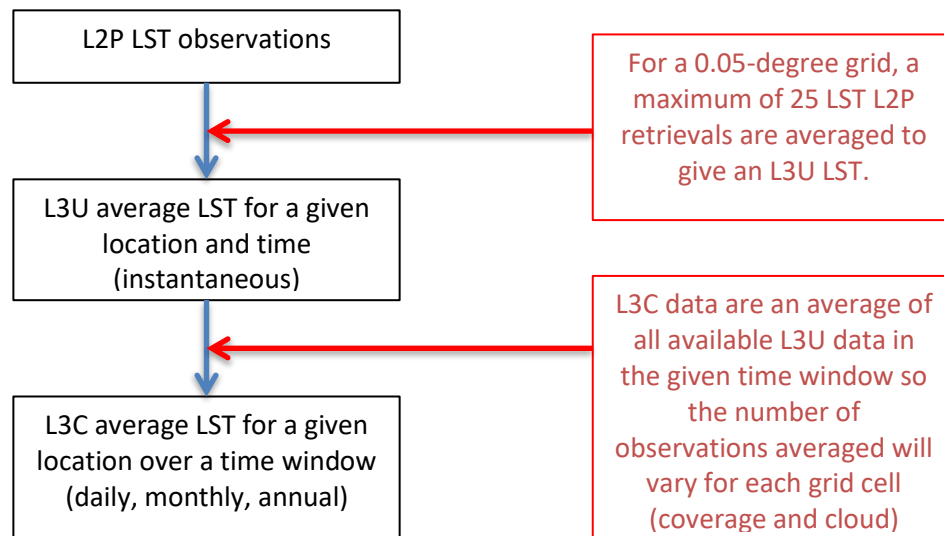


Figure 5-3: Schematic showing the averaging steps for post-processing LST L2 retrievals to L3U and L3C.

Figure 5.3 shows the processing steps for generating L3C data from L2P data. There are two averaging steps:

1. Averaging L2P observations for a single grid cell (instantaneous time frame) to generate L3U.
2. Averaging L3U observations over a given time window to generate temporally averaged L3C products (daily, monthly or annually).

In the first step, the biome information is used to inform the propagation of uncertainty for the surface component into the L3U data. For the second step, these data are no longer available. This is problematic for uncertainty propagation, as each of the L3U observations contributing to the average in the second step is itself an average over a number of L2P observations. The number and location of these L2P observations is dependent on data quality and cloud cover. As a result, where the underlying surface is heterogeneous across the grid cell, the combination of available L2P observations represents different surface types to different degrees.

Without information about the biomes of the L2P pixels contributing to each L3U average, the surface uncertainty component is propagated as if it were uncorrelated between L3U observations. Given the assumption that the uncertainty will be systematic over regions of consistent biome, treating the uncertainties as independent in the averaging to L3C will underestimate of the propagated surface uncertainty component.

The implementation of a strict metrological process here is complicated by the requirement to carry around additional data in the L3U products. For each L3U observation, the biome and associated surface uncertainty component from each of the contributing L2P observations would need to be stored, increasing file size and complexity. This has been done in an offline capacity and is recommended for consideration as an output product. It is also recommended that these L3U products are made available to data users.

In the case of gridding the L3U data at a coarser resolution (a task that may well need to be done by a data user for their application if not disseminated directly by the data supplier), the information from the L2P data on the biome and associated surface uncertainty component would again be required. It is also worth considering here the underlying assumption that the error effects are correlated by biome and whether there is a better method of propagation. There is both in-biome variability within the classification scheme and latitudinal variations in biome composition.

5.1.4.2. New uncertainties relevant to the processing level

Calculation of the arithmetic mean to represent the average gridded LST is based on the assumption that the contributing LST observations representatively sample the LST variation across the grid box. In practice, this is rarely true for infrared LST retrievals as retrievals are only possible under clear-sky conditions. As a consequence, in all cases where cloud obscures some of the grid box, sampling uncertainty is introduced into the averaged LST [RD-9]. This sampling uncertainty is modelled for LST_cci data using the following parameterisation.

$$u(\langle z \rangle)_{samp} = \frac{n_{cld} \sigma_z^2}{n - 1} \quad (5.38)$$

Here, n is the total number of contributing observations to the gridded LST, and n_{cld} is the number of these that are cloudy. σ_z^2 is the variance in LST observations in the vector \mathbf{z} . This current parameterisation for sampling uncertainty has some limitations as it is dimensionally inconsistent and does not account for cases where there are few clear-sky pixels available, which have consistent LSTs but are not representative of the LST variability within the cell. To present an estimate of the variability within a cell has been used, but to improve further would require a significant investigation, which could be initiated in Phase II.

This uncertainty component is uncorrelated between Level 3 grid cells and is therefore added to the uncorrelated (random) uncertainty component as defined in equation 5.23 (along with the atmospheric uncertainty component).

$$u(\langle z \rangle)_i = \sqrt{u(\langle z \rangle)_i^2 + u(\langle z \rangle)_{samp}^2 + u(\langle z \rangle)_{atm}^2} \quad (5.39)$$

5.1.5. L3C and L3S products

L3C and L3S products are ‘collated’ and ‘synthesised’ Level 3 datasets respectively. L3C data are provided on a common grid (as with L3U), with daily L3C products containing the L3U observation closest to the nominal overpass time of the given sensor. Monthly and annual LST products are temporal averages of the daily L3C products. L3C products contain data only from a single sensor, whereas L3S products contain data from two or more different sensors. L3C and L3S products are both produced from L3U inputs, propagating the uncertainty components to give uncertainty components for both L3C and L3S. In this case, the atmospheric fitting uncertainty is propagated as an uncorrelated uncertainty (it is added to the uncorrelated uncertainty component as assumed temporal correlation is very short at 5 minutes – eq. 5.30). However, given the propagation of weather systems at synoptic scales, this temporal correlation length scale could be an underestimate. For the locally systematic uncertainty component (containing the uncertainty from the surface specification), the biome information is not retained for use in the propagation, and it is treated as uncorrelated – this will likely

result in an underestimation of this uncertainty component for the 0.05 degree data. At 0.01 degree, it is assumed that any given pixel only covers one biome as this is commensurate with the resolution of the global land cover data. The large-scale uncertainty component is propagated in the same manner as described above for L3U products. For L3S products there will also be an uncertainty component related to the homogenisation of different satellite products to a common overpass time.

5.2. MODIS, SEVIRI and GOES-16/ABI

Three instrument series use the generalized split window (GSW) algorithm as described in this section. The Moderate Resolution Imaging Spectroradiometer (MODIS) is an instrument payload aboard two polar orbiting satellites: Terra (Earth Observing System AM) and Aqua (Earth Observing System PM). Terra has an equator overpass time of 10.30am and Aqua an equator overpass time of 1.30pm. The Terra satellite was launched in 1999 and the Aqua satellite in 2002. Both MODIS instruments are still making observations 20 years later, despite an anticipated lifetime of 6 years. Only over recent years have additional calibration methods been required to account for instrument degradation.

MODIS Terra has been selected to bridge the gap in the ATSR-SLSTR climate data record between April 2012 with the failure of the Envisat platform, and the subsequent launch of SLSTR in 2016. MODIS instruments make observations in 36 spectral channels, across the infrared and visible spectrum. Of these, 29 channels have a spatial resolution of 1 km at nadir consistent with the ATSR and SLSTR instruments. Channels 31 and 32 provide observations at 11 and 12 microns respectively, which can be used to retrieve LST. MODIS has a much wider swath width (2330 km) than the ATSR and SLSTR instruments. For the purpose of the CDR, both the MODIS and SLSTR data will be made to look 'ATSR like' by cropping the swath appropriately. The instrument characteristics for MODIS Terra are shown in Table 13.

Instrument	Channels (µm)		Availability	Equator Overpass Time
MODIS	0.66, 0.87	250 m resolution	All channels available.	10:30 (Terra) 14:30 (Aqua)
	0.47, 0.56, 1.24, 1.64, 2.13	500 m resolution		
	0.42, 0.44, 0.49, 0.53, 0.57, 0.65, 0.68, 0.75, 0.87, 0.91, 0.94, 1.38, 3.75, 3.96, 4.05, 4.47, 4.52, 6.72, 7.33, 8.55, 9.73, 11.03, 12.02, 13.34, 13.64, 13.94, 14.24	1 km resolution		

Table 13: Instrument characteristics for MODIS Aqua and MODIS Terra.

The MODIS instrument has sufficiently different characteristics from the ATSR instrument series that using a GSW retrieval algorithm is more appropriate for the single sensor than the University of Leicester (UoL) algorithm. For the CDR, the UoL algorithm will be used for consistency with the ATSR and SLSTR instruments. As such, the measurement equation is different from that used for the ATSR instruments and the uncertainty budget needs to be constructed from this baseline. In this section we

discuss the formulation of an uncertainty budget instruments using the generalised split window retrieval algorithm.

The Spinning Enhanced Visible and InfraRed Imager (SEVIRI) instruments fly aboard the Meteosat Second Generation platforms (MSG1-4). These platforms are geostationary, in orbit close to 0 N, 0 E, observing the same part of the globe with a high temporal resolution (15 minute complete cycle time). MSG1 was launched in 2005, MSG2 in 2005, MSG3 in 2012 and MSG4 in 2015. SEVIRI observations are used within LST CCI to produce both a single-sensor time series, and as part of the LST CCI merged products. Table 14 details the instrument characteristics for SEVIRI.

Instrument	Channels (μm)	Availability	Equator Overpass Time	
SEVIRI	0.635, 0.81, 1.64, 3.92, 6.25, 7.35, 8.70, 9.66, 10.8, 12.0, 13.4	4.8 km IFOV, 3 km sampling	All channels available.	15 minute sample time

Table 14: Instrument characteristics for SEVIRI aboard MSG1-4.

The Advanced Baseline Imager (ABI) flies aboard the Geostationary Operational Environment Series (GOES)-16 satellite platform, and observes the western hemisphere every 10 minutes, centred on the equator at 72.5 degrees west. GOES-16 was launched in 2016 and replaced GOES-13 as the operational GOES East satellite in December 2017. Within LST CCI the ABI on GOES-16 is used both as a single-sensor product and in the merged GEO+LEO infrared products. Table 15 summarises the ABI instrument characteristics.

Instrument	Channels (μm)	Availability	Equator Overpass Time	
ABI	0.47, 0.64, 0.86, 1.37, 1.6, 2.2, 3.9, 6.2, 6.9, 7.3, 8.4, 9.6, 10.3, 11.2, 12.3, 13.3	2 km	All channels available.	10 minute sample time

Table 15: Instrument characteristics for ABI aboard GOES-16.

5.2.1. Land Surface Temperature Retrieval

The generalised split window retrieval algorithm [RD-33] is applied to MODIS, SEVIRI and GOES-16/ABI. The measurement equation is shown in equation 5.40 and this is dependent on the brightness temperatures at wavelengths of 11.03 and 12.02 μm at 1 km resolution.

$$LST = \left(A_1 + A_2 \left(\frac{1 - \varepsilon}{\varepsilon} \right) + A_3 \frac{\Delta\varepsilon}{\varepsilon^2} \right) \frac{T_{11} + T_{12}}{2} + \left(B_1 + B_2 \frac{1 - \varepsilon}{\varepsilon} + B_3 \frac{\Delta\varepsilon}{\varepsilon^2} \right) \frac{T_{11} - T_{12}}{2} + C \quad (5.40)$$

The retrieval is dependent on the mean land surface emissivity (ϵ) for the two channels used in the retrieval (ϵ_{11} and ϵ_{12}) and the difference between the land surface emissivity at the two wavelengths ($\Delta\epsilon$) [RD-34].

$$\epsilon = 0.5(\epsilon_{11} + \epsilon_{12}) \quad (5.41)$$

$$\Delta \epsilon = \epsilon_{11} - \epsilon_{12} \quad (5.42)$$

Surface emissivity is specified in the retrieval using data from the Combined ASTER MODIS Emissivity over Land (CAMEL) atlas [RD-60]. The data are provided at a spatial resolution of 0.01 degrees at thirteen wavelengths between 3.6 and 14.3 μm . These wavelengths are used as hinge points for the full emissivity spectra and a base fit can be used to interpolate between them. For the MODIS, SEVIRI and GOES-16/ABI retrievals, emissivity at 10.1 and 12.1 μm is used.

The retrieval uses a number of coefficients A_j , B_j ($j=1,2,3$) and C , which have a dependency on satellite viewing angle and water vapour [RD-34]. The coefficients are banded by both total column water vapour and satellite zenith angle. Satellite zenith angle is divided into 13 bands of width 5° spanning 0-65° and total column water vapour into 8 bands of width 7.5 kg m^{-2} (covering the range 0-60 kg m^{-2}) [RD-34].

Given the definition of the measurement equation in 5.40, the error effects associated with each term can be determined. To do this, error effects are grouped by the measurement term following equation 4.1 where $z = g(\mathbf{y}, \boldsymbol{\beta}) + 0$, where \mathbf{y} is the observation vector, $\boldsymbol{\beta}$ is the retrieval parameter vector and the '+0' term encompasses error effects not directly associated with either of these vectors. Although at present it may not be possible to quantify the uncertainty associated with every error effect, this methodology provides a means to assess progress in characterising the uncertainties in the LST retrieval and identifying remaining gaps.

Measurement term	Normal notation	Effect	Effects expected	Correlation length scale	Attributed uncertainties	Sensitivity
	A_1	1	Satellite zenith angle variability error	s	Not attributed	*
		2	Total column water vapour error	s	TCWV ensemble spread	$\frac{\partial g}{\partial TCWV}$
		3	Total column water vapour and solar zenith angle binning	s	Fitting residual	*
		4	Fitting error	s	Fitting residual	*
	A_2	5	Satellite zenith angle variability error	s	Not attributed	*
		6	Total column water vapour error	s	TCWV ensemble spread	$\frac{\partial g}{\partial TCWV}$
		7	Total column water vapour and solar	s	Fitting residual	*



Measurement term	Normal notation	Effect	Effects expected	Correlation length scale	Attributed uncertainties	Sensitivity
β			zenith angle binning			
		8	Fitting error	s	Fitting residual	*
	A ₃	9	Satellite zenith angle variability error	s	Not attributed	*
		10	Total column water vapour error	s	TCWV ensemble spread	$\frac{\partial g}{\partial TCWV}$
		11	Total column water vapour and solar zenith angle binning	s	Fitting residual	*
		12	Fitting error	s	Fitting residual	*
	B ₁	13	Satellite zenith angle variability error	s	Not attributed	*
		14	Total column water vapour error	s	TCWV ensemble spread	$\frac{\partial g}{\partial TCWV}$
		15	Total column water vapour and solar zenith angle binning	s	Fitting residual	*
		16	Fitting error	s	Fitting residual	*
	B ₂	17	Satellite zenith angle variability error	s	Not attributed	*
		18	Total column water vapour error	s	TCWV ensemble spread	$\frac{\partial g}{\partial TCWV}$
		19	Total column water vapour and solar zenith angle binning	s	Fitting residual	*
		20	Fitting error	s	Fitting residual	*
	B ₃	21	Satellite zenith angle variability error	s	Not attributed	*
		22	Total column water vapour error	s	TCWV ensemble spread	$\frac{\partial g}{\partial TCWV}$
		23	Total column water vapour and solar zenith angle binning	s	Fitting residual	*
		24	Fitting error	s	Fitting residual	*
	C	25	Satellite zenith angle variability error	s	Not attributed	*
		26	Total column water vapour error	s	TCWV ensemble	$\frac{\partial g}{\partial TCWV}$

Measurement term	Normal notation	Effect	Effects expected	Correlation length scale	Attributed uncertainties	Sensitivity
					spread	
		27	Total column water vapour and solar zenith angle binning	s	Fitting residual	*
		28	Fitting error	s	Fitting residual	*
	ϵ_{11}	29	Emissivity error	s	CAMEL emissivity uncertainty	$\frac{\partial g}{\partial \epsilon_{11}}$
		30	Temporal interpolation of emissivity data	s	Not attributed	$\frac{\partial g}{\partial \epsilon_{11}}$
	ϵ_{12}	31	Emissivity error	s	CAMEL emissivity uncertainty	$\frac{\partial g}{\partial \epsilon_{12}}$
		32	Temporal interpolation of emissivity data	s	Not attributed	$\frac{\partial g}{\partial \epsilon_{12}}$
	y	T_{11}	33	Noise	i	0.03 K
34			Calibration error	c	Not attributed	$\frac{\partial g}{\partial T_{11}}$
T_{12}		35	Noise	i	0.04 K	$\frac{\partial g}{\partial T_{12}}$
		36	Calibration error	c	Not attributed	$\frac{\partial g}{\partial T_{12}}$
+0	Geolocation	37	Re-projection of native instrument grid to image grid	s	Not attributed	*
	Cloud Detection	38	Undetected cloud	s	Not attributed	*
	RTM	39	Error in RTM simulation (trace gas profiles, parameterisation).	c	0.03 K	$\frac{\partial g}{\partial T_{11}}$
	NWP	40	Error in RTM inputs (surface temperature and total column water vapour).	c		$\frac{\partial g}{\partial T_{12}}$

Table 16: Error effects for single pixel LST retrieval. Effects are categorised according to the measurement equation term. Where quantified, the values propagated for each effect are specified for MODIS TERRA. *denotes cases where the uncertainty is modelled rather than propagated using a sensitivity coefficient.

Table 16 shows that there are 34 error effects associated with the retrieval parameter vector (β). The first 28 of these are associated with the retrieval coefficients A, B ($j=1,2,3$) and C. Each coefficient has four associated error effects: the first two arise from the use of binned data to parameterise the coefficients. Uncertainties arise both in the data used to select the coefficient bin and the use of a non-continuous function in solar zenith angle and total column water. The total column water vapour uncertainties are specified using an ensemble and propagated through the retrieval equation. The solar zenith angle uncertainties are expected to be small and are not currently attributed. The effects associated with the binning of the coefficients are all fully correlated between coefficients. The third error effect is the uncertainty associated with the bins of total column water vapour and solar zenith angle chosen for the calibration. This error effect is assumed to be folded into the retrieval fitting error at present. Finally, the retrieval model structure does not fully represent the physical system and therefore the fourth error effect is the uncertainty in the retrieval fitting process, parameterised using the fitting residual.

The emissivity estimates in the 11 and 12 μm channels are also part of the retrieval parameter vector. Each emissivity estimate has two error effects associated with it: 1) emissivity estimate error and 2) temporal interpolation error. The first is the error associated with the emissivity estimation process itself, and the second is the error associated with interpolating these estimates to the time of the retrieval. The first is explicitly propagated through the retrieval equation whilst the second is not estimated at present.

There are four error effects associated with the observation vector, \mathbf{y} . These are the instrument noise and calibration errors associated with each channel. The instrument noise is propagated through the retrieval equation according to the sensitivity of the retrieved surface temperature to the observations and accounted for explicitly in the uncertainty budget. The calibration error is not quantified, as this information is not made available in the Level 1 data.

The '+0' term contains the error effects not directly related to the retrieval parameters (β) or the observations (\mathbf{y}). Four sources of error fit into this category for MODIS, SEVIRI and GOES-16/ABI. The first is the geolocation error arising from propagation of the native instrument grid to an image grid. This is not explicitly accounted for in the uncertainty budget. The second is the error due to an imperfect method for detecting clouds. Where clouds remain undetected this will bias the LST retrieval (typically cold). At present this source of uncertainty is not quantified. The final two sources of error are related to the use of a radiative transfer model (RTM) to calculate the retrieval coefficients. The first source of error is in the model simulation itself, specifically in the parameterisations used, and the second is in the numerical weather prediction data used by the RTM to set the boundary conditions. These two sources of error are combined and propagated using the sensitivity of the retrieval to the observations. The quantification of this uncertainty is likely to be an underestimate as it uses a value calculated over ocean surfaces [RD-15] where conditions are more stable than over land.

5.2.2. Level 1 data

Level 1 data are used as input into Level 2 retrievals of geophysical variables (e.g. LST). These Level 1 data have uncertainties associated with them that arise both from the instrument characteristics and the measurement process. Quantifying the uncertainty budget for Level 1 data requires an in-depth analysis of the measurement process, in-orbit conditions and instrument construction [RD-13]. Unfortunately, this type of analysis is not routinely undertaken, and an uncertainty budget is rarely provided with Level 1 data. As such, it is only possible to propagate the uncertainty information routinely provided with the Level 1 data into the retrieval, which is usually limited to an estimate of the retrieval noise in each channel.

5.2.2.1. Uncertainties due to random error effects

5.2.2.1.1 Uncertainties due to instrument noise

One source of uncertainty in the Level 1 data is the noise associated with each channel used in the retrieval equation (errors 21 and 23 in Table 16). In order to propagate this through the retrieval equation the sensitivity coefficient matrix, \mathbf{C} , is required (please refer back to equation 4.9 for more details). In this case, \mathbf{C} can be defined as:

$$\mathbf{C} = \begin{bmatrix} \frac{\partial g}{\partial T_{11}} & \frac{\partial g}{\partial T_{12}} \end{bmatrix} \quad (5.43)$$

where:

$$\frac{\partial g}{\partial T_{11}} = \frac{(A_1 + B_1)}{2} + \frac{(A_2 + B_2)(1 - \varepsilon)}{2\varepsilon} + \frac{(A_3 + B_3)\Delta\varepsilon}{2\varepsilon^2} \quad (5.44)$$

$$\frac{\partial g}{\partial T_{12}} = \frac{(A_1 - B_1)}{2} + \frac{(A_2 - B_2)(1 - \varepsilon)}{2\varepsilon} + \frac{(A_3 - B_3)\Delta\varepsilon}{2\varepsilon^2} \quad (5.45)$$

ε and $\Delta\varepsilon$ are defined in equations 5.41 and 5.42 respectively. The error correlation matrix, \mathbf{S}_ε , is diagonal. Each non-zero element represents the variance due to the instrument noise in each channel. For MODIS, SEVIRI and GOES-16/ABI this follows the same approach used for the ATSR instrument and is specified as the square of the noise equivalent delta temperature (NEdT) at 300 K for each channel. The values used for these instruments are shown in Table 17.

Instrument	Variance T_{11} NEdT	Variance T_{12} NEdT
MODIS AQUA	$(0.02)^2$	$(0.03)^2$
MODIS TERRA	$(0.03)^2$	$(0.04)^2$
MSG1	$(0.11)^2$	$(0.15)^2$
MSG2	$(0.11)^2$	$(0.16)^2$
MSG3	$(0.11)^2$	$(0.15)^2$
MSG4	$(0.11)^2$	$(0.16)^2$
GOES-16/ABI	$(0.1)^2$	$(0.1)^2$

Table 17: T_{11} and T_{12} diagonal elements in the \mathbf{S}_ε matrix for the MODIS AQUA, MODIS TERRA, MSG1, MSG2, MSG3, MSG4 and GOES-16/ABI instruments.

5.2.3. Level 2 data

Level 2 data are the retrieved geophysical variable, e.g. LST. Uncertainties in the Level 2 data arise both from uncertainties propagated from the Level 1 data (as discussed in the previous section) and uncertainties introduced during the retrieval process itself. In this section we characterise the uncertainties in the latter.

5.2.3.1. Uncertainties due to locally systematic error effects

5.2.3.1.1 Uncertainties due to total column water vapour

In the generalised split window algorithm coefficients are calibrated over bands of satellite zenith angle and total column water vapour. An estimate of TCWV *a priori* is required for LST retrieval and is used to select the appropriate coefficients. The uncertainty in this estimate is then propagated through the LST retrieval. The uncertainty is parameterised using the ensemble spread in the Numerical Weather Prediction data that is made available together with the TCWV best estimate. The ensemble systems consist in a set of model runs with perturbed initial conditions; some systems also include perturbations to the model physics, more than one model within the ensemble or different physical parameterisation schemes [RD-45]. Processing of ensemble data can be quite demanding and therefore we currently approximate the instantaneous TCWV spread to a climatology of this spread that depends on actual TCWV, latitude and month.

For this uncertainty (effects 2, 6, 10, 14, 18, 22 and 26 in Table 14), the sensitivity coefficient matrix, \mathbf{C} , consists of the differential of the LST retrieval equation with respect to total column water vapour (TCWV).

$$\mathbf{C} = \left[\frac{\partial g}{\partial TCWV} \right] \quad (5.49)$$

Since the dependence of the measurement equation on TCWV is implicit through all of the coefficients, the differential can be calculated as:

$$\frac{\partial g}{\partial TCWV} = \sum_j \frac{\partial g}{\partial \beta_j} \frac{\partial \beta_j}{\partial TCWV} \quad (5.50)$$

Where $\beta = (A_1, A_2, A_3, B_1, B_2, B_3, C)$ is the vector of coefficients and j represents the j -th class of TCWV. However, β_j is a piece-wise linear function and therefore cannot be differentiated. Instead, we approximate uncertainty propagation to finite differences:

$$\frac{\partial g}{\partial TCWV} \cong \sum_j \frac{\Delta g}{\Delta \beta_j} \frac{\Delta \beta_j}{\Delta TCWV} \quad (5.51)$$

In this case, the LST uncertainty due to TCWV, $u(TCWV)$, will not be computed through the matrix notation, instead:

$$u(TCWV)^2 \cong \sum_j \left(\frac{\Delta g}{\Delta \beta_j} \right)^2 \left(\frac{\Delta \beta_j}{\Delta TCWV} \right)^2 \Delta TCWV^2 = [\Delta g | \Delta TCWV]^2 \quad (5.52)$$

Where $[\Delta g | \Delta TCWV]$ represents variation in g due to all possible variations in TCWV.

Each coefficient β_j , cannot vary with TCWV independently of the remaining coefficient (i.e., we have a fixed set of β_j per class of TCWV) and as such the sum in j is dropped. Since each β_j takes a finite number of values, instead of considering all possible values of $\Delta TCWV$, we need only to consider g for the valid values of β and their error probability distribution, which is determined by the TCWV distribution:

$$u(TCWV)^2 = \sum_k [g(y, \beta(R_k)) - g(y, \beta)]^2 P(TCWV \in R_k) \quad (5.53)$$

Where R_k is the region of the water vapour domain where the k-th value of β is valid. The TCWV error probability distribution is obtained from the ensemble run. Let us assume that the ensemble estimates of TCWV have a normal distribution, $N(\mu_{ENS}, \sigma_{ENS})$, where μ_{ENS} is the ensemble mean and σ_{ENS} is the ensemble standard deviation (or spread). The interval probability is then given by:

$$P(TCWV \in R_k) = F(R_k^u) - F(R_k^l) \quad (5.54)$$

Where F is the cumulative density function of the generic normal distribution $N(\mu_{ENS}, \sigma_{ENS})$, and R_k^u and R_k^l are the upper and lower bounds of the TCWV region R_k . The normal distribution takes values $\in]-\infty, +\infty[$, but the TCWV variable takes only positive values and, in the case of the generalised split window algorithm is effectively limited by the upper limit of the higher TCWV region. It is therefore necessary to normalize the probability $P(TCWV \in R_k)$ to the effective range of possible TCWV values:

$$P(TCWV \in R_k) = \frac{F(R_k^u) - F(R_k^l)}{F(R_N^u) - F(R_1^l)} \quad (5.55)$$

Where N is the number of TCWV regions considered.

5.2.3.1.2 Uncertainties due to coefficient fitting (atmospheric effects)

Uncertainties due to coefficient fitting (error effects 1-14 in Table 16) arise primarily from limitations in the model structure in fully representing the physical system (in this case, the radiative transfer between TOA and surface) and from the coefficient binning based on SZA and TCWV. There is also an uncertainty component associated with the specification of the atmospheric state in the radiative transfer simulations used to calculate the coefficients and the satellite viewing geometry. The combined uncertainty from all of these error effects can be estimated empirically using the residuals from the coefficient fitting process. In the retrieval these are characterised as a function of satellite zenith angle and total column water vapour, both of which are categorized using bands. The satellite zenith angle bands are five degrees in width, spanning angles of 0-65 degrees and the total column water vapour bands are 7.5 kg m⁻² in width, ranging from 0-60 kg m⁻².

The uncertainties are the standard deviation of the double differences between the retrieved and input surface temperatures in the fitting process [RD-7]. This standard deviation (σ) is calculated as:

$$\sigma = \sqrt{\frac{\sum(x - \bar{x})^2}{n}} \quad (5.56)$$

Where

$$x = (LST_{sim} - LST_{ret}) - (LST_{sim} - LST_{NWP}) \quad (5.57)$$

Here the subscripts to equation 5.57 refer to the simulated ('sim'), retrieved ('ret') and input (numerical weather prediction, 'NWP') surface temperatures respectively. 'n' is the number of surface temperature pairs. The standard deviations calculated using this method are presented in Table 18 for each satellite zenith angle and total column water vapour band.

Satellite Zenith Angle	Total Column Water Vapour / kg m ⁻²							
	0-7.5	7.5-15	15-22.5	22.5-30	30-37.5	37.5-45	45-52.5	52.5-60
0-5	0.1397374	0.1906502	0.3269909	0.4201471	0.5520666	0.5255013	0.4376333	0.4180112
5-10	0.1400361	0.1913468	0.3282242	0.4213339	0.5538996	0.5272474	0.4388275	0.4194894
10-15	0.1412796	0.1933246	0.3313085	0.4249771	0.5597443	0.5325294	0.44360938	0.4247408
15-20	0.1436432	0.1968351	0.3362969	0.4312518	0.5695301	0.2417954	0.4518316	0.433856
20-25	0.1472791	0.2009236	0.3432307	0.4406297	0.5838836	0.5551182	0.4638663	0.4476363
25-30	0.1542108	0.2062539	0.3525505	0.4537698	0.6025053	0.5738518	0.4804446	0.4662907
30-35	0.1593711	0.2134587	0.3650315	0.472076	0.6277122	0.5983022	0.5032856	0.4918718
35-40	0.1678901	0.2265631	0.3822142	0.495861	0.6622258	0.6300033	0.5342761	0.5269526
40-45	0.1811672	0.2423774	0.4007928	0.526875	0.7066834	0.6722192	0.5762372	0.5745986
45-50	0.1951527	0.2536512	0.4262932	0.5671594	0.7645003	0.7287358	0.6341143	0.6402901
50-55	0.2110682	0.2748969	0.4624019	0.6182972	0.8512186	0.8066604	0.7155972	0.7333723
55-60	0.2352481	0.3066246	0.5101285	0.6893211	0.9967552	0.918269	0.8352454	0.8690413
60-65	0.2643704	0.3460157	0.5765274	0.7919971	1.194713	1.083928	1.015079	1.07252

Table 18: Residual uncertainties in the coefficient fitting process. Uncertainties are presented as standard deviations and would be squared when used as diagonal elements of the error correlation matrix, S_{ϵ} .

5.2.3.1.3 Uncertainties due to emissivity estimation

Land surface emissivity in the 11 and 12 μm channels is input into the measurement equation (5.40) to retrieve LST from MODIS, SEVIRI and GOES-16/ABI. Any error associated with the estimate of these values will propagate through the retrieval equation, resulting in a source of uncertainty in the retrieved LST (error effects 29 and 31 in Table 16). The emissivity retrieval itself has a physical basis, but the errors associated with this emissivity estimate are likely to be locally correlated with an assumed correlation length scale of 0.05 degrees. The sensitivity coefficient matrix for the propagation of this uncertainty is given in (5.58):

$$C = \begin{bmatrix} \frac{\partial g}{\partial \epsilon_{11}} & \frac{\partial g}{\partial \epsilon_{12}} \end{bmatrix} \quad (5.58)$$

The derivatives of the retrieval equation by which these uncertainties are propagated are given in 5.47 and 5.48. The error correlation matrix, S_{ϵ} is diagonal, with each non-zero element representing the variance of the error distribution associated with each emissivity estimate. These values are taken from the Combined ASTER and MODIS Emissivity over Land (CAMEL) atlas, and incorporate spatial, temporal and algorithm variability uncertainties [RD-61].

5.2.3.2. Uncertainties due to large-scale systematic error effects

There are two sources of error that are correlated over long spatio-temporal scales, for example the lifetime of the instrument.

1. Calibration errors in the instrument which may have a channel dependence

2. Errors arising from using radiative transfer modelling to simulate radiance in the retrieval coefficient derivation.

The uncertainty from (1) is what remains after correcting for any unknown bias in the data. Propagation of calibration uncertainties is usually reliant on the provision of this information by the Level 1 data producers. In the absence of this information and given assessments of very low systematic errors in the T_{11} and T_{12} observations [RD-37, RD-38] this uncertainty is not attributed at present (and assumed to be small). The uncertainty from the radiative transfer modelling can be estimated by assessing the sensitivity of the model to perturbations in the input data. This is done in the context of AATSR sea surface temperature retrievals in RD-15 for the 11 μm channel and found to be of order 0.03 K. This value is adopted here for MODIS also, and applied to both the T_{11} and T_{12} observations. As this was estimated with reference to sea surface temperature simulations, it is likely to be an underestimation over land.

This value of 0.03 K for both the 11 and 12 μm channels is propagated using the sensitivity matrix with respect to the observation vector as given in equation 5.43. The sensitivity terms are given in full in equations 5.44 and 5.45.

5.2.3.3. Correlations length scales of Level 2 uncertainty components

In the Level 2 data products, uncertainty components are group together according to their correlation length scales in order to facilitate correct propagation to higher-level products (which may undergo spatial and/or temporal averaging). The correlation length scales associated with all of the uncertainty components discussed in this section are shown in Table 19.

Error effect	Correlation length scale
Instrument noise	Uncorrelated
Sub-pixel emissivity variability	Uncorrelated
Emissivity estimation	Biome dependent
Atmospheric fitting	5 km / 5 minutes [RD-28, RD-29]
Radiative Transfer Modelling	Instrument record

Table 19: Correlation length scales for the error effects characterised in Level 2 MODIS, SEVIRI and GOES-16/ABI data.

The provision of uncertainty information in the Level 2 products follows the same template as that described for the ATSR and SLSTR products. The total uncertainty is provided along with four individual uncertainty components: 1) uncorrelated uncertainty, 2) large-scale systematic uncertainty, 3) locally correlated atmospheric uncertainty and 4) locally correlated surface uncertainty. The two locally correlated systematic uncertainties are split because there are different correlation length scales associated with each.

The correlation length scales assumed for the atmospheric uncertainty component are consistent with the ATSR products, with a spatial and temporal length scale of 5 km and 5 minutes respectively [RD-28, RD-29]. These correlation length scales are significantly shorter than those assumed over the ocean (100 km and 1 day, which are more similar to synoptic scales). This is due to the concept that more localised meteorological conditions develop over the land than the ocean. As discussed previously, the validity of these assumptions is recommended for further investigation in Phase II of LST CCI to see

whether the local or synoptic atmospheric conditions are the dominant factor and whether these correlation length scales should vary as a function of latitude or longitude.

5.2.4. Level 3 data

Level 3 products are produced on a common grid at 0.01 or 0.05 degree resolution. Three types of Level 3 products can be produced in any given processing chain: 1) L3U – these are ‘uncollated’ products, where a single L2 orbit or full disk observation is placed on a regular latitude-longitude grid. 2) L3C – these are ‘collated’ products, where two or more orbits/disks are combined from the same instrument. 3) L3S – these are ‘synthesised’ products, which combine L3 data from two or more sensors.

The LST L3U value in any given grid cell is calculated using the arithmetic mean of LST observations falling within geographical limits of the grid cell. This can consist of up to 25 observations when re-gridding 1 km resolution data (for 0.05 degree products), but the total will be dependent on both cloud cover (all L3 products) and over-lapping orbits (L3C and L3S products only). For the 0.01 resolution data, typically only 1-2 pixels fall into any given grid cell, sometimes with fractions of pixels overlapping the defined bounds of the cell. In this case the partially overlapping observations are also averaged, weighted by their fractions. Similarly, the uncertainties are propagated following the methodology described here, but weighted by their fraction. The LST in any given grid cell is calculated using:

$$LST_{grid} = \frac{1}{n} \sum_{i=1}^n LST_i \quad (5.59)$$

We can use the measurement equation form given in 4.2 in addition to equation 5.59 to produce a breakdown of the error effects for Level 3 data. The measurement equation takes the form $\langle z \rangle = g(\mathbf{z}, \boldsymbol{\gamma})$. Note that we use ‘ \mathbf{z} ’ and ‘ $\boldsymbol{\gamma}$ ’ rather than ‘ \mathbf{y} ’ and ‘ $\boldsymbol{\beta}$ ’ when defining the observation and parameter vectors as we have moved up one level in the data production. The error effects associated with Level 3 MODIS, SEVIRI and GOES-16/ABI data are show in Table 20.

Measurement term	Normal notation	Effect	Effects expected	Correlation length scale	Attributed uncertainties	Sensitivity
z	z _n	1	LST noise	i	Quantified at L2	$\frac{\partial h}{\partial z}$
		2	Input data – surface effects (emissivity).	i	Quantified at L2	$\frac{\partial h}{\partial z}$
		3	Retrieval error – surface effects (emissivity)	s	Quantified at L2	$\frac{\partial h}{\partial z}$
		4	Retrieval error – atmospheric effects (emissivity, coefficient fitting).	s	Quantified at L2	$\frac{\partial h}{\partial z}$
		5	RTM and NWP simulation error	c	Quantified at L2	$\frac{\partial h}{\partial z}$
		6	Cloud Detection	s	Not attributed	*
		7	Geolocation	s	Not attributed	$\frac{\partial h}{\partial z}$
		8	Calibration	c	Not attributed	$\frac{\partial h}{\partial z}$
y	Weighting	9	Weighting of retrieved pixels contributing to averaged product	s	0	*
+0	Sampling uncertainty	10	Clear-sky pixel representivity of LST across gridded domain	s	Modelled	*

Table 20: Error effect for averaging MODIS, SEVIRI and GOES-16/ABI LST products. Effects are categorised according to the measurement equation term. Where quantified, the values propagated for each effect are specified. *denotes cases where the uncertainty is modelled rather than propagated using a sensitivity coefficient.

At Level 3, there are eight error effects associated with the LST input vector, **z**. Five of these (errors 1-5) are quantified within the Level 2 data, and these can be propagated appropriately into the Level 3 product. These are the noise (propagated through from the Level 1 data), the surface effects from emissivity parameterisation, the atmospheric effects from the coefficient fitting and the RTM and NWP errors. Three further effects: from cloud detection, geolocation and calibration (errors 6-8 in the table) are not quantified within the Level 2 data.

There is one error effect associated with the measurement equation parameter, **y**, and that is the weighting applied when calculating the average. At present, equal weighting is given to all values in the observation vector, **z**, and therefore this uncertainty is equal to zero. Other approaches can be taken, which may be of more relevance under certain conditions (for example in regions of rapidly varying biome). For a fuller discussion of these options please refer to section 5.1.4.

At Level 3 the ‘+0’ term includes the uncertainty due to sub-sampling. When using infrared observations, LST cannot be retrieved in the presence of clouds, which frequently results in under-sampled grid cells when averaging data. This component of the uncertainty budget is modelled.

5.2.4.1. Propagated uncertainties

There are five uncertainty components that are propagated from the Level 2 data into the Level 3 data. As with the ATSR instrument, the propagation is done independently for uncertainty components with different correlation length scales.

5.2.4.1.1 Uncorrelated (random) uncertainties

The first two components (1 and 2 in Table 20) are combined in the Level 2 data to give a single uncorrelated uncertainty component. The sensitivity coefficient for the propagation of uncertainty is the derivative of the measurement equation with respect to \mathbf{z} . This sensitivity matrix (\mathbf{C}) is consistent across all uncertainty components that are propagated rather than modelled and is shown in equation 5.60.

$$\mathbf{C} = \begin{bmatrix} \frac{\partial h}{\partial z_1} & \dots & \frac{\partial h}{\partial z_n} \end{bmatrix} \quad (5.60)$$

Differentiating equation 5.59 with respect to \mathbf{z} (LST) gives the sensitivity.

$$\frac{\partial h}{\partial z} = \frac{1}{n} \quad (5.61)$$

The correlation matrix, \mathbf{R} , in this case is the identity matrix as uncertainties are uncorrelated between pixels. The propagated uncertainty component, $u(\langle z \rangle)_i$, is then given in 5.62.

$$u(\langle z \rangle)_i = \frac{1}{\sqrt{n}} \sum_n u(z)_i \quad (5.62)$$

5.2.4.1.2 Fully correlated large-scale uncertainties

The large-scale uncertainty component that comes from the RTM and NWP errors (component 5 in Table 20) is fully correlated over the gridded domain. The sensitivity matrix, \mathbf{C} , is the same as that given in equation 5.60 but the \mathbf{R} matrix differs in this case. Here the correlation matrix, \mathbf{R} , is equal to \mathbf{J} , i.e. all values including the off-diagonal terms are equal to 1. The propagated uncertainty, $u(\langle z \rangle)_c$, is therefore the average of the input large-scale uncertainty components.

$$u(\langle z \rangle)_c = \frac{1}{n} \sum_n u(z)_c \quad (5.63)$$

5.2.4.1.3 Locally systematic uncertainties

The locally systematic uncertainties have two components, one associated with the atmosphere and one associated with the surface. The reason for providing these uncertainties separately is that the assumed correlation length scales of these components differ, as shown in Table 19. The spatial correlation length scale for the atmospheric component is 5km, so on the L3U grid this is considered fully correlated and treated in the same way as the fully correlated large-scale uncertainties. The sensitivity matrix, \mathbf{C} , is identical to that shown in equation 5.60, and the correlation matrix, \mathbf{R} , is equal to

\mathbf{J} , ie. all values in the matrix are equal to 1. The propagated atmospheric uncertainty component ‘atm’, is therefore the average of the atmospheric uncertainty components associated with each LST measurement (z), as shown in equation 5.64.

$$u(\langle z \rangle)_{atm} = \frac{1}{n} \sum_n u(z)_{atm} \quad (5.64)$$

At Level 3, this atmospheric uncertainty component is considered to be uncorrelated (as the spatial correlation length scales are equal to the grid cell size and temporal correlations are assumed to be very short (5 minutes)). This is therefore added to the uncorrelated uncertainty component provided with the Level 3 data.

$$u(\langle z \rangle)_i = \sqrt{u(\langle z \rangle)_i^2 + u(\langle z \rangle)_{atm}^2} \quad (5.65)$$

For the surface component of the locally systematic uncertainty, the same uncertainty propagation process is used as in the case of the ATSR instrument series. The assumption made is that the uncertainties are fully correlated within observations sharing a land cover class, but uncorrelated between observations where the land cover class is different. The present implementation of the uncertainty propagation is a two-step approach. The first step is to take each land cover class grouping within the measurements (z) that form part of the average. Within each group, uncertainties are assumed to be fully correlated. The sensitivity matrix, \mathbf{C} , is identical to that shown in equation 5.60, the correlation matrix is equal to \mathbf{J} , and the uncertainty estimate as a function of biome is given in 5.66.

$$u(\langle z \rangle)_{biome} = \frac{1}{n} \sum_n u(z|biome) \quad (5.66)$$

Following this first step, there are now ‘ m ’ uncertainties, where $m \neq n$, unless each member of the vector \mathbf{z} has a different land cover class. The assumption is then made that the subset of uncertainties ‘ m ’ are independent as correlation is assumed to be a function of land cover class. These uncertainties therefore average down as a function of $1/\sqrt{m}$ to give the locally correlated surface uncertainty component (‘surf’) at Level 3.

$$u(\langle z \rangle)_{surf} = \frac{1}{\sqrt{m}} \sum_n u(z)_{biome} \quad (5.60)$$

This two-step implementation does not strictly follow the laws of propagation of uncertainty and leads to a small underestimate in the magnitude of this uncertainty component. A worked example that illustrates this is given in Section 5.1.4.1.4. This propagation can be undertaken in a single step by correctly populating the correlation matrix, \mathbf{R} , setting off-diagonal terms equal to one where observations share a land cover class. All of the required information is available in order to take this approach, and this is recommended for implementation.

Similarly, the retention of biome information for the correct propagation of this uncertainty component to higher-level products (L3C and L3S) is also recommended, although it is acknowledged that this requires a methodology for retaining additional data, possibly as an offline auxiliary dataset. The reasons for retaining this information are discussed in detail in section 5.1.4.1.4.2, but briefly, losing information on the uncertainty correlation will result in an underestimation of the total uncertainty.

5.2.4.2. New uncertainties relevant to the processing level

The LST in a gridded product is calculated using the arithmetic mean. The assumption here is that the LST measurements contributing to this mean value fully represent the variability in the LST within the grid cell. In practice, this is rarely true for LST retrievals using infrared channels, as these are only possible under clear-sky conditions. Where clouds exist, a part of the gridded domain is obscured. We account for this by including a sampling uncertainty as part of the Level 3 LST uncertainty estimate. This uncertainty is modelled using the parameterisation in equation 5.68.

$$u(\langle z \rangle)_{samp} = \frac{n_{clld} \sigma_z^2}{n - 1} \quad (5.68)$$

In equation 5.57, n_{clld} is the number of cloudy observations in a give grid cell, n is the total number of observations in that grid cell and σ_z^2 is the variance in the LST observations in the vector \mathbf{z} . This parameterisation has some limitations as it is dimensionally inconsistent, and does not correctly account for situations where few LST observations are available, which have consistent LST values but are not representative of the LST variability across the grid cell. Further investigation would be required to develop this parameterisation further.

The sampling uncertainty is uncorrelated between Level 3 grid cells and is therefore added to the uncorrelated uncertainty component in addition to the atmospheric uncertainty component.

$$u(\langle z \rangle)_i = \sqrt{u(\langle z \rangle)_i^2 + u(\langle z \rangle)_{atm}^2 + u(\langle z \rangle)_{samp}^2} \quad (5.69)$$

5.2.5. L3C and L3S products

These products are created using an identical methodology to that applied to the ATSR instrument series. Please refer to section 5.1.5 for full details.

5.3. SSM/I and SSMIS

The microwave LST product will be built using radiances observed by the Special Sensor Microwave/Imagers (SSM/I since 1987) and its more recent version the Special Sensor Microwave Imagers Sounder (SSMIS since 2003). These instruments fly on board Defence Meteorological Satellite Program (DMSP) near polar orbiting satellites, providing passive microwave observations twice a day with an incident angle of 53 degrees. The main characteristics of these instruments are presented in Table 7. Instrument swath widths are close to 1400 (SSM/I) and 1700 (SSMIS) km, providing a 1-2 days revisiting time depending on acquisition latitude.

Instrument	Channels (GHz)	Ground Resolution (km)	Satellite platform (years)	Equator Overpass Time
SSM/I	19.35	69x43	F13 (1995-2008)	~6.30 AM/PM
	22.235	50x40		
	37.0	37x28		
	85.50	15x13		
SSMIS	19.35	73x41	F17 (2009-2015)	~6.30 AM/PM
	22.235	73x41	F18 (2016-2020)	
	37.0	41x31		
	91.665	14x13		

Table 21: Instrument characteristics for SSM/I [RD-46] and SSMIS [RD-47]. Vertically and horizontally polarized BTs are available at all frequencies, apart from the 22.235 GHz channel, which is only vertically polarized. SSMIS also observe at other frequencies, but only the ones used for the LST estimation are listed. The ground resolution corresponds to the 3db-Field of View (FOV) of the projected ground footprint.

SSM/I and SSMIS are differently designed instruments and not just one sequential instrument series. As SSMIS provides a continuation of the basic SSM/I observed frequencies, both instruments can be used together to build a data record of brightness temperatures. Nevertheless, they are not expected to give identical brightness temperatures per se, and the sensors require an inter-calibration before their brightness temperatures can be used to derive the microwave LST data record. For the LST_cci project, the brightness temperatures are sourced from the Fundamental Climate Data Record of Microwave Imager Radiances [RD-48], where the brightness temperatures from the different SSM/I and SSMIS instruments have been inter-calibrated to reduce changes related to inter-sensor differences. A common LST retrieval is then applied to process the whole Terabyte data record.

5.3.1. Land Surface Temperature Retrieval

The brightness temperatures observed by a microwave space-borne radiometer at frequency ν and polarization p assuming surface specular reflection and non-scattering atmosphere may be written:

$$\begin{aligned}
 Tb_{\nu,p} &= T_v^\uparrow + \tau_\nu [\epsilon_{\nu,p} T_{e\nu} + (1 - \epsilon_{\nu,p}) T_v^\downarrow] = \\
 &= (T_v^\uparrow + \tau_\nu T_v^\downarrow) + \epsilon_{\nu,p} (\tau_\nu T_{e\nu} - \tau_\nu T_v^\downarrow) = \\
 &= A_\nu + \epsilon_{\nu,p} (B_\nu T_{e\nu} + C_\nu)
 \end{aligned}
 \tag{5.70}$$

Where τ_ν is the total atmospheric transmittance along the sensor line of sight, T_v^\uparrow and T_v^\downarrow represent the upwelling and downwelling atmospheric emission, respectively, $\epsilon_{\nu,p}$ is the surface emissivity, $T_{e\nu}$ is the effective emission temperature of the surface, and the A_ν , B_ν and C_ν terms are abbreviations of the corresponding terms. Dependence of these variables on sensor viewing angle is omitted since we observe at a constant zenith angle close to 53 deg.

The effective emission temperature can then be derived by:

$$Te_v = \frac{Tb_{v,p} - A_v - \epsilon_{v,p}C_v}{\epsilon_{v,p}B_v} \quad (5.71)$$

This effective temperature is called the microwave LST. However, it should be noted that at some specific locations, especially in very dry and sandy areas, the effective emission temperature could be different from the skin temperature measured in the thermal infrared. This is because of the relatively large penetration of the microwave radiation into the sub-surface for these conditions, so the emission temperature does not only correspond to the surface skin [RD-49].

The previous equation derives LST from one single observing channel. In order to better constrain the inversion problem, LST will be retrieved using simultaneously a larger number of frequency channels. This allows to better take into account the atmospheric absorption and emissivity variations in the retrieval [RD-50], similar to the infrared retrievals, where the double-channel algorithms are more suitable to deal with the atmospheric absorption and emissivity effects. If the retrieval uses all channels listed in Table 1, there will then be seven measurement equations similar to the previous equation, and estimating the LST requires solving the corresponding system of equations.

In practice, instead of solving the system of equations for each observation, the LST retrieval is based on approximating the relationship between the brightness temperatures and the LST by a non-linear regression, with the coefficients of the regression determined with a calibration database [RD-50]. To deal with the emissivity variation and further improve the regression, pre-calculated microwave monthly mean emissivity estimates are also used as regressors, together with the brightness temperatures. Concerning the atmosphere, no regressors related to the temperature or water vapour are further added, but the information is introduced into the regression by the brightness temperature variations of the 22 GHz channel, which is close to a water vapour line and therefore sensitive to changes in atmospheric conditions.

The non-linear regression is built by a standard multi-layer perceptron. Multi-layer perceptrons are a type of neural network commonly used to reproduce transfer functions between observations and related geophysical parameters given their proven capability to approximate any continuous function with an arbitrary precision [RD-51]. The details about the exact implementation can be found in [RD-50]. During the calibration phase, the neural network adjusts a set of parameters by minimizing a cost function determined by the set of input-output examples of the calibration dataset. They can be regarded as the regression coefficients of the non-linear model provided by the neural network, or the retrieval coefficients of the inversion algorithm.

Once the neural network is calibrated, the transfer function defined by the neural network becomes the measurement equation, which depends on the 7 channel brightness temperatures, the corresponding climatological emissivities, and the retrieval coefficients:

$$LST = f(T_m, e_m, a_n) \quad (5.72)$$

Where T_m , are the brightness temperatures for channels 19 GHz, vertically polarized (V) ($m=1$), 19 GHz horizontally polarized (H)($m=2$), 22 GHz V ($m=3$), 37 GHz V ($m=4$), 37 GHz H ($m=5$), 85/91 GHz V ($m=6$), and 85/91 GHz H ($m=7$), e_m are the corresponding climatological emissivities for the same channels, and

an are the retrieval coefficients, $n = 1:161$. The function f is differentiable, and either analytical or perturbation-based differentiation can be used to estimate the sensitivity of the function f to its inputs. To relate this back to equation 4.1, z is the retrieved LST, y are the observations (T_m), and β includes the retrieval coefficients a_n , but also the emissivities, e_m . This is different from the infrared measurement equation, where the retrieval coefficients have dependencies on fractional vegetation cover, biome, and precipitable water vapour. In the microwave measurement equation the retrieval coefficients are fixed once the neural network is calibrated, but the dependency of z on the emissivities is introduced by having them as inputs to the function f .

Similar to the infrared, the main error effects associated with the terms in the measurement equation can be listed. Table 2 gives a breakdown of the error effects. The errors associated with the terms y and β are similar in nature to their infrared counterparts. Other errors are specific to the regression model and calibration dataset. The regression model used is relatively complex, and may not be optimal for different reasons, even if is parameterized as good as possible. In principle, the fitting residuals should be indicative of the optimality of the neural network, but some effects could still be missing. For instance, the neural network may be over-fitting to the calibration dataset, with small fitting residuals, but may not perform as optimally when inverting new observations not present in the calibration dataset. There can also be missing input parameters to the regression model, as not all the brightness temperature variability is captured by the emissivity variations. And there can be errors in the calibration dataset itself. For instance, the climatological emissivities and LST in the dataset come from previous inversions of brightness temperatures, so they are certainly subject to errors.

Measurement term	Normal notation	Effect	Effects expected	Correlation length scale	Attributed uncertainties	Sensitivity
β	$a_{1\dots n}$	1	Fitting error	s	Fitting residual	$\frac{\partial g}{\partial a}$
	$e_{1\dots m}$	2	Emissivity error	s	Emissivity uncertainty (location dependent)	$\frac{\partial g}{\partial e}$
γ	$T_{1\dots m}$	3	Calibration error	c	Not attributed	$\frac{\partial g}{\partial T}$
		4	Noise in the retrievals	i	Noise uncertainty (channel-sensor dependent)	$\frac{\partial g}{\partial T}$
+ 0	Regression model structural errors	5	Error linked to a not optimal model	i,c,s (depending on error)	Not attributed	*
	Regression dataset missing inputs	6	Error linked to unexplained input variability	i,c,s (depending on error)	Not attributed	*
	Regression dataset variables errors	7	Error linked to original uncertainty in the dataset variables	i,c,s (depending on error)	Not attributed	*

Table 22: Main error effects for single pixel LST retrieval. Effects are categorised according to the measurement equation term. *denotes cases where the uncertainty cannot be propagated using a sensitivity coefficient.

The LST retrievals are certainly more uncertain in the microwave than in the infrared. This is not just related to the use of a more complex model in the measurement equation, but to a more complex relationship between the microwave emission and changes in the surface and atmospheric conditions. In principle the uncertainty associated to the brightness temperatures and emissivity inputs could be propagated through the regression model. However, this propagation of uncertainty will only estimate the LST error that originates directly from the input uncertainty. As discussed above, this error propagation does not account for the inherent errors of the calibration dataset (how good it reproduces the “true” relationship between brightness temperatures and the LST) and the neural network itself (how good the neural network can approximate this relationship). Therefore, we propose in the next sections a derivation of total uncertainty to have more robust error estimation.

5.3.2. L1 data

Similar to the infrared retrievals, the uncertainty due to a random error effect in Level 1 data is the instrumental noise. These are given in Table 3 for the SSM/I and SSMIS instruments. In the microwave region, the Rayleigh-Jeans approximation of the Planck’s law is valid, and with the emissivity defined as

the ratio of the radiance of a grey body with respect to the radiance of a black body at the same physical temperature, the brightness temperature becomes the direct product of the emissivity and the physical temperature. Therefore, the sensitivity coefficients of matrix C for each observing channel (equation 4.9) are just then the inverse of their corresponding emissivity. The emissivity is location and time dependent, and much more varying than in the infrared, so only climatological values are at hand in the implemented retrieval scheme. In principle, average emissivity maps could be used to have a first idea about the error effect of the Level 1 instrumental noise. But, as discussed in the previous Section, we favour a derivation of total uncertainty including Level 1 and Level 2 error effects, and this Level 1 uncertainty will not be estimated.

Instrument	Channels (GHz)	Variance NE Δ T (K)	
		V-pol	H-pol
SSM/I	19.35	(0.45) ²	(0.42) ²
	22.235	(0.74) ²	
	37.0	(0.38) ²	(0.37) ²
	85.50	(0.69) ²	(0.73) ²
SSMIS	19.35	(0.35) ²	(0.35) ²
	22.235	(0.45) ²	
	37.0	(0.22) ²	(0.22) ²
	91.665	(0.19) ²	(0.19) ²

Table 23: T_m diagonal elements in the S_e matrix for the SSM/I [RD-1] and SSMIS [RD-2] instruments.

5.3.3. L1 and L2 data together

The microwave calibration dataset is built with real observed brightness temperatures, retrieved LST estimates from a detailed inversion of these observations [RD-52]. A time-location dependent climatological emissivity database has been also added to provide a reference emissivity for each sample in the dataset [RD-53]. Given the nature of this calibration dataset, it can be argued that most of the sources of Level 1 and Level 2 uncertainty are included in this dataset. Therefore, this information can be used not only to calibrate the regression model, but also to estimate an LST uncertainty based on inspecting the dispersion of values in the input-output space of the calibration dataset [RD-54].

For each combination of brightness temperatures and emissivities, the deterministic function of the regression model will output a single LST value. In order to associate an uncertainty value to that LST estimation, a small subset of the input space around that combination can be selected, and the corresponding dispersion in LST values in the calibration output space used as a measure of uncertainty. In practical terms, this can be done by dividing the multi-variable input space in a number of narrow bins, followed by the calculation, for each selected bin in the input space, of the standard deviation of the LST error (i.e., the difference between the LST values associated to that input bin and the corresponding LST estimates from the regression model). A lookup table storing bins and uncertainties can be created, and searched for each LST retrieval to associate an uncertainty to each LST estimation.

This approach is illustrated in Figure 5-4, where the regression problem is simplified by regressing only the brightness temperatures of the 37 GHz vertically polarized channel on the corresponding LST of the

calibration dataset. The blue lines show the deterministic output of the regression model, the black circles the mean value of the LST for a number of bins of brightness temperatures, and the black horizontal lines the \pm one standard deviation of the LST for that bin, centred on the mean value. As expected, most of the LST mean values coincide with the regression model output, i.e., the regression model performs well and is able to find the expected LST value for each given brightness temperature. The standard deviations characterize the vertical dispersions representing the uncertainty in the brightness temperature – LST relationship. This dispersion is a characteristic of the calibration dataset, and it is the result of (1) expected variability, i.e., the observed brightness temperatures are affected by variations in other atmospheric and surface parameters, not just the LST, and (2) uncertainty in the calibration brightness temperatures (e.g., the instrumental noise) and associated LST values (e.g., the retrieval error of these LST estimates). This dispersion is independent of the regression model, and cannot be overcome unless additional information is added to the inversion scheme. When the remaining brightness temperatures and corresponding emissivities are added as inputs, the dispersion per bin is reduced and the regression model is able to estimate LST with a smaller uncertainty.

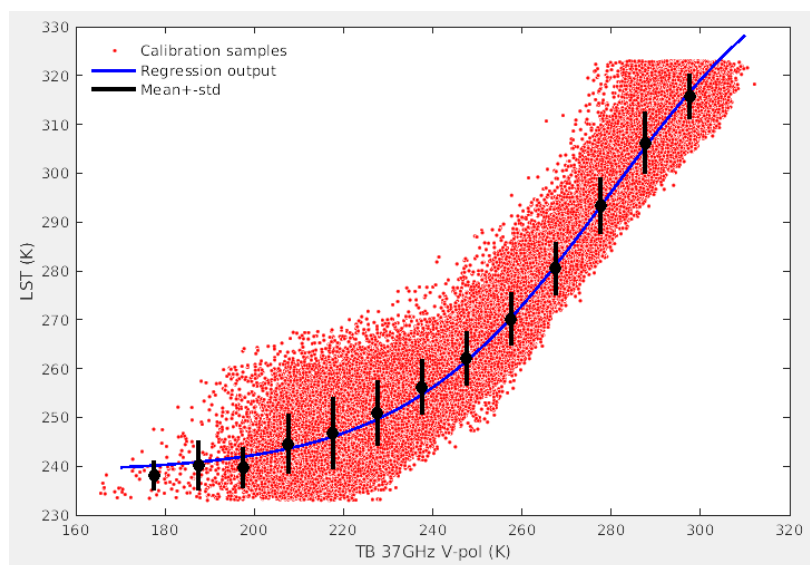


Figure 5-4: Illustration of a single-channel regression model and calibration dataset. A neural network is trained to retrieve LST from the SSM/I 37 GHz vertically polarized brightness temperatures (TB). Red dots are the samples in the calibration dataset, and the neural network output is represented in blue. The horizontal axis has been divided into 5 K TB bins, and for each bin the mean (black circles) and \pm one standard deviation (black line centred around the mean) are given. See the text for more details.

In practice, the multi-dimensionality of the input space complicates the bin selection. Also, storing the dispersion values in a lookup table results in discrete uncertainty estimation. A more convenient implementation, and the one currently used, is to adopt the technique of [RD-54], where a clustering technique is used to facilitate the bin selection, and the uncertainty estimation is incorporated in the regression model itself, to provide a continuous mapping also for the uncertainty. This approach is illustrated in Figure 5-5. First, a neural network is calibrated to provide a first regression model and allow a first estimation of the retrieval error, calculated as the difference of the retrieved LST and the corresponding target LST. Then, a k-mean clustering technique [RD-55] is used to classify the samples of

the calibration dataset into a number of coherent clusters, and the retrieval error is estimated for each cluster. This is followed by calibration of a new regression model having as output the LST and the retrieval error, using the same calibration dataset but with the associated errors estimated with the clustering technique added. This procedure can be iterated until there is a convergence on the estimated error, i.e., the error estimation from the output of the neural network agrees with the error derived from the difference between retrieved and target LST.

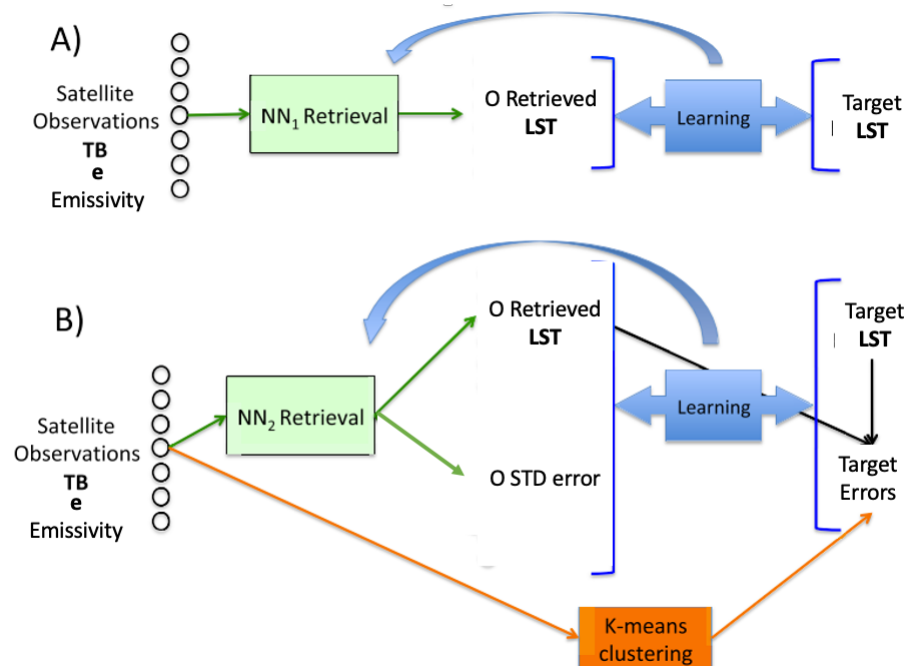


Figure 5-5: Illustration of (A) a traditional LST estimation with a Neural Network (NN), and (B) the proposed scheme where both the LST and an estimation of the LST error are provided by the NN. See the text for more details. Diagram adapted from Figure 2 in [RD-54].

A limitation of this approach is that it provides a total uncertainty value, characterizing Level 1 and Level 2 errors together, without the possibility of propagating uncertainties individually to produce an uncertainty breakdown. Although this breakdown can be of importance for some applications, or to further propagate the uncertainty to next processing levels, it is believed that for this first LST-cci microwave data record the total uncertainty derivation can produce a more robust and useful estimation than a partial breakdown of uncertainties, where only small number of error effects can be taken into account.

An example of estimated uncertainty is given in Figure 5-6. The top panel shows the retrieved LST for day 2012/07/02 for the ascending overpass of SSM/I around 6.30 AM, while the bottom panel displays the estimated uncertainty. In general, the larger uncertainties are located in places where our expected knowledge about the microwave inversion problem suggests difficult inversions. In most cases, these are areas where the emissivity can change rapidly. In this case, the climatological emissivity used as input to the regression model can be poorly representing the true surface conditions. For instance, this happens in snow-covered areas, surfaces that become humid due to rainfall or inundation, or transition regions where the vegetation growth can have large variations from year to year. Coastal regions can also display large uncertainty, as the true emissivity can be very low if water is present in the swath

position of the SSM/I observation, which is not always properly captured by the closest emissivity estimate selected from the climatology. In arid regions large uncertainties can be related to the difficulties of the inversion in regions due to the large penetration depth of the microwaves and the related sub-surface emission.

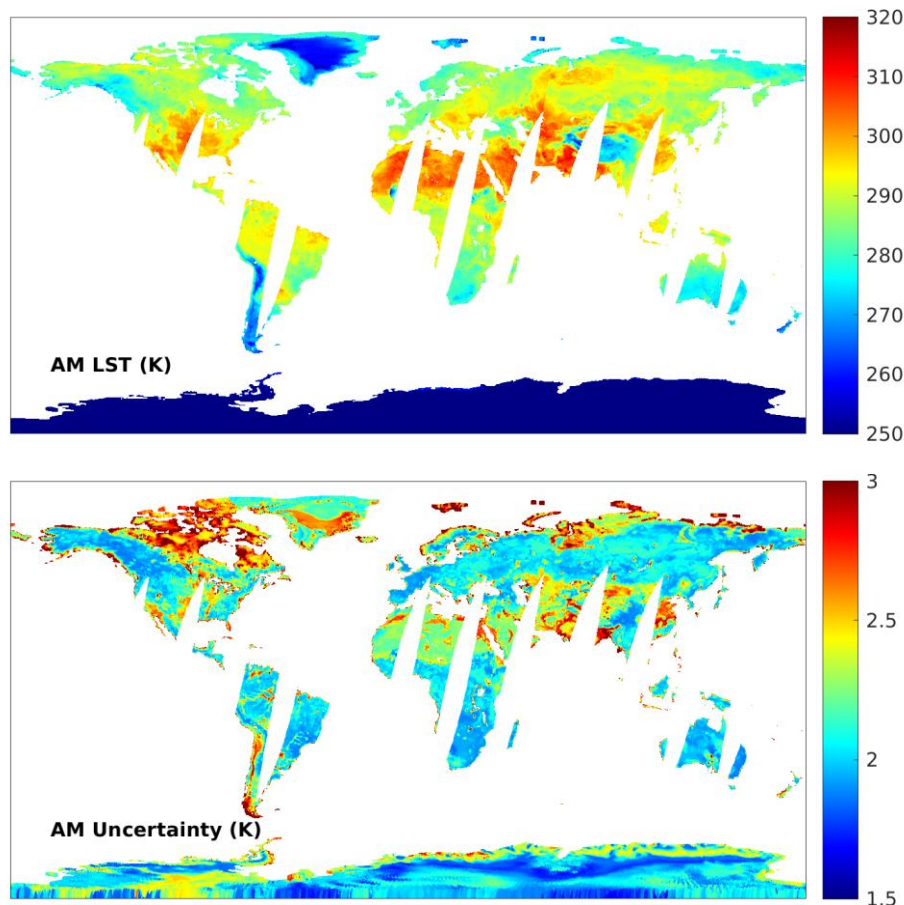


Figure 5-6: Example of retrieved LST (top) and associated uncertainty (bottom). Plotted the morning retrievals from the SSM/I overpass at ~6.30 AM local time.

5.3.4. L3 data

Microwave Level 3 products are those where data are placed onto a common grid at 0.25-degree resolution. The LST value within any given grid box can be selected from the closest Level 2 value (daily product), or calculated as the arithmetic mean of all LST retrievals of the grid box for time averages (monthly from daily, or yearly from monthly). In general, we can write:

$$LST_{grid} = \frac{1}{n} \sum_{i=1}^n LST_i \quad (5.73)$$

For the Level 3 daily, $n=1$, as we select only one Level 2 estimate (the closest to centre of the grid box), while for Level 3 monthly and Level 3 yearly n is the number of days per month with available LST estimates, or the number of months per year, respectively.

Using the form of the measurement equation given in 4.2, $\langle z \rangle = g(\mathbf{y}, \boldsymbol{\beta})$, we can define the error effects associated with the averaged LST product. These are shown in Table 4. As there is not a Level 2 uncertainty breakdown, but just a total uncertainty value, there is only one overall expected effect. For the error propagation, the original uncertainties are assumed to be independent, as specific correlation length scales cannot be attributed without an uncertainty breakdown. This is clearly a simplification, as some degree of correlation is expected in the LST estimate, both in term of spatial (e.g., contiguous grid boxes) and time (e.g., day to day) scales. The result is a likely underestimation of Level 3 uncertainty, as the addition of uncorrelated quantities decreases the uncertainty more than the addition of correlated quantities.

Measurement term	Normal notation	Effect	Effects expected	Correlation length scale	Attributed uncertainties	Sensitivity
z	z_n	1	Overall retrieval error effect	i	Quantified at L2	$\frac{\partial h}{\partial z}$
\mathbf{y}	Weighting	6	Weighting of retrieved pixels contributing to averaged product	s	0	*
+0	Coverage uncertainty	7	Representativity of original LST across gridded domain	s	Not attributed	*

Table 24: Error effects for averaging LST products. Effects are categorised according to the measurement equation term. * denotes where the uncertainty cannot be propagated using a sensitivity coefficient.

As the Level 3 daily product is derived by assigning the closest Level 2 values to each grid box, no uncertainty propagation is needed. Nevertheless, a new source of error arises from the re-gridding, as the selected Level 2 value will never truly represent the area of the Level 3 grid boxes. This uncertainty is very difficult to characterize, so it is not attributed.

For the Level 3 monthly product, as the individual Level 3 daily uncertainties are assumed to be uncorrelated, the \mathbf{R} matrix is the identity matrix, \mathbf{I} . The sensitivity coefficient is obtained by differentiating h with respect to z , resulting in an uncertainty scaled by $1/\sqrt{n}$.

$$\frac{\partial h}{\partial z} = \frac{1}{n} \quad (5.74)$$

$$u(\langle z \rangle)_i = \frac{1}{\sqrt{n}} \sum_n u(z)_i \quad (5.75)$$

The same considerations applies to the Level 3 yearly product, the Level 3 monthly uncertainties are added and assumed to be uncorrelated, propagated in a similar way to the Level 3 daily uncertainties.

6. Harmonisation, Drift and Time Corrections

Generating climate data records (CDRs) of LST typically requires the combination of data from different satellites to form a longer time series. Combining these data requires the application of one or more adjustments to some (or all) of the data inputs and these have associated uncertainties, which need to be accounted for. In broad terms, four types of adjustment fall into this category:

1. Harmonisation of all sensors in a CDR to a single reference sensor.
2. Correction for orbital drift in one or more sensors over time (could be a calibration drift or a positional drift affecting the equator overpass time).
3. Corrections for different equator overpass times of the different sensors in the series.
4. Correction of all data to a single local time.

These are not all necessarily applicable to every CDR, but where they are applied, an associated uncertainty budget should be constructed. In this section we detail the uncertainty budgets associated with the infrared single-sensor CDR and the microwave products.

6.1. Harmonisation and calibration drift correction

The harmonisation and calibration drift corrections with reference to IASI are applied to both the infrared single-sensor CDR (ATSR-2, AATSR, MODIS Terra and SLSTR-A) and to the merged infrared products.

6.1.1. Harmonisation and calibration drift correction with reference to IASI

A detailed outline of the proposed harmonisation steps can be found in RD-56. Here we describe only the details relevant for the construction of the uncertainty budget. The measurement equation for the inter-calibration of each sensor with respect to IASI is given in equation 6.1.

$$BT_{calib_sens} = BT_{sens} + BT_{corr} \quad (6.1)$$

BT_{sens} is the brightness temperature for the instrument to be calibrated against IASI. BT_{corr} is a sensor-specific correction to that brightness temperature, made with reference to the brightness temperature differences between that sensor and IASI. The result of this correction is the inter-calibrated brightness temperature (BT_{calib_sens}). These differences are provided in the form of a look-up table at monthly resolution. The error effects table associated with this measurement equation is shown below (Table 25). Please note that the attribution and sensitivity columns of Table 25 have yet to be completed, as this is a recommended uncertainty budget only, not yet applied to the data products.

Measurement term	Normal notation	Effect	Effects expected	Correlation length scale	Attributed uncertainties	Sensitivity
y	BT_{corr}	1	Approximation made by using a simple Planck function to convert from radiance to BT	c		
		2	Calibration limited to 60-90 degrees south	c		
		3	IASI data processor variable for reference data	c		
		4	Sampling uncertainty in definition of matches	s		
		5	Cloud contamination	s		
		6	Match-up process – time and viewing geometry differences	s		
+ 0		7	Linear fit	c		
		8	Extrapolation of fit to data beyond lifetime of IASI	c		

Table 25: Error effects table for the harmonisation of infrared sensors with reference to IASI.

The first set of error effects (1-6) is associated with the calculation of the brightness temperature correction. Error effect 1 occurs because a simple Planck function is used to convert radiance to brightness temperature for all sensors. Using a single wavelength for this conversion will introduce a radiance dependent error, which could be eliminated by convolving the Planck function with the spectral response function of the observing instrument. If this approach were not taken, then the radiance dependent uncertainty in making this approximation would need to be calculated. The second error effect occurs because the brightness temperature correction term is calculated using data limited to 60-90 south. This is not representative of the full temperature range observed globally and therefore does not account for temperature dependence in the inter-calibration outside of the range covered by the near-polar matches.

The IASI data that has been used as a reference has been produced using different versions of the IASI data processor (i.e. incremental updates to the IASI time series use different processing versions). This may introduce systematic changes in the IASI data due to processor changes (error effect 3). The last three error effects relate to the matching process between the IASI observations and those of the sensor to be corrected. Error effect 4 relates to sampling uncertainty introduced in the matches both by only using clear-sky observations, and by matching L3U gridded observations to the IASI footprint rather than using data on the L2 image grid. Error effect 5 arises from possible cloud contamination of data that can occur in the case of cloud masking failure despite the use of strict cloud contamination thresholds. Finally, differences in the sensor viewing geometry and time of observations between the matched data points will also introduce an uncertainty due to differences in the conditions under which the surface is observed by the two sensors (error effect 6).

There are also two error effects that are part of the ‘+0 term’, associated with the fitting to the data. The first is the use of a linear fit. The relationship between the MODIS and IASI data is not linear, so this assumption will introduce uncertainties that are larger at both ends of the time series. The second is the extrapolation of the data beyond the lifetime of the IASI and MODIS sensors. This extrapolation is required for a period of more than 10 years prior to the launch of IASI in order to include all of the ATSR-2 data record for example (part of the single sensor CDR).

6.1.1.1. How to quantify the uncertainties in the harmonisation to IASI

For the time period in which IASI is operation, the uncertainties can be addressed as follows. The error in assuming a simple Planck function for the radiance to brightness temperature conversion (error effect 1) can be assessed by comparing the brightness temperature calculated using the channel’s nominal wavelength with that using the full spectral response function convolved with the Planck function. e.g.

$$B_{\varphi}(T) = \frac{\int_{v_{min}}^{v_{max}} B(v, T)\varphi(v)dv}{\int_{v_{min}}^{v_{max}} \varphi(v)dv} \quad (6.2)$$

Where φ is the spectral response function (SRF), v_{min} and v_{max} define the boundaries of the SRF and B is the Planck function [RD-57]. The uncertainty will be radiance dependent and could be modelled as the standard deviation of these differences, but once the code to use instrument specific conversion to brightness temperature is written, using this instead of the single wavelength assumption would eliminate this source of uncertainty. This uncertainty component associated with this assumption could be of magnitude $\sim 0.1-0.5$ K. RD-57 provides a good example of the uncertainties introduced when using an effective wavenumber for this calculation.

To address the uncertainty introduced by changes in the IASI processor, the number of changes throughout the time series used should be identified, along with the impact of those changes on the observed radiance. The magnitude of these changes over time can then be used to inform the uncertainty estimate for error effect three. A timeline of the processor updates is provided in RD-58 in addition to an estimate of the relative impact on these updates on both radiance and temperature. Error effects 4, 5 and 6 are all folded into the matchup process. To quantify these uncertainties the standard deviations of the brightness temperature differences between IASI and the reference sensor in a given month could be used.

For brightness temperature corrections extrapolated before the launch of IASI, it isn’t possible to directly attribute the uncertainties via the data matching process, as the data do not exist. One way to estimate the uncertainty would be to apply two linear fits to the data; one using all data available in the time series and the second using only the data in the first five years of the time series. Extrapolate both backwards in time, using the absolute difference between the two as an order-of-magnitude estimate of the uncertainty (which will increase linearly with time in the non-data period). Arguments exist for using either fit to make the correction in this instance, and either could be justified as possible representations of what occurs prior to the launch of IASI, therefore since it is not known (or, by this method, knowable) which is more realistic, their difference scales the possible level of uncertainty (to an order of magnitude). This extrapolation uncertainty is common for a given time.

To calculate the locally correlated uncertainty arising from the variability around the linear fit to the data, the residuals to the fit could be used.

6.2. Adjusting for differences in equator overpass time

The single-sensor CDR uses data from ATSR-2, AATSR, MODIS-T and SLSTR-A. There is a 30-minute time difference in the equator overpass time between each pair of sensors (AATSR and SLSTR-A are at 1000/2200 local time and ATSR-2 and MODIS-T at 1030/2230 local time). Production of a continuous time series of data for these sensors requires a time correction to the data from AATSR and SLSTR-A.

6.2.1. Adjustment for differences in equator overpass time for the single-sensor CDR

The time correction is applied in LST space using matches against MODIS as the reference sensor. MODIS is chosen as this sensor overlaps with both AATSR and SLSTR-A, which are to be adjusted. The time difference between the two observations (AATSR to MODIS or SLSTR to MODIS) typically falls within a 45-minute time window, given the nominal 30-minute difference in overpass times. The measurement equation for this adjustment is as follows.

$$LST_{sens_mod} = LST_{sens} + LST_{corr} \quad (6.3)$$

Here LST_{sens} is the LST retrieved from the sensor to be adjusted, and LST_{corr} the adjustment with reference to the corresponding MODIS LST. These adjustments are applied using a look-up table where the correction is characterised as a function of time of day, location, land cover class and the time difference between the observations, to produce LST_{sens_mod} . The dimensions of the look-up table bins are day/night, 10-degree latitude band and 1-minute bins for the sensor time differences. Table 26 shows the error effects associated with this LST adjustment. Please note that the attribution and sensitivity columns of this table have yet to be completed, as this is a recommended uncertainty budget only, not yet applied to the data products.

Measurement term	Normal notation	Effect	Effects expected	Correlation length scale	Attributed uncertainties	Sensitivity
y	LST_{corr}	1	Sampling uncertainty in the matching process	s		
		2	Cloud contamination	s		
+0		3	Uncertainty in the mean correction	c		
		4	Uncertainty in the LST difference on a particular day.	s		

Table 26: Error effects table for adjustment of AATSR and SLSTR-A data to a nominal equator overpass time of 1030/2230.

Error effect 1 associated with the LST correction term is the sampling uncertainty that is introduced in the match-up process. This arises both from uneven geographical sampling due to the presence of cloud and the use of gridded observations that have already been averaged in time and space. The second error effect is from cloud detection failures, meaning that some cloud will be present in the matches used to estimate the LST adjustment even where strict cloud detection thresholds are applied. There are also two error effects associated with the '+0 term'. The first of these is the uncertainty in the

mean correction to the LST difference, and the second the uncertainty in the assumption that the mean correction is applicable on any given day, given the particular atmospheric and surface conditions.

The approach as defined in RD-56 suggests that the correction will be made using the mean differences in each time bin. Given that these data are noisy, applying a linear fit to these observations and using this may be more appropriate for minimising the error in the correction for any given time difference. If this approach is taken, the large-scale uncertainty on the mean correction (error effect 3) can be estimated using the standard error on this linear fit. The local uncertainty in the LST difference on a particular day (error effect 4), and the uncertainties from sampling and cloud contamination (error effects one and two) can be estimated using the standard deviation of the LST differences in each time bin.

6.3. Correcting data to a nominal satellite overpass time

The microwave CDR requires a correction to local solar time to be made, to account for orbital drift in the contributing sensors. This correction will provide an estimate to a constant local solar time which does not change with location, therefore also correcting the local solar time changes arising from the instrument scanning with a particular orbit and ground swath width. This correction is applied after inter-calibration following the method of RD-59.

6.3.1. Time correction for microwave products

The nominal overpass time of the microwave LST product drifts in time because the satellite platforms carrying the SSM/I and SSMIS instruments do not correct for orbital drift. To facilitate climate studies, the microwave LST product includes an optional LST offset that can be added to the original retrieved LST value to provide a new LST estimate at 0600 and 1800 local time. Due to the satellite orbit inclination and width of the observing ground swath, the nominal equator crossing time is only valid at the centre of the ground swath crossing the equator. This is not a particularity of the microwave instruments, but common to all polar orbiting sensors. The differences to the nominal time depend on the inclination of the orbit and the scanning velocity of the instrument. This is illustrated in Figure 6-1 (top-left), where the time differences of the observing time with the 1800 nominal time are shown for the L3C product on 2005/06/03. This implies that the microwave LST adjustments do not only correct for the drift in local time, but also take care of the time differences related to the characteristics of the instrument swath.

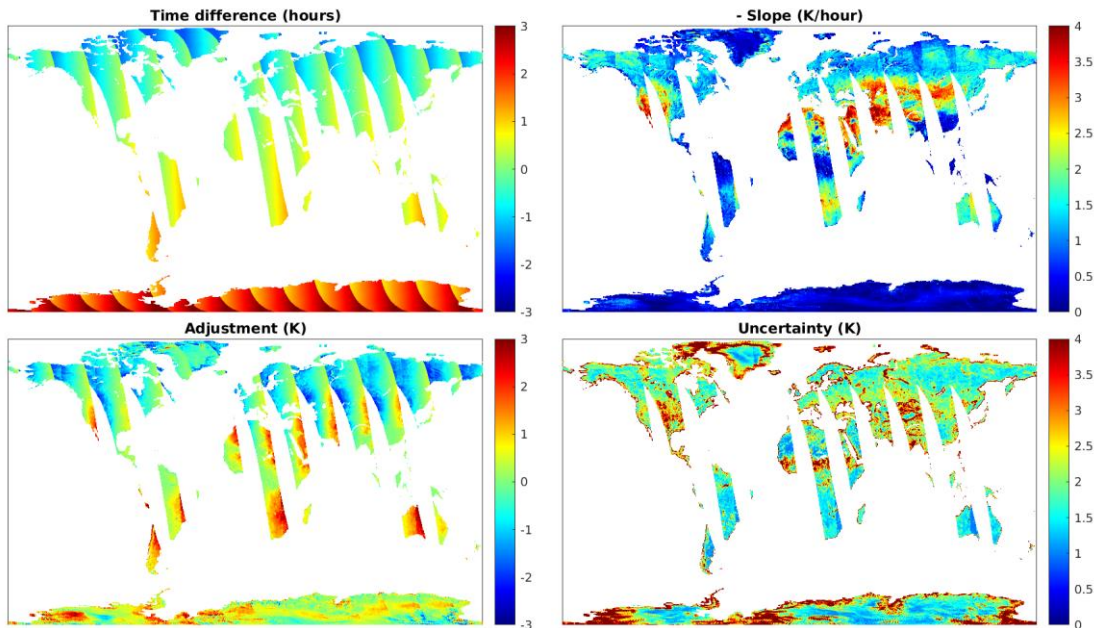


Figure 6-1: Example of time adjustment for the SSM/I ascending overpass on 2005/06/03. Plotted are the time difference of the overpass local time and 1800 (top-left); the negative of the slopes used to derive the LST adjustment (top-right); the LST adjustment (LST_{corr}) derived by multiplying the time differences and the slopes (bottom-left), and; the uncertainty associated with the LST adjustment (bottom-right). See the text for more details.

The LST adjustment is applied to the instruments SSM/I on board the satellite F13, and SSMIS on board F17. Two other SSMIS sensors are used to work out the adjustment, onboard the F16 and F18 platforms. The adjustment is based on pairs of LST differences between these instruments for 10 years of coincident overpasses. The measurement equation then takes a similar form to the adjustment for different satellite overpass times:

$$LST_{sens_mod} = LST_{sens} + LST_{corr} \quad (6.4)$$

Where LST_{sens} is the L3C daily LST retrieved from the F13 or F17 sensor to be adjusted, LST_{corr} the adjustment with reference to the F16 and F18 SSMIS instruments, and LST_{sens_mod} is the adjusted L3C daily LST. Notice that, compared with the infrared: (1) microwave LST is derived not only for clear-sky, but also for cloudy conditions; (2) LST estimates depend more on the surface emissivity, and; (3) surface emissivity varies more with changes in the surface conditions. This makes any attempt to derive a LST adjustment quite uncertain as its value depends on the local conditions of each particular day. For instance, the presence of clouds dampens the amplitude of the diurnal cycle, so the LST adjustment will be smaller. Likewise, a humid soil will warm less because part of the incoming radiation will be used to dry the soil. Therefore, only an approximated LST adjustment can be derived without information on the specific conditions for a particular day and time of the day.

In practice the LST adjustment is derived by estimating an average ratio of daily LST changes with respect to the corresponding local time changes for each continental cell of the L3C product grid. To calculate this ratio for a given Day-of-Year (DOY) and location, for each cell and 30 days around the selected DOY, the available pairs of LST differences and corresponding local time differences are first

selected, and then divided in three bins according to the local time of the F13 and F17 observation, with the bins being local time < 0500(1700), between 0500(1700) and 0700(1900), and > 0700(1900). For each DOY, cell, and local time range, the slope of a linear fit to the existing matches and the spread around the fit are stored in a look-up table. An example of the slopes of DOY 154 applied for the LST adjustments to 1800, 2005/06/03, are given in 6-1 (top-right). As this is the late afternoon overpass, the slopes are negative. Notice that the plot shows the negative of the slope with a positive colour scale. The slopes with largest negative values are visible at arid areas, where the amplitude of the diurnal cycle is the largest. As expected, forested areas and ice surfaces have slopes closer to zero as the LST varies less during the day.

The look-up table is then used to derive the LST_{corr} for an observation at a given date, location, and local time. An example is provided in 6-1 for day 2006/06/03, where the local time difference to 1800 (top-left) is multiplied with the corresponding slope (top-right) providing the LST_{corr} (bottom-left). The LST_{corr} can take values as large as +/- 3K, coinciding with areas with the largest local time differences and largest slopes.

As discussed previously, the uncertainty associated to LST_{corr} is expected to be large due to the particularities of the microwave retrieval. Table 27 shows the main error effects associated with this LST adjustment. First, the daily LST estimates have an associated uncertainty. A second error effect is related to the sampling uncertainty that is introduced in the match-up process, as the L3C product is based on observations gridded from the original swath ground positions. A third error is related to the fact that the applied linear fit to derive the slope at a particular day, location, and local time, is not directly related to the specific surface and atmospheric conditions of that day and time. As described previously, the derived slopes use matchups in a running window of 30 days, which includes pairs of LST differences for different years, and therefore different conditions, and for a given range of local time differences established by the selected bins. Even if the bins were changed to cover much narrower local time conditions, the proposed scheme will still provide a “mean” correction based on the average conditions of the 10 analysed years for that very specific local time. The final error effect (5) is the uncertainty that arises when changing between two different correction slopes at the time thresholds of 0500/1700 and 0700/1900.

Measurement term	Normal notation	Effect	Effects expected	Correlation length scale	Attributed uncertainties	Sensitivity
y	LST _{corr}	1	Uncertainty associated to using LST differences representing typical conditions	s	Variability around a specific time difference	*
		2	Sampling uncertainty in the matching process	s		*
+0	Daily correction	3	Uncertainty in the LST difference on a particular day.	s		Variability around the mean linear fit
	Mean correction	4	Uncertainty in the mean correction	c	*	
	Change of correction slope	5	Uncertainty in step-changes at 0500/1700 and 0700/1900 local time of correction slopes	s	Not attributed	*

Table 27: Error effects table for time differences corrections for microwave data

To derive an uncertainty estimate for each location, day, and local time, we use the spread of the LST differences around the linear fit stored together with the slope value in the look-up table. This variability includes the first two errors, but the third one is only accounted for as an “averaged” uncertainty, with the uncertainty for the specific conditions not being attributed. Still, the derived values can be useful to provide a view of uncertainty. An example is given for the LST adjustment on 2006/06/03 in 6-1 (bottom-right). Typical values are in the range 1-2 K, but the values can be as large as 4K, typically occurring at places where the LST used in the fits were highly variable. For instance, this is the case in coastal regions, where the coarser resolution of the microwave observation contaminates the LST retrievals with radiation emitted by the water entering the field of view of the instrument. Large uncertainties are also observed in transition regions where the local conditions can change from year to year (e.g., changes in plant growth, soil moisture, precipitation). This is visible in the transition zone between the arid regions of the Northern Africa and the forested areas of Central Africa, and in some regions in North America and Asia. The final uncertainty in changing the LST correction slopes is not presently attributed.

7. Specification of uncertainty information used in LST retrieval

The information required to calculate the uncertainty budget for the ATSR and SLSTR instruments is contained within a look-up table for each sensor. These files are in netCDF format and are read by the retrieval code. The structure of this look-up table is consistent between sensors and provided in section 6.1.

7.1. Look-up Table Structure

Each of the look-up tables has a set of global attributes that detail the contents of the file, the creator of the file and the appropriate contact for users of the file who have any questions about its contents. These are given in Table 14. The global attributes also contain some data format information pertaining to the file type (netCDF4), conventions and dataset details. The creation time of the file is of course file dependent, and is not included explicitly in Table 14.

Global Attributes	
Conventions	"CF-1.4"
title	"LST error auxiliary dataset for ATS_GT2"
institution	"University of Leicester"
source	"RTTOV simulated uncertainties"
contact	"djk20@le.ac.uk"
netCDF_version	"netCDF4"
dataset_name	"LST error ATS_GT2"
creation_time	-- file dependent --

Table 28: Global attributes for look-up tables used in the uncertainty budget calculation for AATSR.

Table 15 gives the details of the dimensions used in the look-up tables. The table includes the dimension name as found in the file (column 1), the dimension size (column 2) and then a definition of the contents of the dimension (column 3). These dimensions allow the contents of the file to be stratified by channel, biome, satellite zenith angle, time of day (day/night) and total column water vapour as appropriate.

Dimensions	Value	Contents
n_biome	28	Number of biomes
n_channel	2	Number of channels
n_satze_band	5	Number of satellite zenith angle bands
n_tcwv_band	1	Number of total column water vapour bands
sl_channel	6	Character length of 'char' variable
n_large_scale	1	Number of large scale uncertainty components
n_diurnal	2	Number of diurnal components (day/night)
n_biome_all	29	Number of biomes including water class

Table 29: Dimensions of the look-up tables used in the uncertainty budget calculation for AATSR.

There are eleven variables contained within the look-up table files Table 16). The first five describe the dimensions used for the uncertainty components. These are the biomes, channels, satellite zenith angles, total column water vapour bands and times of day appropriate to the uncertainty components provided. The final six variables contain the data required to calculate the uncertainty budget itself. The details of those applicable to the ATSR and SLSTR retrievals are as follows:

- i. The noise equivalent delta temperatures (NEdT) used in the propagation of this uncertainty component into the retrieval (u_ran_y).
- ii. The atmospheric fitting uncertainty in the retrieval coefficient calculation (u_loc_fit).
- iii. The geolocation uncertainty (delta LST expected by mis-representing the underlying biome).
- iv. The large scale systematic uncertainty for propagation into the retrieval (u_sys).

Variable	Type	Dimensions
biome	Byte	(n_biome)
channel	Char	(n_channel, sl_channel)
satze_band	Float	(n_satze_band)
tcwv_band	Float	(n_tcwv_band)
diurnal	Byte	(n_diurnal)
u_ran_y	Float	(n_channel)
u_ran_emis	Float	(n_channel, n_biome)
u_loc_fit	Float	(n_tcwv_band, n_satze_band, n_biome, n_diurnal)
u_loc_emis	Float	(n_channel, n_biome)
u_loc_geo	Float	(n_biome_all, n_biome, n_diurnal)
u_sys	Float	(n_large_scale)

Table 30: Variables contained within the look-up table used in the uncertainty budget calculation. Information provided includes the variable name, the variable type and the dimensions of the variable.

Table 17 describes the attribute metadata provided with each of the variables in the look-up table. Thitypically includes a long name describing the data in more detail, the units of the data and values of flags where appropriate. In one case (for the NEdT data) a reference is included and this is file specific.

Variable	Attribute	Attribute Content
biome	long_name	“Biome code corresponding to biome index”
	flag_meanings	“ ”
	flag_values	1b, 2b, 3b, 4b, 5b, 6b, 7b, 8b, 9b, 10b, 11b, 12b, 13b, 14b, 15b, 16b, 17b, 18b, 19b, 20b, 21b, 22b, 23b, 24b, 25b, 26b, 27b, 28b
channel	long_name	“Channel corresponding to channel index”
	flag_meanings	“ ”
	flag_values	1b, 2b
satze_band	long_name	“Satellite Zenith Angle lower band value (degrees) corresponding to satze band index”
	flag_meanings	“ ”
	flag_values	1b, 2b, 3b, 4b, 5b
tcwv_band	long_name	“Total Column Water Vapour lower band value (degrees) corresponding to tcwv band index”
	flag_meanings	“ ”
	flag_values	1b

Variable	Attribute	Attribute Content
diurnal	long_name	Diurnal code corresponding to diurnal index
	flag_meanings	“ “
	flag_values	1b, 2b
u_ran_y	long_name	“Estimate of NEDTs”
	units	“kelvin”
	comment	-- file specific --
u_ran_emis	long_name	“Estimate of random error due to emissivity”
	units	“kelvin”
u_loc_fit	long_name	“Estimate of locally correlated error due to atmospheric fitting”
	units	“kelvin”
u_loc_emis	long_name	“Estimate of locally correlated error due to emissivity”
	units	“kelvin”
u_loc_geo	long_name	“Estimate of locally correlated error due to geolocation”
	units	“kelvin”
u_sys	long_name	“Estimate of large scale systematic uncertainty applicable to all pixels”
	units	“kelvin”

Table 31: Attributes associated with each variable contained within the look-up tables used in the uncertainty budget calculation.

8. Provision of Uncertainties in LST CCI Products

Within LST_cci products, uncertainty information is provided with each LST measurement. The exact information provided is dependent on the product type, and in some cases a full breakdown of the uncertainty components by correlation length scale is provided (as discussed throughout this document), whilst in others only the total uncertainty is included. This section describes the uncertainty information provided with each product type.

8.1.1. LST_cci product types

It useful here to define the different product types produced within the LST_cci project, as these will be discussed more extensively below. Data are provided in four formats: L2P, L3U, L3C and L3S, with the format dependent on the data type [RD-21]. The LST data provided within the project are diverse, and the following data differences all determine the most appropriate data type for each data record:

- i. Single sensor data records or multi-sensor data records
- ii. Polar orbiting or geostationary satellites
- iii. Infrared or microwave products
- iv. Single sensor ‘type’ data records or merged products

The required temporal resolution is also important in determining the most appropriate file format. Within the LST_cci project, data are provided at the following time resolutions:

- i. ‘Instantaneous’ orbit or geostationary disk
- ii. Daily
- iii. Monthly
- iv. Annually

The differences between the L2P, L3U, L3C and L3S data formats are given in Table 14, using definitions provided in RD-21.

Product Type	Description
L2P	Geophysical variables at the full resolution of the instrument, in a satellite projection with associated geographical information.
L3U	Spatially averaged version of the L2P data.
L3C	L3U data from a single instrument that have been combined and temporally averaged.
L3S	L3U data from multiple instruments that have been combined and temporally averaged onto a common grid.

Table 32: Description of data product types produced within the LST_cci project (taken from RD-21).

8.1.2. L2P, L3U, L3C and L3S uncertainty information

The L2P, L3U, L3C and L3S products all provide the total uncertainty in the LST per datum, as well as a complete breakdown of the associated uncertainty components: uncorrelated (random) uncertainty, locally systematic uncertainty (atmosphere and surface components) and large-scale uncertainty. Table 19 presents the variable names for these different components within the LST_cci products.

Uncertainty Component	Naming convention within LST_cci products
Uncorrelated (random) uncertainty	lst_unc_ran
Locally systematic surface uncertainty	lst_unc_loc_sfc
Locally systematic atmospheric uncertainty	lst_unc_loc_atm
Large scale systematic uncertainty	lst_unc_sys
Total uncertainty	lst_uncertainty

Table 33: Mapping of uncertainty components to variable names within L2P, L3U, L3C and L3S products.

All of the uncertainty variables in the L2P and L3U products are stored as 16 bit signed integers. The dimensions of these variables for L2P data are shown in Table 20. These data are provided on the orbit swath and consequently the spatial dimensions reflect the satellite image grid (ni and nj). The time dimension of these files must always be '1' as these contain data from a single orbit.

Dimension	long_name
time	Time dimension; must be 1 for L2P data
nj	Along track dimension
ni	Across track dimension

Table 34: Variable dimensions for uncertainty components in L2P data.

The dimensions of the uncertainty variables in L3U, L3C and L3S products are given in Table 21. These data are provided on a regular grid and therefore the spatial dimensions of these data are latitude and longitude. The time dimension for these products should also be '1' as they contain a single orbit on a regular grid.

Dimension	long_name
time	Time dimension
lat	Latitude dimension
lon	Longitude dimension

Table 35: Variable dimensions for uncertainty components in L3U, L3C and L3S data.

Each of the variables provided in the L2P and L3U products has a number of attributes associated with it that describe the data and how to read them correctly. The first of these is the 'long_name' of the

variable. This contains some free text that gives a more detailed description of the variable contents than the variable name itself. The long_name is different for each of the uncertainty components and the full list of long names is provided in Table 22.

Uncertainty Component	long_name
lst_unc_ran	uncertainty from uncorrelated errors
lst_unc_loc_sfc	uncertainty from locally correlated errors on surface scales
lst_unc_loc_atm	uncertainty from locally correlated errors on atmospheric scales
lst_unc_sys	uncertainty from large-scale systematic errors
lst_uncertainty	land surface temperature total uncertainty

Table 36: 'long_names' for uncertainty components in L2P, L3U, L3C and L3S products.

The remaining attributes provided with the uncertainty data are in common between all of these variables and are summarised in Table 23. Each variable has attributes that describe the units and coordinates of the data. Valid minimum and maximum values for the data are given which are relevant for checking that the data have been read correctly when used. In addition to this, the data are scaled in order to reduce the storage space required for each variable. To revert the data back to its original format the offset and scale factor are required to reverse the scaling. Finally the value used to represent missing data is also provided (in the attribute _FillValue).

Attribute	Meaning	Value
units	Text description of the units	kelvin
_FillValue	A value used to indicate array elements containing no valid data	-32768
add_offset	To be added to the variable after multiplying by the scale factor to recover the original value	0
scale_factor	To be multiplied by the variable to recover the original value	0.001
valid_min	Minimum valid value for this variable once they are packed (in storage type)	0
valid_max	Maximum valid value for this variable once they are packed (in storage type)	10,000
coordinates	Identifies coordinate variables	lat lon

Table 37: Common variable attributes for uncertainty components in L2P, L3U, L3C and L3S products.

9. Validation of Uncertainties

One advantage of calculating uncertainties within the retrieval process itself (rather than with reference to an external dataset) is that these can be independently validated in addition to the LST retrieval. Validation of uncertainties will inform the both the data producer and data user of how representative the uncertainty budget is of the full uncertainty associated with each datum e.g. it will demonstrate whether the main (largest) uncertainty sources are well captured within the budget. It is important to note here that large uncertainties do not indicate bad quality data. Good data can have a large, well-validated uncertainty. Uncertainties can also be used in the validation of the LST data to prescribe upper and lower bounds for measurement differences.

9.1. Techniques

One commonly used technique for validation of retrieved LST data is to compare this with an independent measurement of LST. Typically this independent measurement is made using an in-situ radiometer measurement, in a site deemed appropriate for in-situ to satellite comparisons. Assessing the suitability of the validation site includes consideration of the site homogeneity, length of in-situ data record, characteristics of the in-situ radiometer and any seasonal changes in local vegetation [RD-10]. In this section we discuss the techniques for validating uncertainties on the assumption that a representative independent dataset exists, well matched temporally with the satellite observations.

To validate retrieved surface temperature, the total uncertainty can be compared with the standard deviation of the difference between retrieved and independent LST estimates. Here, the assumption is that the differences between the in-situ and satellite LST estimates produce an error distribution from which the standard deviation is representative of the uncertainty. To take this approach, it must be kept in mind that the in-situ data also have an associated uncertainty, and this (along with any uncertainty in the matching process) determines the lower limit on the uncertainty validation. We can express the uncertainty in the satellite to in-situ observations differences using equation 9.1. The uncertainty in the difference (u_{diff}) is the sum in quadrature of the uncertainty in the satellite observation, and in-situ measurement, along with the geophysical uncertainty of comparing a point measurement with an area average (space) and comparing measurements made at different times. For microwave LST there is an additional geophysical uncertainty due to the measurement depth of the temperature.

$$u_{diff} = \sqrt{u_{sat}^2 + u_{insitu}^2 + u_{space}^2 + u_{time}^2 + u_{depth}^2} \quad (9.1)$$

An example of uncertainty validation is shown in Figure 7.1. The data shown in this instance are sea surface temperatures, but the methods are directly transferrable to LST data. Considering first the top left-hand panel, the plot shows the standard deviation of the retrieval minus in-situ SST differences (y-axis) as a function of the retrieval uncertainties (x-axis). These are shown using the vertical black lines, mirrored about the zero line on the y-axis. The dashed lines above and below zero on the y-axis show the ‘ideal’ uncertainty model. Where the total uncertainty exceeds the uncertainty in the in-situ data, these lines follow the 1:1 ratio. The uncertainty in the in-situ data and geophysical uncertainties in the match up process prevent the ideal model from reaching zero, in this case the assumed uncertainty in the in-situ data is ~ 0.18 K.

Where the solid lines fit well within the ideal model (as in the top right panel), this shows that the uncertainty model validates well. Where the lines fall short of the model, the uncertainties in the

product being validated are an over-estimate, i.e. these would need to be shifted to the left to agree with the ideal model. Conversely, where the solid lines exceed the model, the product that is being validated under-estimates the uncertainties.

For the validation of LST products, the plots will also show the number of matchups used to derive the statistics, as in-situ data are much more limited than is the case with sea surface temperature.

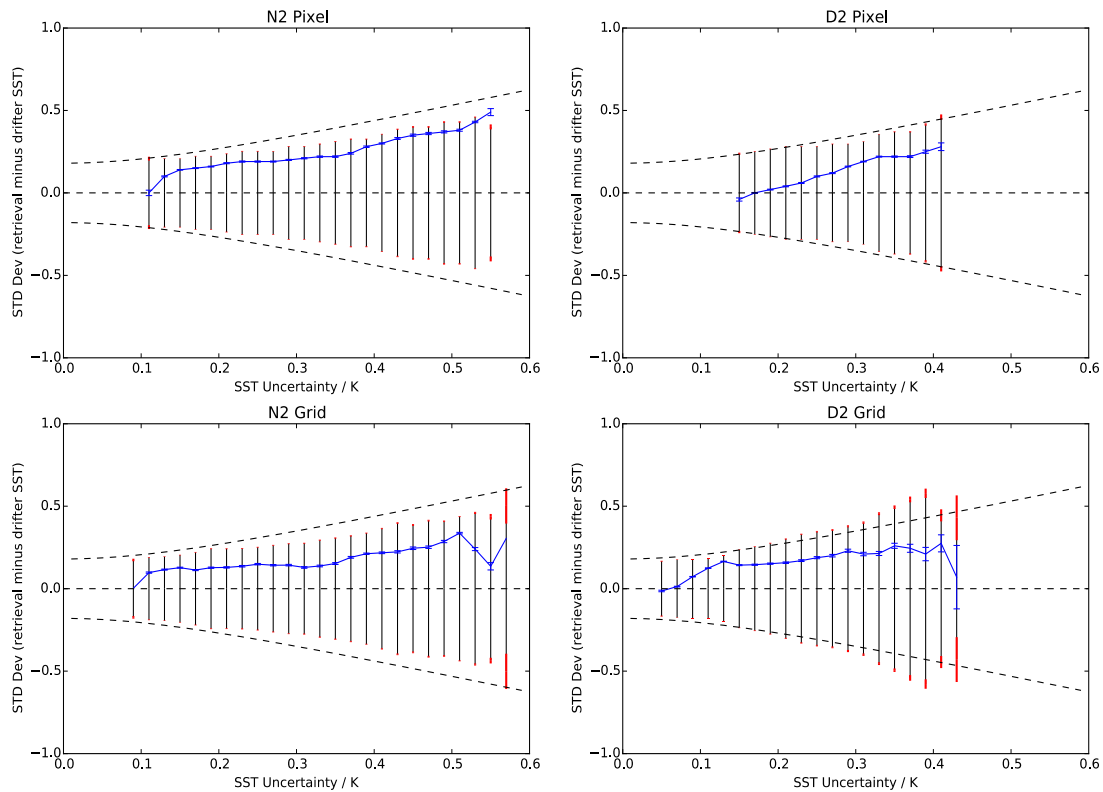


Figure 9-1: An example of uncertainty budget validation. Data are retrieved sea surface temperatures validated using in-situ observations from buoys. Two different retrievals are shown for ATSR data – L2 per pixel datasets (top), and gridded L3 products (bottom). Retrievals are nadir two-channel (N2) and dual-view two-channel (D2) where the channels used are 10.8 and 12 microns. Dashed lines denote the idealised uncertainty model, whilst solid lines represent the standard deviation of the retrieval minus in-situ differences. The blue line shows the SST bias and the red lines are the uncertainties on the retrieved uncertainty.

10. APPENDIX: How to use LST CCI Uncertainty Products

As described in section 9 and throughout this document, LST_cci products are provided with uncertainty estimates per datum. The products include the total uncertainty for each LST measurement as well as a breakdown of the uncertainty components in accordance with their spatial correlation length scales; uncorrelated, locally systematic (atmospheric and surface components at Level 2) and large-scale systematic. The potential uses for LST data within climate applications are diverse and varied, including, for example:

- ❖ Assimilation of LST into numerical weather prediction or other models.
- ❖ Surface energy balance studies.
- ❖ Understanding urban heat islands.
- ❖ Assessing long-term changes in LST and relating this to crop yields and sustainability.
- ❖ Investigating temperature extremes and changing patterns in surface heating.

Within these applications, users are often required to manipulate the LST data in one or more of the following ways:

- ❖ Combining LST's of different origins.
- ❖ Assessing the significance of differences between LST's.
- ❖ Deriving new products through the propagation of LST data.
- ❖ Data assimilation into climate or numerical weather prediction models.

In all cases, correct use of the data requires propagation of the associated uncertainties into the given application. To understand why this is important, it is perhaps useful to consider why uncertainties might vary across a given product (Level 2 or Level 3). Considering first Level 2 data, there is an uncertainty component related to the derivation of the retrieval coefficients. This has a dependence on total column water vapour, and has a tendency to increase in wetter atmospheres. There is also an uncertainty component related to geolocation, essentially in assigning the correct biome to the observation. Where the land surface is more heterogeneous with rapid variations in the land cover, this uncertainty will be larger than in more homogeneous regions. In the example of gridded products (Level 3 data), the uncertainty has a dependence on sampling within a grid cell. If lots of observations are available to calculate LST within a grid cell, the uncertainty will typically be lower than when few observations are available. In the sections below a couple of worked examples are provided that describe how uncertainty information should be used in different scenarios. Note that these examples have been adapted for LST from those presented in the SST CCI Uncertainty Characterisation Report [RD-20].

10.1. Using uncertainty information from Level 2 products

10.1.1. Example 1: Is the LST from a Level 2 product significantly different from a matched independent in-situ radiometer measurement?

To compare a satellite retrieved LST with an in-situ LST measurement the total uncertainty would be used. This total uncertainty is also referred to as the standard uncertainty and represents an estimate of the standard deviation of all the error distribution for all error sources. The in-situ radiometer measurement would also have an associated uncertainty. We therefore have two measurements plus

their associated uncertainties, where the subscript ‘L2’ represents the retrieved data and the subscript ‘in-situ’ the radiometer data.

$$LST_{L2} \pm \varepsilon_{L2}$$

$$LST_{in-situ} \pm \varepsilon_{in-situ}$$

The significance of the difference between the two measurements $LST_{L2} - LST_{in-situ}$ can be interpreted with reference to the combined measurement uncertainty in the difference using an appropriate statistical technique, e.g. a student's t-test. The combined measurement uncertainty in the difference is:

$$\sqrt{\varepsilon_{L2}^2 + \varepsilon_{in-situ}^2}$$

10.1.2. Example 2: What is the uncertainty in my calculation of outgoing LW infrared flux from the land surface arising from the measurement uncertainty in the Level 2 LST product I am using?

To calculate thermal emission from the land surface, an equation along the lines of $E = \varepsilon\sigma T^4$ would be appropriate. Here, E is the thermal emission, ε is the surface emissivity and σ is the Stefan Boltzmann constant. T is the LST from the L2 product. In this example we would again use the total uncertainty provided with the LST estimate. Using the methodology for propagation of error, the uncertainty in E arising from the LST uncertainty is $4\varepsilon\sigma T^3$. It is important to note that the LST used is not the only source of uncertainty in this calculation.

10.2. Using uncertainty information from Level 3 products

10.2.1. Example 1: What is the best estimate of the average LST over an area of 0.25 degrees latitude by 0.25 degrees longitude using L3U LST data?

The Level 3 LST L3U product is gridded at a resolution of 0.05 x 0.05 degrees (latitude and longitude). To estimate the average LST across the 0.25-degree domain we need to calculate an average that includes up to 25 Level 3 LST estimates. Two options are available for calculating the average:

- i. A simple arithmetic mean with equal weight given to each contributing LST estimate.
- ii. A weighted mean reflecting the difference in the uncertainties associated with each contributing LST estimate.

An argument can be made for either approach as follows:

- iii. If significant LST variability were expected across the 0.25-degree cell, the first approach would ensure that all contributing LST estimates are evenly represented in the average.
- iv. If minimum uncertainty in the LST estimate across the 0.25-degree domain is required, assuming that LST variability across the cell is negligible and the 25 LST estimates are essentially repeated measurements of the same LST.

In this example we will consider the second option, but note that for LST this may only be appropriate in more homogeneous regions. In forming a weighted mean we would use the following equation for the best estimate of the average.

$$\bar{x} = \left(\sum \varepsilon_i^{-2} x_i \right) / \left(\sum \varepsilon_i^{-2} \right)$$

Where i is an index running over the 25 contributing LST estimates, x is the LST and ε is the LST uncertainty. This equation gives the higher weighting to those LST estimates with lower uncertainty estimates.

One question still remains; which uncertainty estimate should we use? In this case, the total uncertainty is not the most appropriate measure. This is because it contains uncertainty estimates that are highly correlated between the LST's contributing to the average (those included in the locally systematic and large-scale systematic components). As the correlation of these components is almost perfect across the spatial domain for which the average is being calculated, these should not influence the weight given to any particular LST estimate used to calculate the average. The appropriate uncertainty component to use to define the weights is therefore the uncorrelated component from random error effects (provided within the product). This includes factors such as instrument noise and sampling uncertainty that vary between the LST estimates for each Level 3 cell on this scale.

10.2.2. Example 2: What is the total uncertainty in the averaged LST calculated in example 1 (section 9.2.1)?

The uncorrelated uncertainty in \bar{x} from random error effects in the 25 contributing LST estimates being averaged is given by $\left(\sum \varepsilon_i^{-2} \right)^{-1/2}$, which leads to the standard reduction in random error when calculating an average. The total uncertainty also includes components from the locally systematic or structured error effects (s) and the large-scale common error effects (c). To estimate these contributions, the average value for each across the cell is sufficient. They should differ little if at all between the 25 contributing LST estimates and do not average down over the scale on which they are correlated. The total uncertainty can then be estimated as follows remembering that uncertainties add in quadrature.

$$u(LST) = \sqrt{\left(\sum \varepsilon_i^{-2} \right)^{-1} + \varepsilon_s^2 + \varepsilon_c^2}$$

Here, ε_s^2 is the average of the locally systematic uncertainty and ε_c^2 is the average of the large-scale systematic uncertainty for the 25 contributing LST estimates.

End of Document